A NEW DRUG TRIGGERING MECHANISM IN THERMOSENSITIVE NANOPARTICLES USING A LOW-MELTING-POINT POLYMER

ALI DABBAGH

FACULTY OF MEDICINE
UNIVERSITY OF MALAYA
KUALA LUMPUR

2016

A NEW DRUG TRIGGERING MECHANISM IN THERMOSENSITIVE NANOPARTICLES USING A LOW-MELTING-POINT POLYMER

ALI DABBAGH

THESIS SUBMITTED IN FULFILMENT OF THE REQUIREMENTS FOR THE DEGREE OF DOCTOR OF PHILOSOPHY

FACULTY OF MEDICINE
UNIVERSITY OF MALAYA
KUALA LUMPUR

2016

UNIVERSITY OF MALAYA

ORIGINAL LITERARY WORK DECLARATION

Name of Candidate: **ALI DABBAGH**

Registration/Matric No: **MHA130085**

Name of Degree: **DOCTOR OF PHILOSOPHY**

Title of Thesis ("this Work"):

A NEW DRUG TRIGGERING MECHANISM IN THERMOSENSITIVE NANOPARTICLES USING A LOW-MELTING-POINT POLYMER

Field of Study: **BIOMEDICAL IMAGING**

I do solemnly and sincerely declare that:

(1) I am the sole author/writer of this Work;
(2) This Work is original;
(3) Any use of any work in which copyright exists was done by way of fair dealing and for permitted purposes and any excerpt or extract from, or reference to or reproduction of any copyright work has been disclosed expressly and sufficiently and the title of the Work and its authorship have been acknowledged in this Work;
(4) I do not have any actual knowledge nor do I ought reasonably to know that the making of this work constitutes an infringement of any copyright work;
(5) I hereby assign all and every rights in the copyright to this Work to the University of Malaya ("UM"), who henceforth shall be owner of the copyright in this Work and that any reproduction or use in any form or by any means whatsoever is prohibited without the written consent of UM having been first had and obtained;
(6) I am fully aware that if in the course of making this Work I have infringed any copyright whether intentionally or otherwise, I may be subject to legal action or any other action as may be determined by UM.

Candidate's Signature Date:

Subscribed and solemnly declared before,

Witness's Signature Date:

Name:
Designation:

ABSTRACT

Thermosensitive nanocarriers are increasingly used to allow time and site-specific drug release with minimized systemic toxicity. Thermal-triggered drug release is often governed by coil-globule, membrane disruption, and micellization mechanisms. However, premature and slow drug release, low stability, and insufficient bioavailability remain challenging in most nanocarriers which utilize these triggering mechanisms.

This work aimed to introduce a new triggering mechanism using polymers with gel-liquid phase transition at hyperthermia and thermal ablation temperatures. This phase transition could generate structural defects in nanocarriers and thus facilitate drug release. In addition, for accurate assessment of the heated region during in vitro evaluation of nanocarriers, a novel thermosensitive phantom was developed.

Nanocarriers were synthesized using mesoporous silica nanoparticles (MSNs) as drug reservoir and two polymer formulations including polyacrylamide (PAA) and polyethylene glycol (PEG) as the protective nanoshells. The graft-from and graft-to techniques were respectively employed to prepare PAA-MSNs and PEG-MSNs. The phase transition behaviours as well as various chemical, morphological, and thermal properties of these nanocarriers were characterized and their drug loading and release potentials were investigated using doxorubicin as a hydrophilic model drug. Magnetic resonance-guided focused ultrasound (MRgFUS) was also employed as a typical thermal modality to evaluate the drug release rates in short-term treatment intervals. The required phantom for MRgFUS experiments was developed using a thermochromic dye with reversible discolouration at hyperthermia range. Various physical, thermal, and acoustic properties of this phantom were measured to ensure their proximity to those of human

soft tissues. The thermosensitive behaviour of this phantom was evaluated using radiofrequency (RF) and MRgFUS experiments. The aqueous solutions containing drug-loaded nanocarriers were further embedded within the phantom and sonicated by MRgFUS to determine their efficacy as adjuvants to this thermal modality.

Spectrophotometry analysis of the phantom showed a threshold temperature of 50±3°C with a 6°C difference between the onset and ending discolouration temperatures. The contrast change at focal point during sonication also allowed visualization of the thermal lesion in magnetic resonance images. The onset transition temperatures of PAA-MSNs and PEG-MSNs were 45.1±3.4°C and 40.4±1.8°C, respectively. The peak transition temperature of PEG-MSNs was also 20°C lower than that of PAA-MSNs, resulting in significantly sharper phase transitions. Drug release measurements for PAA-MSNs showed 11.5±2.4% leakage at 37°C after 30 minutes, while this value was significantly increased to 20.2±4.3% in PEG-MSNs. However, the maximum release ratio in PEG-MSNs (68.2±3.7%) was obtained at 50°C which was 10°C lower than that of PAA-MSNs (67.6±2.5% at 60°C). The drug release ratio from PEG-MSNs (45.5±3.1%) under MRgFUS exposure was also significantly higher than PAA-MSNs (39.2±2.2%).

Melting of polymer shells at hyperthermia and thermal ablation temperature ranges could provide thermal-triggered drug release from the core-shell nanocarriers with relatively low undesired release at physiological temperature. The drug release ratio from PEG-MSNs at physiological temperatures was higher than PAA-MSNs. However, the maximum drug release in these nanocarriers was obtained in significantly lower temperatures. Both PAA-MSNs and PEG-MSNs exhibited high loading efficiencies and rapid drug release rates at increased temperatures which make them promising for application as adjuvants to thermal modalities.

ABSTRAK

Nanocarrier termosensitif semakin digunakan untuk memberi masa dan pengeluaran ubat khusus dengan keracunan sistemik yang minimum. Terma yang mencetuskan pengeluaran ubat sering dikawal oleh lingkaran titisan, gangguan membran, dan mekanisma 'micellization'. Walau bagaimanapun, beberapa batasan termasuk pengeluaran ubat pramatang dan lambat, kestabilan yang rendah, dan ketidakcukupan bioavailabiliti pada sasaran kekal mencabar dalam kebanyakan nanocarrier yang menggunakan mekanisma sasaran ini.

Projek ini bertujuan untuk memperkenalkan satu sasaran mekanisma baru menggunakan nanocarriers polimer dengan fasa peralihan gel-cecair pada hipertermia/suhu ablasi terma. Peralihan fasa ini dapat menghasilkan kecacatan struktur dalam nanocarrier dan seterusnya memudahkan penyebaran ubat kepada alam sekitar. Selain itu, untuk penyebaran tepat bagi rantau yang panas ketika penilaian in vitro nanocarriers, termosensitif nanocarriers novelti telah dibangunkan.

Nanocarriers telah disintesis menggunakan lapisan nanopartikel mesoporous silika (MSNs) sebagai bekalan ubat dan dua formulasi polimer termasuk polyacrylamide (PPT) dan polyethylene glycol (PEG) sebagai pelindung nanocarries. Percantuman-daripada dan teknik cantuman-kepada masing-masing digunakan untuk menyediakan PAA-MSNs dan PEG-MSNs. Tindakan peralihan fasa serta pelbagai sifat-sifat kimia, morfologi, dan haba nanocarriers ini telah dicirikan dan muatan/pengeluaran ubat yang berpotensi telah dikaji menggunakan doxorubicin sebagai model hydrophilic ubat. Magnetik resonans yang berpandukan kepada fokus ultrabunyi (MRgFUS) juga bertindak sebagai tipikal modaliti haba untuk menilai kadar pengeluaran ubat dalam selang rawatan jangka pendek. Nanocarriers yang diperlukan untuk eksperimen MRgFUS dibangunkan menggunakan

pewarna termochromik dengan perilaku perubahan warna secara berbalik pada julat hipertermia atas. Pelbagai ciri fizikal, haba dan akustik nanocarriers diukur untuk memastikan kedudukan dekat pada tisu lembut manusia. Tindakan termosensitif nanocarriers ini dinilai oleh frekuensi radio (RF) dan eksperimen MRgFUS sebagai kaedah haba terpilih.

Analisis spektrofotometri nanocarriers menunjukkan suhu ambang 50±3°C dengan perbezaan 6°C di antara permulaan dan akhir suhu perubahan warna tersebut. Perubahan yang ketara pada pusat tumpuan semasa 'sonication' juga meningkatkan visualisasi terma lesi dalam imej magnetik resonans. Suhu peralihan awal PAA-MSNs dan PEG-MSNs masing-masing berada di sekitar 45.1±3.4°C dan 40.4±1.8°C. Suhu peralihan puncak PEG-MSNs juga 20°C lebih rendah daripada PAA-MSNs, mengakibatkan peralihan fasa yang lebih ketara. Pengukuran pengeluaran ubat PAA-MSNs menunjukkan kebocoran 11.5±2.4% dalam larutan akueus pada 37°C selepas 30 minit, nilai ini telah meningkat dengan ketara kepada 20.2±4.3% pada PEG-MSNs. Walau bagaimanapun, nisbah pengeluaran ubat maksimum dalam PEG-MSNs (68.2±3.7%) telah diperoleh pada suhu 50°C iaitu 10°C lebih rendah daripada PAA-MSNs (67.6±2.5% pada 60°C). Nisbah pengeluaran ubat daripada PEG-MSNs (45.5±3.1%) di bawah pendedahan MRgFUS juga jauh lebih tinggi daripada PAA-MSNs iaitu (39.2±2.2%).

Walaupun nisbah pengeluaran ubat pada suhu fisiologi adalah lebih tinggi dalam PED-MSNs, keluaran ubat maksimum dalam nanocarriers telah diperoleh dalam suhu lebih rendah berbanding dengan PAA-MSNs. Kedua-dua PAA-MSNs dan PEG-MSNs menunjukkan kecekapan muatan yang tinggi dan kadar pengeluaran ubat yang pesat pada suhu meningkat menyebabkan potensi untuk aplikasi sebagai adjuvan untuk kaedah terma.

ACKNOWLEDGMENTS

First and foremost, I would like to express my gratitude to Prof. Dr. Basri Johan Jeet Abdullah, Prof. Dr. Mohd Hamdi Abd Shukor, Prof. Dr. Noor Hayaty Abu Kasim, and Associate Prof. Dr. Hadijah Abdullah for their continuous supervision. This project could not be carried out without their unflagging support.

I extend my deepest appreciation and love to my family for their unfaltering patience, encouragement, and sacrifices to help me achieve my goals.

Special thanks to Dr. Reza Rahbari, Dr. Reza Mahmoodian, Dr. Mahdi Sparham, Dr. Sadjad Naderi, Dr. Bijan Rahmati, Dr. Emad Sadeghian Nejad, Dr. Mohammad Mehrali, and Dr. Mahdi Mehrali for their insightful and stimulating comments, which helped me to improve the quality of my research.

Finally yet importantly, I would like to show my regards to Prof. Dr. Rosnah Mohd Zain, Dr. Yeong Chai Hong, Dr. Anand Ramanathan, Dr. Priyadarshni Bindal, Dr. Saad A. Khan, Dr. Erum Zain, Ms. Nur Farha Abdul Halim, Dr. Mohamed Abdulmonem, Dr. Ahmed Madfa, Mrs. Chanthiriga Ramasindarum, Mrs. Helen Ng. Lee Ching, Eng. Hassan Ismail, Mr. Yus Hafizul, Mrs. Zarina Idris, all lectures, professors, officers, and staffs who spent their valuable time to provide logistic support needed for completion of this study.

Thank you.

TABLE OF CONTENTS

LIST OF FIGURES

LIST OF TABLES

LIST OF SYMBOLS AND ABBREVIATIONS

SYMBOLS:

B	:	Magnetic flux density
c	:	Speed of sound
C	:	specific heat capacity
C_b	:	Blood specific heat
Db*	:	Yellow/blue CIELAB value
DE*	:	Total colour difference
DL*	:	Darkness/lightness CIELAB value
E_m	:	Maximum drug encapsulation value
H	:	Magnetic field strength
P_{cav}	:	The (inertial) cavitation threshold
Q	:	Heat deposition in a medium by radiofrequency
t	:	Process time
T	:	Temperature
T_0	:	Room temperature
T1	:	Longitudinal relaxation time
T2	:	Transverse relaxation time
T_b	:	Blood temperature
T_C	:	Liposome phase transition temperature
T_{cog}	:	Coagulation temperature
T_{CP}	:	Clouding point
T_{ec}	:	Ending temperature of colouration
T_{ed}	:	Ending temperature of discolouration

T_{oc}	:	Onset temperature of colouration
T_{od}	:	Onset temperature of discolouration
W_b	:	Blood flow rate
α	:	Attenuation coefficient
ε'_r	:	Dielectric constant (real part of relative permittivity)
f	:	Frequency
κ	:	Thermal conductivity
ρ	:	Density
σ	:	Electrical conductivity

ABBREVIATIONS:

AA	:	Acrylamide
AFM	:	Atomic force microscopy
ANOVA	:	Analysis of variance
AMF	:	Alternating magnetic fields
AMSN	:	Activated mesoporous silica nanoparticles
APR	:	N-acryloyl pyrrolidine
APS	:	Ammonium persulphate
BSA	:	Bovine serum albumin
CAA	:	Citric acid anhydrate
CAM	:	Citric acid monohydrate
CG	:	Coil-globule
CMC	:	Critical micellar concentration
CMT	:	Critical micellar temperature
CST	:	Critical solution temperature
CTAB	:	Cetyltrimethyl ammonium bromide
DMAM	:	N,N-dimethyl acrylamide
DPPC	:	Dipalmitoyl phosphocholine
DSC	:	Differential Scanning Calorimetry
DSPC	:	Distearoyl phosphatidylcholine
DSPE	:	Distearoyl phosphatidyl ethanolamine
EPR	:	Enhanced permeability and retention
EW	:	Egg white
FT-IR	:	Fourier transform infrared spectroscopy

FUS	:	Focused ultrasound
GDL	:	D-glucono-δ-lactone
HIFU	:	High intensity focused ultrasound
HSPC	:	Hydrogenated soy phosphocholine
IPN	:	Interpenetrating polymer network
ISM	:	Industrial, scientific and medical
LCST	:	Lower critical solution temperature
LGTT	:	Lower gel transition temperature
LIT	:	Laser-induced thermal ablation
LMV	:	Large multilamellar vesicle
LTSL	:	Lysolipid-containing thermosensitive liposome
MD	:	Membrane disruption
MGC	:	Micelle gelation concentration
MI	:	Micellization
MPPC	:	Monopalmitoyl phosphocholine
MR	:	Magnetic resonance
MRgFUS	:	Magnetic resonance-guided focused ultrasound
MRI	:	Magnetic resonance imaging
MSN	:	Mesoporous silica nanoparticles
MSPC	:	Monostearoyl phosphatidylcholine
MW	:	Microvawe
NIPMAM	:	N-isopropyl methacrylamide
NIR	:	Near-infrared
NISAA	:	Non-ionic surface-active agent

ODA	:	Octadecyl acrylate
PA	:	Photo absorbance
PAA	:	Polyacrylamide
PAA-MSN	:	Polyacrylamide-coated mesoporous silica nanoparticles
PAC	:	Polyacrylic acid
PBO	:	Poly(1,2-butylene oxide)
PBS	:	Phosphate buffered saline
PE	:	Polyethylene
PEG	:	Polyethylene glycol
PEG-MSN	:	Polyethylene glycol-coated mesoporous silica nanoparticles
PEO	:	Polyethylene oxide
PLGA	:	Poly(lactic acid-co-glycolic acid)
PNIPAM	:	Poly(N-isopropyl acrylamide)
PPO	:	Polypropylene oxide
PRF	:	Pulse repetition frequency
PTSL	:	Polymer-modified thermosensitive liposome
PVA	:	Polyvinyl acetate
PVC	:	Polyvinyl chloride
REP	:	Reference phantom
RES	:	Reticuloendothelial system
RF	:	Radiofrequency
SAR	:	Specific absorption rate
SCT	:	Sodium citrate tribasic dehydrate
SEM	:	Scanning electron microscopy

SP	:	Superparamagnetic behaviour
SPR	:	Surface plasmon resonance
SUV	:	Small unilamellar vesicle
TCD	:	Thermochromic dye
TCP	:	The clouding point
TGA	:	Thermogravimetric analysis
TEM	:	Transmission electron microscopy
TEMED	:	N,N,N’,N'-tetramethyl ethylene-diamine
TEOS	:	Tetraethyl orthosilicate
TEVS	:	Triethoxy vinylsilane
TSL	:	Thermosensitive liposome
TSP	:	Thermosensitive phantom
TTSL	:	Traditional thermosensitive liposome
UCST	:	Upper critical solution temperature
UGTT	:	Upper gel transition temperature
UV-Vis	:	Ultraviolet-Visible spectroscopy
VMSN	:	Vinyl-modified MSNs

LIST OF APPENDICES

CHAPTER 1: INTRODUCTION

Targeted drug delivery systems with controllable period and rate of drug release have received increasing attention in pharmaceutical science. In such drug delivery systems, the diagnostic or therapeutic agents are navigated through the body by means of "smart" nanocarriers which can intelligently target the diseased site and unload their content with controllable rates (Lien et al., 2008). An ideal nanocarrier should eliminate the incomplete kill zone by precise delineation of the boundaries between the affected region and surrounding tissues (Gilstrap et al., 2011).

The time and site-specific drug release with minimized off-site effects is often achieved using nanocarriers which respond to a specific stimulus, acting in the target. A number of stimuli including heat, light, electricity, magnetic field, pH, redox microenvironment, or ultrasound could be employed for the purpose of localized drug delivery. These stimuli generally induce chemical, physical, or structural changes in the delivery system and thus facilitate drug diffusion into the surrounding medium. In particular, when stimuli are specific to the disease pathology, the nanocarriers become active rather than passive participants and respond uniquely to the pathological triggers, resulting in improved efficacy of their therapeutic potential (Ganta et al., 2008).

Temperature is among the most effective triggering stimuli which has been extensively employed to exert the synergistic effect of hyperthermia and pharmacotherapy (Ganta et al., 2008). Temperature-based drug delivery method generally relies on thermosensitive nanocarriers which transfer their cargo through the body and release in a region specifically heated above the physiological temperature (Tang et al., 2011). Encapsulation of therapeutic agents such as chemotherapeutics in thermosensitive

nanocarriers could effectively decrease their systemic toxicity and prolong their circulation time (Maya et al., 2013; Parodi et al., 2013).

Thermal sensitivity is usually governed by a sudden alteration of at least one property of the nanocarriers against temperature, triggering sufficient drug dosages immediately in the diseased region. Ideally, thermosensitive nanocarriers must preserve their payload at physiological temperature and quickly discharge it into a locally heated region to counteract rapid clearance by the bloodstream (Gil et al., 2004).

Thermosensitive nanocarriers can be fabricated using various inorganic and organic compounds including polymers, lipids, self-assembling micelles, metals, and carbon-based nanostructures (Gilstrap et al., 2011). The materials required for fabrication of nanocarriers are mostly selected according to the diagnostic or therapeutic objective, payload characteristics, heating mechanism, applied temperature range, material biocompatibility, and the administration method (Ganta et al., 2008). These materials exhibit different mechanisms of thermal-sensitivity which could significantly influence the efficacy of nanocarriers during hyperthermia and thermal ablation procedures (Gilstrap et al., 2011). A number of parameters including the temperature, rate, and intensity of response to the external heat source could drastically influence the success of these triggering mechanisms. Therefore, understanding the mechanisms of thermal-triggered drug release and their underlying parameters in different smart materials is important in order to design appropriate nanocarriers which could be effectively combined with various thermal modalities in clinical setting.

1.1 Research Background

Drug release from thermosensitive nanocarriers mostly relies on mechanisms such as membrane disruption, coil-globule transition, and micellization. For instance, drug release from lysolipid-containing thermosensitive liposomes occurs by dissociation of lipid membrane and formation of stabilized defects at temperatures ranging between 39°C to 42°C, resulting in the preferred routes for rapid discharge of the entrapped drug (Gasselhuber et al., 2012b; Needham et al., 2013; Ta et al., 2013).

The coil-globule transition is mostly seen in polymers with lower critical solution temperature (LCST) (Deshmukh et al., 2014; Ruiz et al., 2007; Scherzinger et al., 2014; Ward et al., 2011; Yan et al., 2011; Yang et al., 2011). The increased hydrophobicity of these polymers upon a slight heating above their LCST results in a conformational transition from swollen coils to collapsed globules which in turn provides mechanical pressure to squeeze the encapsulated drug outwards (Bekhradnia et al., 2014; Li et al., 2013c).

Triblock copolymers such as poloxamers (e.g. polyethylene oxide-polypropylene oxide-polyethylene oxide (PEO-PPO-PEO)) are typical examples of thermosensitive materials which exhibit micellization mechanism (Chen et al., 2007; Chiappetta et al., 2007; Yapar et al., 2013). At micellar volumetric fractions above a specific threshold, these micelles entangle together upon heating and undergo three-dimensional and crystal-like packing, producing a hydrogel network (Yapar et al., 2013). When heating is continued, phase separation and clouding due to the dissociation of the stiff gel network favours the release of entrapped drug.

Recently, a novel mechanism of drug release using thermosensitive capping agents have been proposed. In this mechanism, a porous matrix (e.g. mesoporous silica nanoparticles) is blocked by capping agents such as double helix DNA (Derfus et al., 2007; Ruiz Hernandez et al., 2011), or pseudorotaxane-based nanovalves (Thomas et al., 2010), which rapidly dissociate in the hyperthermia temperature range and allow an "on-off" drug release from the porous structure. The porous nanocore provides a high loading capacity as well as sufficient mechanical and chemical stabilities in the physiological environment.

The aim of all these thermosensitive systems is to increase the dosage of available therapeutic drugs at the affected region with minimal negative influence on the surrounding tissues. Although these drug delivery systems have shown promising in vitro and in vivo efficacies, several shortcomings must be overcome prior their actual application in treatment of human diseases. Therefore, most of these thermosensitive nanocarriers are currently undergoing clinical trials in different phases against various types of malignant cells and few formulations have been approved for clinical application.

1.2 Problem Statement

Although various mechanisms of thermal sensitivity for controlled drug release have been suggested, a number of limitations such as undesired drug release at body temperature, slow drug release rate at target tissue, low stability and desorption in physiological environment, and low bioavailability of the encapsulated drug remain challenging in most thermosensitive nanocarriers which rely on these triggering mechanisms. For instance, although some thermosensitive liposomal formulations have

undergone pharmaceutical development and commercialization (e.g. ThermoDOX®), their functionality has been mostly examined in environments free of biomolecules and plasma proteins that may cause rapid lipid desorption. A number of studies have reported the rapid desorption of lysolipids from thermosensitive liposomes when administrated in vivo, resulting in hampered thermal sensitivity and premature drug leakage at physiological temperature (Banno et al., 2010; Chiu et al., 2005; De Smet et al., 2010; Ta et al., 2010). Some evidences also indicated that lysolipids might dissociate from liposomes upon dilution (Chiu et al., 2005). A low efficacy of drug encapsulation is another limitation of thermosensitive liposomes which may provide insufficient drug dosage for an effective tumour treatment (Ta et al., 2013; Xing et al., 2011).

In phase-transitional polymers which exhibit coil-globule mechanism, a relatively low mechanical strength is among the primary concerns which hinders their in vivo application (Bekhradnia et al., 2014). Although fabrication of these nanostructures in core-shell form could increase their mechanical stability, collapse of the polymer shell at temperatures above LCST may suppress the drug penetration outward from the reservoir core (Yang et al., 2008).

The clinical efficacy of thermosensitive micelles is also limited due to a number of limitations such as inconsistency of phase transition temperature and insufficient stability in physiological media. For instance, the transition temperature of poloxamers is highly dependent on their concentration in aqueous solutions. Therefore, when used in vivo, these triblock copolymers fail to exhibit a similar transition temperature to that observed in in vitro experiments. Moreover, poloxamers may not remain stable for more than several hours in bloodstream and thereby, long-term delivery of these compounds continues to be a challenge (Jeong et al., 2002).

In thermosensitive nanocarriers which employ capping agents, considerable drug release at physiological temperature is the crucial challenge which results in relatively high systemic toxicities and low therapeutic dosages available in the target. For instance, in vitro drug release ratios above 30% were observed in DNA-capped mesoporous silica nanoparticles incubated at 37°C for 15 minutes (Ruiz Hernandez et al., 2011).

The current research is an attempt to develop a new mechanism of drug release in order to address some of the above-mentioned limitations such as insufficient loading capacity, low mechanical stability, and high ratios of drug release at body temperature. Nanocarriers were synthesized in core-shell nanostructure using a porous drug reservoir and polymeric shells with melting temperatures within the hyperthermia and thermal ablation range. It is assumed that the thermal energy generated by hyperthermia modalities could rapidly dissociate the protective shell and facilitate drug release from the porous core into the surrounding environment. The onset melting temperature of the polymer layer must be sufficiently above physiological temperature and below the upper limit of therapeutic thermal ablation range to obtain minimized drug release ratio in healthy tissues and consequently, lower systemic toxicity. To the best of our knowledge, this study is the first attempt to produce thermosensitive nanocarriers based on the melting temperature of the encapsulating shell.

Similar to any novel diagnostic or therapeutic option, the developed thermosensitive nanocarriers require in vitro assessment and verification in terms of their efficacy and shortcomings prior examination in in vivo models. The ideal medium for in vitro investigation of these drug delivery systems is the real tissue of clinical interest which presents the closest approximation to the clinical practice. However, due to the substantial complications in supply and maintenance of the real tissues as well as difficulties in

standardization of the obtained results, thermosensitive phantoms with similar properties to target tissues are often utilized for these high-temperature studies. A multitude of formulations has been proposed to prepare thermosensitive phantoms. However, the majority of these formulations suffer from inaccurate estimation of the thermal profile during exposure to various thermal modalities.

In the present study, a new thermosensitive phantom containing a thermochromic dye for hyperthermia and thermal ablation studies were formulated to provide a reversible thermal-sensitivity behaviour with a more accurate threshold temperature compared to that of currently-used thermosensitive agents.

1.3 Research Aim and Objectives

The current research aims to utilize a combination of hyperthermia and thermosensitive nanocarriers for rapid release of therapeutic drugs with sufficient dosages in a locally heated region. Therefore, the following are the research objectives:

1. To fabricate a thermosensitive tissue-mimicking phantom as a platform for in vitro studies of the thermosensitive nanocarriers.
2. To prepare a polyacrylamide-mesoporous silica (PAA-MSN) nanoparticle and characterize their thermal and drug release behaviours for hyperthermia application.
3. To prepare a polyethylene glycol-mesoporous silica (PEG-MSN) nanoparticles and characterize their thermal and drug release behaviours for hyperthermia application.

1.4 Contribution of Research

In this research, the thermal sensitivity behaviour in nanocarriers of therapeutic drugs were simplified using low-melting-point materials. This new mechanism of thermal sensitivity could open a wide area of research to develop a variety of thermosensitive carriers with tailored properties and more precise thermal responses (e.g. sharper and faster phase transitions) using different low-melting-point materials. In comparison to other mechanisms of thermal sensitivity, the suggested mechanism allows selection of a broader range of materials with diverse properties for synthesis and development of thermosensitive nanocarriers. The immediate outcome and contribution of this research to the world of knowledge comprises two research articles and a review paper published in scientific journals.

In this work, we also introduced a novel thermosensitive phantom which could be used for visualization of the temperature distribution during heating and cooling processes, evaluation of the heating and cooling rates, acoustic and electromagnetic dosimetry, and calibration of thermal devices. A low preparation cost due to a little amount of required thermosensitive agent as well as their ability to be fabricated at flexible temperatures, makes these phantoms prominent for various thermal applications. The outcome of this part of research have been published in two review and research publications.

1.5 Research Motivation

Crucial limitations of the current thermosensitive drug delivery systems provided an inspiration to develop a new mechanism of thermal sensitivity in smart nanocarriers using

core-shell nanostructures with low-melting-point polymer nanoshells. It was assumed that the gel-liquid phase transition of the polymer nanoshell at increased temperatures could facilitate penetration of the therapeutic drug encapsulated inside these nanostructures. This new mechanism of thermal sensitivity could address a number of existing limitations such as low mechanical stability, insufficient loading capacity, and undesired drug release at physiological temperature, opening a wide research area for more effective delivery of various diagnostic and therapeutic agents using nanocarriers with tailored properties.

1.6 Research Scope

The present research aims to integrate the materials science, biomedical engineering, and pharmaceutical science in order to develop nanocarriers with fast response to various non-invasive thermal modalities. However, prior characterization of these drug carriers, a thermosensitive tissue-mimicking phantom with customized properties needs to be produced for conducting the required in vitro studies. This phantom was fabricated by a facile and reproducible technique which allows a mass production in laboratories for calibration, analytical, and experimental purposes. Moreover, various acoustic and thermal properties of the phantom were quantified and their potential in representation of the thermal lesion was examined using radiofrequency (RF) and magnetic resonance-guided focused ultrasound (MRgFUS) modalities. However, the optical and electrical properties of this phantom formulation were not measured in the current research.

In order to synthesize the smart nanocarriers, two different polymers were employed. Various chemical, morphological and thermal properties as well as the carrier/drug relationship were examined to understand the drug release behaviour when these

nanocarriers are exposed to the heat gradients. The nanocarriers were also sonicated using MRgFUS modality to evaluate the drug release rates in short-term intervals. However, the cytotoxicity tests, in vitro examination in simulated body fluids, and in vivo studies fall beyond the scope of this project and may be performed in further research.

1.7 Thesis Structure

In the current chapter, a brief introduction of the project concept was presented and the current challenges addressed in this research were explicated. Based on the existing limitations, the research objectives were clarified and the scope of this study was outlined. In Chapter 2, a comprehensive background into various triggering mechanisms of thermosensitive materials under hyperthermia condition is presented. This chapter also covers a detailed review of various thermal phantoms, synthesis techniques, and recommended applications. Chapter 3 primarily concerns the first research objective in fabrication and characterization of the thermosensitive tissue-mimicking phantom and investigation of their thermosensitive behaviour under hyperthermia condition. In chapter 4, the proof-of-concept study (objective 2) using polyacrylamide nanoshells is carried out to evaluate the potential of the new triggering mechanism for effective drug release at high temperature regimens. The third objective is addressed in chapter 5, which presents the synthesis, characterization, and in vitro examination of the mesoporous silica nanoparticles coated by polyethylene glycol nanoshells. Chapter 6 finally concludes the obtained results and provides recommendations for potential areas of research in further studies. The flow of the various project activities is summarized in Figure 1.1.

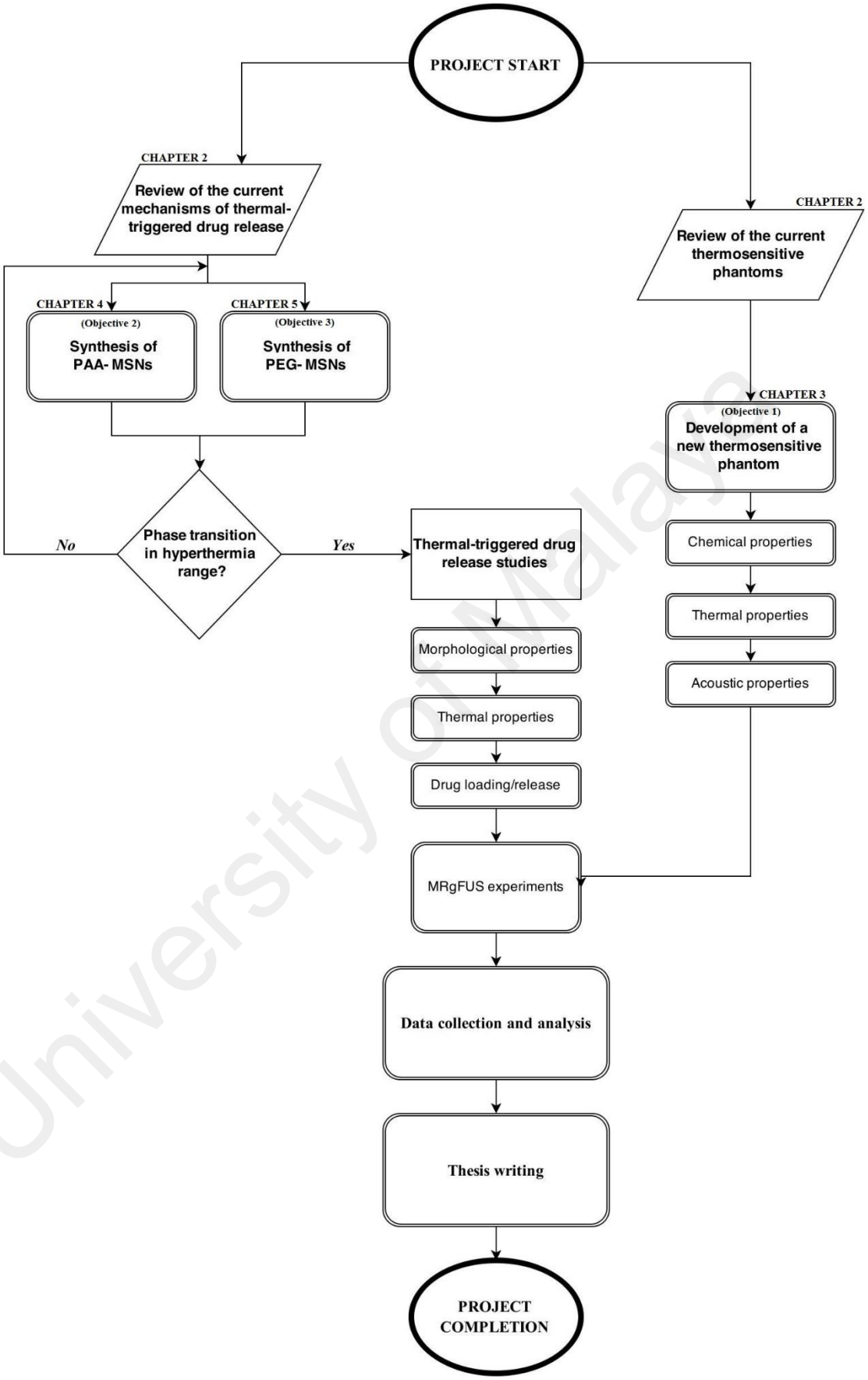

Figure 1.1: A schematic of the activities carried out in the current research.

CHAPTER 2: LITERATURE REVIEW

2.1 Triggering Mechanisms of Thermosensitive Nanoparticles

Nanoparticle-based drug delivery is an innovative method which has been employed to achieve reduced systemic toxicity, improved drug retention in circulation, and increased intratumoural drug accumulation via the enhanced permeability and retention (EPR) effect (Li et al., 2013a). However, the structure heterogeneity of tumour vasculature inflicts an irregular drug extravasation within the affected region (Jain et al., 2010; Vaupel et al., 2010). Moreover, due to the complexity of interstitial tumour matrix as well as the limited interstitial fluid flow, diffusion of nanoparticles in the extravascular extracellular space remains challenging (Chrastina et al., 2011). The intratumoural nanoparticle accumulation could be enhanced by employing mild hyperthermia as an adjunctive therapy to increase the perfusion and permeability in tumour vasculature (Hervault et al., 2014; Vaupel et al., 2010). Furthermore, increased permeability of cell membrane, inhibition of DNA-repair, and higher rates of cytotoxic chemical reactions at elevated temperatures could lead to an enhanced cytotoxicity of antineoplastic agents under hyperthermia condition (Issels, 2008; May et al., 2013).

The efficacy of nanoparticle-based hyperthermia could further be improved using thermosensitive nanocarriers of chemotherapeutic agents (Li et al., 2008). The thermosensitive nanocarriers should ideally preserve their cargo at physiological temperature and quickly release it into a locally heated tumour to counteract rapid clearance by bloodstream (Mura et al., 2013). These carriers can be fabricated using a diversity of organic and inorganic compounds including biocompatible polymers (Gong et al., 2013; Qiu et al., 2001; Ward et al., 2011), lipids (Dicheva et al., 2014; Kneidl et

al., 2014; Ta et al., 2013), self-assembling amphiphilic micelles (Croy et al., 2006; Kedar et al., 2010; Talelli et al., 2011). Thermosensitive nanostructures may also be made using metallic (Cherukuri et al., 2010; Huff et al., 2007; Kumar et al., 2011; Lee et al., 2011; Sharifi et al., 2012), or carbon-based compounds (Iancu et al., 2011; Klingeler et al., 2008; Singh et al., 2013) which directly act as therapeutic adjuvants, rather than carrying other therapeutics, through enhancing the heat deposition rate within the affected region. Thermal sensitivity is often determined by a sharp nonlinear alteration in at least one characteristic of these materials during the temperature change. The onset and ending temperatures, rate, and intensity of this property change could significantly influence the efficacy of thermosensitive nanostructures under hyperthermia condition.

The current section provides a comprehensive review of the most widely observed triggering mechanisms of thermosensitive nanoparticles and outline their main features and shortcomings. Several mechanisms of thermal sensitivity such as coil-globule, membrane disruption, and micellization transitions are generally applied for thermal-triggered drug release; whereas, enhanced heat generation under hyperthermia modalities is often obtained by employing materials with superparamagnetic behaviour, or photo-absorbing ability. Recently, fabrication of hybrid nanostructures has allowed simultaneous application of both drug and heat triggering mechanisms for a faster drug delivery and improved hyperthermia condition. It is noteworthy that a number of other mechanisms have recently shown potential for application in nanoparticle-based hyperthermia systems. However, the focus of this review is only on the mechanisms which their efficacy has successfully been established through extensive in vitro and in vivo studies. Understanding the substantial parameters that influence these triggering

mechanisms could aid in selection of appropriate thermosensitive nanostructures and thermal modalities according to the specific experimental and clinical condition.

2.1.1 Coil-globule Phase Transition

Coil-globule phase transition of the thermosensitive polymers has recently found increasing interest for effective release of therapeutics under hyperthermia condition. The unique characteristic of thermosensitive polymers is their discontinuous water-solubility change at a specific temperature referred to as the critical solution temperature (CST). In the concentration–temperature phase diagrams, CST is a temperature where both coil-shaped soluble polymer chains and insoluble polymer globules are present in the aqueous medium (Okada et al., 2005; Schmaljohann, 2006; Seuring et al., 2012; Yamauchi et al., 2007).

CST could generally be categorized into lower critical solution temperature (LCST) and upper critical solution temperature (UCST). LCST is considered as the minimum temperature in the concentration–temperature phase diagram where the phase separation occurs in the polymer solutions (Wu et al., 2011; Zarzyka et al., 2014). UCST by contrast is the maximum temperature in the phase diagram where the polymer solution changes from phase-separated to a single-phased solution (Wu et al., 2011; Yin et al., 2014). The phase separation due to the temperature changes is often accompanied by a discontinuous volumetric collapse of the polymer network in aqueous solution. Therefore, the phase transition at elevated temperatures results in negative and positive temperature-dependent

volumetric changes in LCST and UCST polymers, respectively. The volumetric ratio between the swollen and collapsed states is often less than tenfold (Annaka et al., 1992).

2.1.1.1 Mechanisms of Coil-Globule Phase Transition

The coil-globule phase transition in thermosensitive polymers is governed by the balance between repulsive and attractive electrostatic forces that respectively favour the polymer swelling and collapse behaviour (Polotsky et al., 2013). According to the mean field theory, discontinuity of the volumetric phase transition is controlled by the ionization degree as well as the persistence length of the polymer chains. In general, increased ionization or stiffness of the polymer chains leads to a discontinuous transition and higher volumetric changes. The volumetric changes above tenfold could be resulted in the polymer network by increasing the swelling pressure via polymer ionization. Therefore, the polar solvents (e.g. aqueous solution) play an important role in obtaining a discontinuous volumetric phase transition in thermosensitive polymers. Although, the organic solutions may also provide discontinuous volumetric phase transition when the polymer chains are highly ionized (Annaka et al., 1992). The electrostatic forces needed for the coil-globule phase transition in aqueous solutions of thermosensitive polymers are often produced by hydrophobic and cooperative hydrogen bonding interactions (Deshmukh et al., 2014; Ilmain et al., 1991; Scherzinger et al., 2014; Yang et al., 2013). The other intermolecular forces such as Van-der-Waals and attractive ionic interactions are not considered as crucial forces in coil-globule phase transition of thermosensitive polymers (Ilmain et al., 1991).

(a) Hydrophobic Interaction

The presence of moderately hydrophobic groups (which allow partial dissolution in aqueous medium) such as methyl, ethyl, or propyl is a common characteristic of LCST polymers. At temperatures below LCST, water molecules near the hydrophobic polymer coils form highly ordered structures, called ice-bergs, via an exothermic and spontaneous hydrogen bonding process which decreases both enthalpy and entropy of the mixture. Although the energy of this hydrophobic interaction is about few kcal.M^{-1}, it could significantly stabilize the polymer configuration (Shibayama et al., 1993). At temperatures above LCST, the water molecules leak out from the polymer due to the breakage of hydrogen bonds, resulting in coil-globule phase transition accompanied by precipitation of the polymer (Figure 2.1) (Li et al., 2013c).

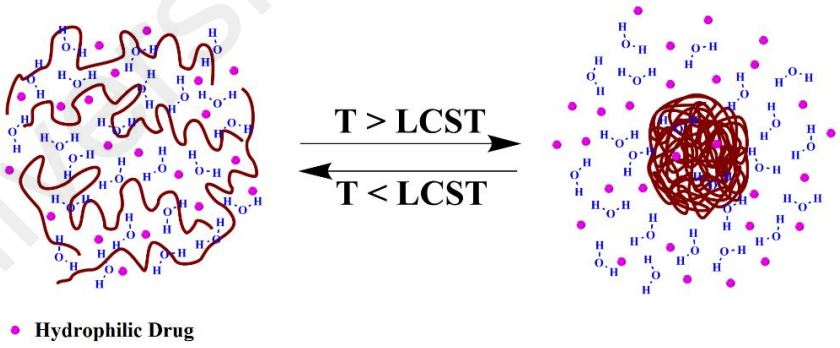

Figure 2.1: A schematic of the coil-globule transition in LCST polymers due to the hydrophobic effect. Collapse of the polymer chains provides a compressive force, leading to leakage of the aqueous solution out of the globule structure.

From the thermodynamics perspective, the LCST and UCST phase transitions due to the hydrophobic interaction are respectively controlled by entropy and enthalpy balances. At LCST, the entropic gain from the release of hydrogen-bonded aqueous molecules becomes higher than entropy loss because of polymer collapse, resulting in increased overall entropy (Pennadam et al., 2004; Shibayama et al., 1993; Ta et al., 2013). Moreover, the entropic gain of the whole system becomes more significant compared to the enthalpic contribution of hydrogen bonds between aqueous molecules and the polymer chain (Pennadam et al., 2004; Ta et al., 2013). UCST by contrast is a temperature at which the enthalpic effect because of the ordered state of aqueous molecules around the polymer chains becomes less than the entropy loss (Ta et al., 2013; Ward et al., 2011).

(b) Cooperative Hydrogen Bonding

A positive temperature-dependent volumetric phase transition (swelling at UCST system) via the cooperative hydrogen bonding interaction is mostly observed in interpenetrating polymer networks (IPNs) comprised of two independent networks intermingled but not chemically bonded to each other (Ilmain et al., 1991; Shibayama et al., 1993). At temperatures below UCST, the formation of intermolecular hydrogen bonds between the interpenetrating chains results in the formation of continuous ladder-like complexes that probably cause water-insolubility and volumetric shrinkage. However, the temperature rise presumably initiates the dissociation of the hydrogen bonds, allowing expansion of the polymer complex (Figure 2.2) (Katono et al., 1991). Dissociation of the initial hydration bonds between the interpenetrating complex units also promotes the

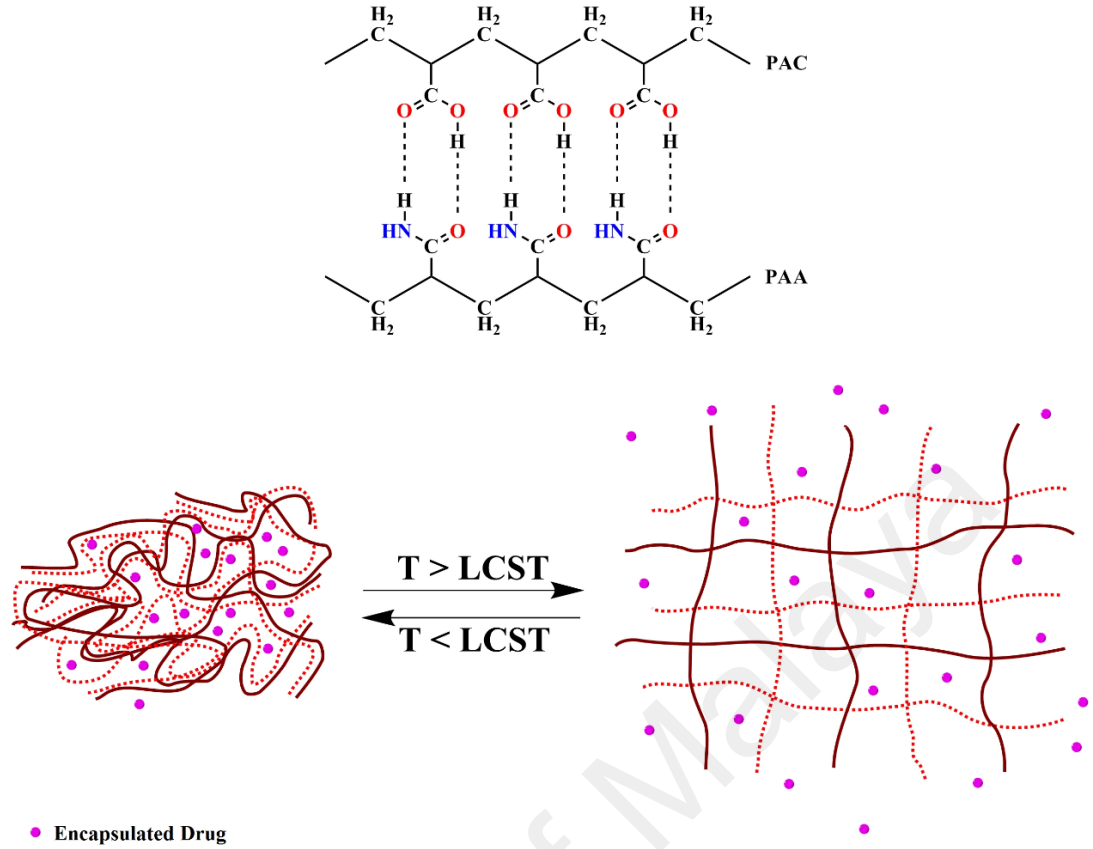

Figure 2.2: A schematic of a) hydrogen bonding between polyacrylic acid (PAC) and polyacrylamide (PAA) chains; b) positive temperature-dependent volumetric phase transition in UCST system via cooperative hydrogen bonding interaction.

cooperative breakage of contiguous complexes (zipper effect), leading to free solubilization of the interpenetrating chains and a drastic volumetric expansion at higher temperatures (Katono et al., 1991).

Helix-coil transition, which is mostly observed in random gel networks (e.g. gelatine), is another example of an intermolecular association by hydrogen bonding. In this mechanism, two or more polymer chains generate a helix conformation at low temperatures that forms physical junctions in the gel network. However, in spite of

obtaining a positive temperature-dependent volumetric change in both IPNs and random gels, a sigmoidal transition above a specific transition temperature range is only observed in IPNs. On the contrary, the random gels undergo a relatively simple, exponential swelling during heating. The difference in the swelling mechanisms of IPNs and random gels with similar compositions is proposed to result from the continuity of the hydrogen bonds between the interpenetrating chains of IPNs which cause zipper effect. In the random gels, due to the relative isolation and discontinuity of complex units, independent dissociation of complexes within the gel matrix may not induce the zipper effect (Katono et al., 1991).

2.1.1.2 Current Challenges and Future perspective

Although the coil-globule phase transition is among the mostly studied triggering mechanisms, the materials which show this thermosensitive behaviour have not achieved clinical application due to a number of intrinsic disadvantages (Patenaude et al., 2012). Most of the polymers which exhibit coil-globule transition possess dubious biocompatibility and biodegradation (Patenaude et al., 2012). Moreover, the transition temperatures of these polymers are often not initially appropriate for hyperthermia application and need be modified via copolymerization with other hydrophilic or hydrophobic comonomers to alter their hydrophobic-hydrophilic balance. In general, the hydrophobic moieties decrease the LCST, while the hydrophilic comonomers result in an opposite effect. For instance, the phase transition temperature of poly(N-isopropyl acrylamide) (PNIPAM) could be increased from 32°C to above 37°C by copolymerization with hydrophilic moieties such as ethylene glycol (Gan et al., 2002),

acrylamide (Shen et al., 2006; Xie et al., 2007), dimethyl acrylamide (Shen et al., 2006), and acrylic acid (Zhang et al., 2007). However, the excessive ratios of hydrophilic moieties could divide the continuous PNIPAM chains into short segments and hamper their hydrophobic aggregation forces (Kaneko et al., 1998).

The phase transition of the thermosensitive polymers mostly occurs in a temperature range rather than specific temperature values and their transition temperatures are thus referred to as "cloud points" in some literature (Roy et al., 2013). The presence of a hysteresis between the heating and the cooling curves results in two intermediate states, giving four states with thermodynamic stability including: coil, crumpled coil, molten globule, and globule (Wang et al., 1999). The nature and molar concentration of the comonomers (Kujawa et al., 2006), presence of co-solvents or additives (Lutz et al., 2006), and solvent quality could also affect the phase transition temperature (Lien et al., 2008). For instance, substitution of water with deuterated water results in a 1-2°C increase in the LCST of PNIPAM (Wang et al., 1999).

The insufficient mechanical stability of polymeric nanocarriers under load-bearing conditions is another limitation which may impede their clinical application. These materials could undergo deterioration during peristaltic movements in the gastrointestinal tractus, or because of exposure to the interstitial or intramuscular shear forces (Bekhradnia et al., 2014). Therefore, clinical application of these nanocarriers requires long-term cytotoxicity investigation and sufficient control of their phase transition temperature range, mechanical strength, collapse intensity, and surface properties (Bekhradnia et al., 2014; Roy et al., 2013).

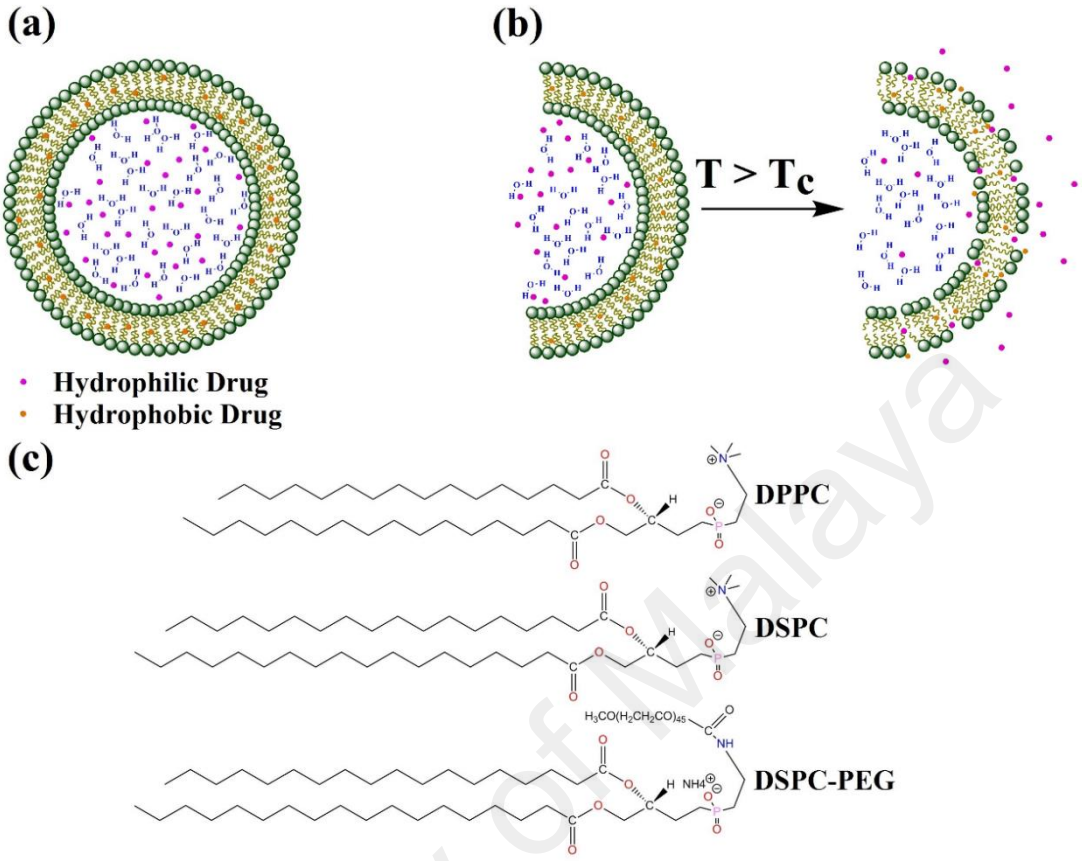

Figure 2.3: a) A two-dimensional schema, representing the typical structure of a TTSL; b) thermal-triggered phase transition of TTSLs. Increased bilayer fluidity at temperatures above Tc results in drug release; and c) chemical structures of the lipid chains used in fabrication of TTSLs.

2.1.2 Membrane Disruption

Drug release by dissociation of the nanocarriers at hyperthermia temperature range is a triggering mechanism which is mostly observed in thermosensitive liposomes. Liposomes are spherical vesicles consisted of aqueous interior cores surrounded by lipid

bilayer shells (Figure 2.3a) which form by self-assembly of amphiphilic lipids in aqueous solutions (Torchilin, 2005).

The enhanced delivery of anticancer drugs into tumour tissue using thermosensitive liposomes (TSLs) and hyperthermia was firstly reported in 1978 (Yatvin et al., 1978). Afterwards, various lipid formulations have been examined to generate TSLs with improved stability and triggering behaviour. The biocompatibility, sharp phase transition, rapid and concentration-free response, high loading capacity, mechanical Strength, and tuneable physical properties make these nanostructures prominent for hyperthermia application.

2.1.2.1 Triggering Mechanisms in Thermosensitive Liposomes

The current TSL formulations could be organized into five categories including traditional thermosensitive liposomes (TTSLs), lysolipid-containing thermosensitive liposomes (LTSLs), polymer-modified thermosensitive liposomes (PTSLs), magneto-liposomes, and bubble-generating thermosensitive liposomes, which are briefly reviewed in the following.

(a) Traditional Thermosensitive Liposomes (TTSLs)

The thermosensitive triggering potential of TTSLs is mainly relied on their structural transition from the gel state to a crystalline-phased liquid when heated above a specific temperature (T_C) (Koning et al., 2010; Lindner et al., 2004; Needham et al., 2001;

Needham et al., 2013). The initial TTSL formulations were generally comprised of dipalmitoyl phosphocholine (DPPC), a saturated fatty acid with 16-carbon chains, and a T_C around 41°C. In general, saturated fatty acids with longer alkyl chains exhibit higher T_C range (Landon et al., 2011). Therefore, TTSLs with higher T_C ranges could be obtained by incorporation of longer saturated lipids such as distearoyl phosphatidylcholine (DSPC) with 18-carbon chains and T_C of 54°C into the initial formulation (Yatvin et al., 1978).

Lipid membranes of TTSLs are condensed and ordered in the gel phase with highly extended hydrocarbon chains, constrained to the two-dimensional membrane sheets. When the lipid membranes are heated, the mobility of lipid head groups is gradually increased and at temperatures around T_C, a trans-to-gauche alteration occurs in the alignment of the C-C bonds in the hydrocarbon chains. The lipids at these interfaces often exhibit mismatches in molecular packing and hydrophobic conformation, as well as highly permeable membranes. Although at temperatures above T_C the bilayer is completely molten, but individual lipid molecules remain confined to the two-dimensional membrane sheets with more free and rapid movement within these sheets, making the membrane highly permeable and fluidized. Therefore, the encapsulated drugs could easily diffuse out of the structure due to the formation of preferred routes in the membrane (Figure 2.3b) (Ta et al., 2013). Formation of the permeable bilayer at T_C is often determined by irregular increase of ion mobility across the membrane (Hays et al., 2001).

During the synthesis process, rehydration of the dry lipid sheets at temperatures above T_C generates large multilamellar vesicles (LMVs) followed by small unilamellar vesicles (SUVs). When the liposomes are cooled again to temperatures near T_C, the solid domains

with different orientations are nucleated within the molten membrane. Eventually by completion of the transition, the solidified domains with different orientations create grain boundaries in the membrane (Landon et al., 2011), resulting in planar defects within the physical structure of lipid bilayers. Therefore, the lipid membranes possess a faceted and granular structure rather than homogeneous sheets with perfect arrangement. Moreover, the grain boundaries within the liposome membrane are the preferred regions for formation of molten domains during heating and thus, their presence increases the membrane permeability during the phase transition (Ta et al., 2013).

Although TTSLs show enhanced drug release at mild hyperthermia range, but they could not provide a sufficient quantity and rate of drug release. Therefore, these TTSLs are often modified by incorporating other lipids such as distearoyl phosphocholine (DSPC) (Nibu et al., 1995) or hydrogenated soy phosphocholine (HSPC) (Gaber et al., 1995) in order to increase the packing mismatch and thus obtain higher permeability (Figure 2.3c). However, incorporation of lipids with longer alkyl chains into the DPPC-based liposomes may cause increased T_C and broader transition intervals.

The TTSL formulations often need be given stealth properties by a biodegradable layer of polyethylene glycol (PEG) (Li et al., 2013b; Li et al., 2010), polysaccharides (Turner et al., 2012; Wang et al., 2010), polyoxazolines (Woodle et al., 1994; Zalipsky et al., 1996), N-substituted acrylamides (Yamazaki et al., 1999), Polyhydroxyethyl L-glutamine (Romberg et al., 2005), polyhydroxyethyl L-asparagine (Romberg et al., 2007a), or amino acids (Romberg et al., 2008; Romberg et al., 2007b) to decrease their aggregation susceptibility and clearance by reticuloendothelial system (RES). For example, protection of TTSLs by PEG could result in a tenfold increase of drug concentration in tumours due

to their prolonged presence in bloodstream (Lasic et al., 1995). However, incorporation of PEG as well as cholesterol (used to improve serum stability) to the DPPC/HSPC liposomes could negatively influence the thermal sensitivity of these formulations (Gaber et al., 1995).

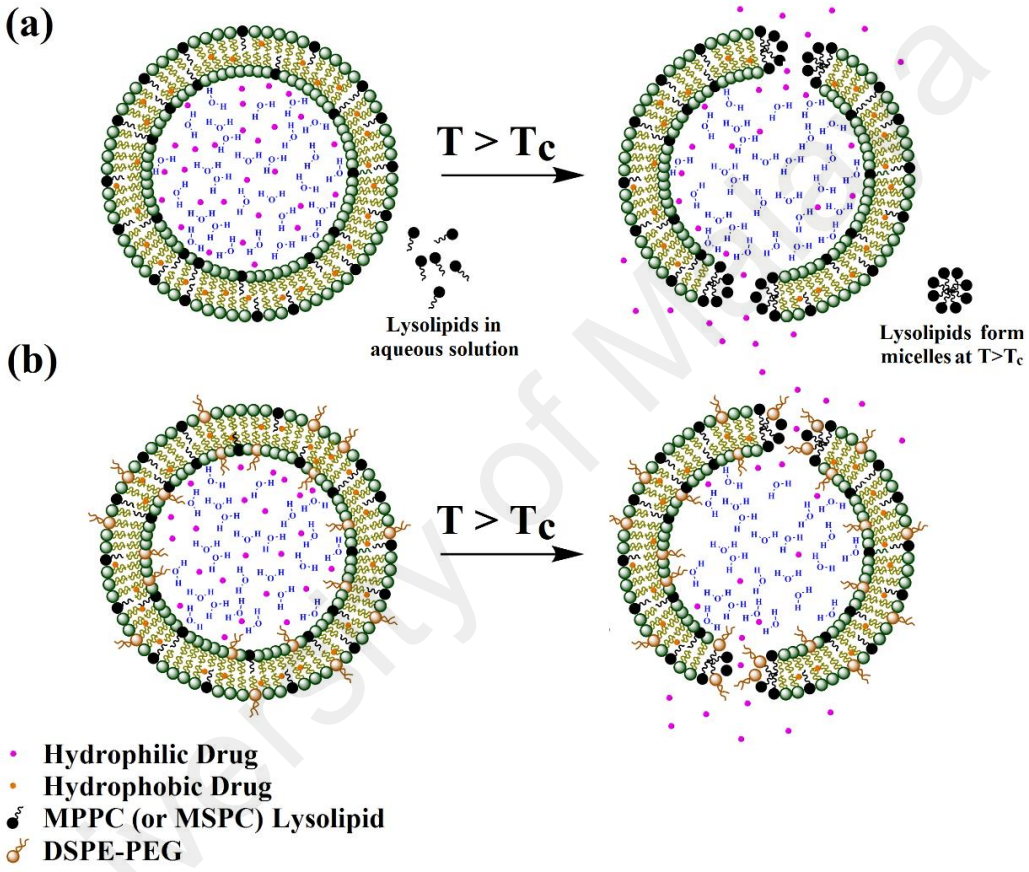

Figure 2.4: A schematic of the defect formation mechanism in TSLs due to the incorporation of a) lysolipid, and b) lysolipid with DSPE-PEG. Formation of micelles at threshold temperature results in enhanced permeability of the lipid bilayer. The addition of DSPE-PEG also improves the stability of pores produced within the lipid bilayer.

(b) Lysolipid-Containing Thermosensitive Liposomes (LTSLs)

Sharp phase transition (i.e. a burst release) is a crucial parameter for delivering effective and lethal dose of encapsulated drug as well as avoiding the occurrence of multidrug resistance in malignant tissue (De Smet et al., 2011). One prominent approach for obtaining a sharp phase transition in TSL formulations is to entrap lysolipids (lipids with only one acyl chain) such as monopalmitoyl phosphocholine (MPPC) or monostearoyl phosphatidylcholine (MSPC) into the TTSL membranes, which results in decreased T_C and improved drug release rate. For instance, presence of 10% MPPC in the membrane results in an approximately 50% faster drug release at 42°C and reduction of T_C from 43°C to 39–40°C (Anyarambhatla et al., 1999; Needham et al., 2000).

The improved triggering behaviour in LTSL formulations is generally relied on generation of nanopores and defects in the lipid bilayer at temperatures near T_C due to the lysolipid micellization and dissolution, respectively (Figure 2.4a) (Landon et al., 2011). Lysolipids are generally composed of a single hydrocarbon chain and a relatively large head group with a positive intrinsic charge, which form micelles when dispersed in a solution (Ta et al., 2013). During membrane melting at temperatures around T_C, lysolipids accumulate at the boundaries due the increased mobility of the lateral lipids at this region. The accumulated lysolipids further micellize and thus form stabilized nanopores within the lipid bilayer. Moreover, desorption of fairly water-soluble lysolipids at temperatures near T_C generates molecular-scale defects through which the entrapped drugs could be released. However, experimental evidences indicate that the lysolipids are still present within the bilayer after dialysis above T_C and thus, the rapid drug diffusion is mostly governed by the formation of stabilized nanopores at molten grain boundary

areas rather than the vacancy defects left from lysolipid desorption (Mills et al., 2005). The stability of bilayer pores could be further improved by incorporation of distearoyl phosphatidyl ethanolamine-polyethylene glycol (DSPE-PEG2000) into the LTSL formulation (Figure 2.4b) (Landon et al., 2011).

(c) Polymer-Modified Thermosensitive Liposomes (PTSLs)

The membrane disruption rate in response to thermal energy could also be increased by incorporation of LCST polymers within the TSL bilayer. At temperatures above LCST, dehydration of polymer chains destabilizes the liposomal structure and provides preferred routes for rapid leakage of the entrapped drug (Figure 2.5a) (Kono, 2001; Ta et al., 2010). Incorporation of thermosensitive leucine zipper peptide into TTSLs could also combine the attractive features of TTSLs with the dissociative, unfolding properties of these peptides (Figure 2.5b) (Al-Ahmady et al., 2012).

PNIPAM copolymerized with various anchoring monomers including octadecyl acrylate (ODA) (Zhou et al., 2012), didodecylacrylamide (Kono et al., 2002), acrylamide (AA) (Han et al., 2006; Hayashi et al., 1999), and acrylic acid (Mackinnon et al., 2009) is the most extensively used polymer for improving the thermal sensitivity of lipid membranes. The long saturated chains of ODA strongly interact with the hydrophobic chains of the lipid bilayers, providing lower desorption of PNIPAM-co-ODA compared to lysolipids. However, the addition of 1% ODA decreases the LCST of PNIPAM from 32°C to 27°C and thus negatively affects the stability of TSLs at physiological condition (Kono et al., 1994). In contrast, the LCST of PNIPAM is increased to 39°C when AA is

used as anchor site, resulting in more stability of TSLs at physiological temperature (Hayashi et al., 1999).

The type of incorporated comonomers significantly influences the PTSL triggering performance. For instance, although the LCSTs of PNIPAM copolymerized with N-isopropyl methacrylamide (NIPMAM), N,N-dimethyl acrylamide (DMAM), and N-acryloyl pyrrolidine (APR) are approximately identical (~40°C), TSLs sensitized by these polymers exhibit different phase transition behaviours. In general, more hydrophobic comonomers (e.g. NIPMAM) provide stronger interactions with lipid membrane and thus, increase the membrane disruption and drug release rates (Yoshino et al., 2004).

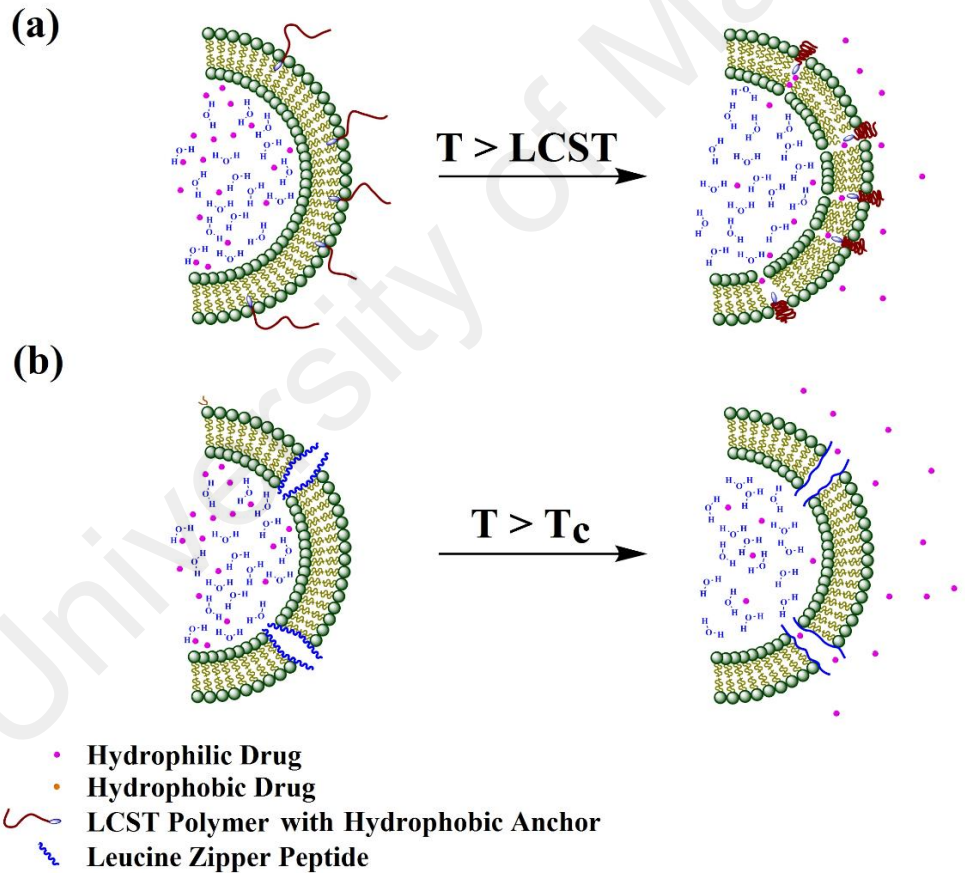

Figure 2.5: Thermal-triggered drug release from TSLs due to the a) coil-globule transition of a LCST polymer, and b) unfolding of a leucine zipper peptide.

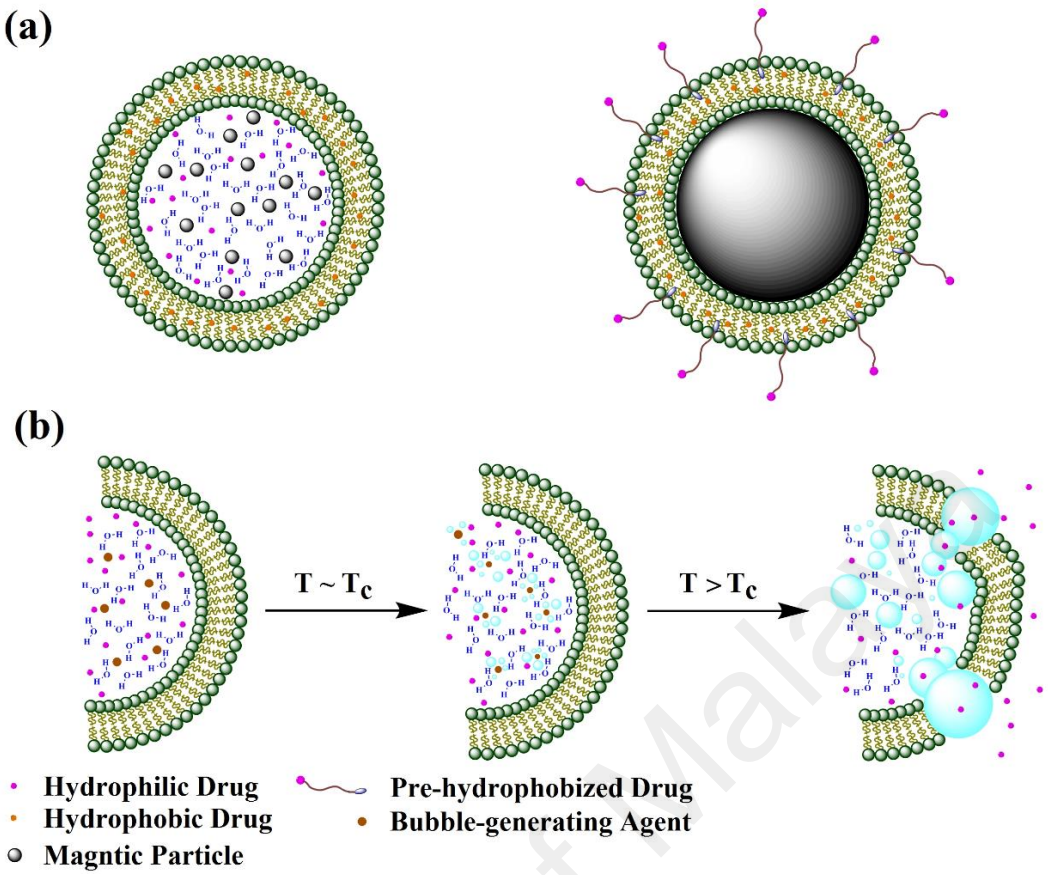

Figure 2.6: A schematic representation of a) two different magneto-liposome structures. Drug pre-hydrophobization is necessary when the inner volume of TSLs is occupied by a single magnetic nanoparticle core; b) bubble-generating liposomes. Thermal-triggered generation of bubbles via decomposition of ammonium bicarbonate produces permeable pores for discharge of the entrapped drug.

(d) Magneto-liposomes

Superparamagnetic iron oxide nanoparticles are a class of negative T_2-contrast agents which can be incorporated in the liposomal formulations in order to enhance their intracellular delivery for magnetic resonance imaging (MRI) purposes (Faria et al., 2013; Giustetto et al., 2013; Lorenzato et al., 2013; Pradhan et al., 2014). Appropriate selection

of the phospholipid bilayer could result in a significant intracellular uptake of iron oxide nanoparticles with no cytotoxic effects (Soenen et al., 2007; Soenen et al., 2009). The presence of the magnetic core also allows delivering magneto-liposomes to the target site by using an extracorporeal magnetic field.

The superparamagnetic behaviour and high thermal conductivity of iron oxides could also be used to increase the heat deposition rate within the lipid membrane and thus promote drug release rate in the target tumour (Amstad et al., 2011; Spera et al., 2014). A drug release ratio up to 40% could be achieved by heating the magneto-liposomes using 214 KHz pulsed alternating magnetic field for ten times (Podaru et al., 2014). A recent study has also shown that hydrophobic magnetic nanoparticles can facilitate drug release by increasing bilayer permeability through magnetic-impelled motions of nanoparticles rather than destruction of the lipid structure (Qiu et al., 2013).

The iron oxide nanoparticles could form a single core by complete occupation of the aqueous central cavity (Soenen et al., 2007) or provide several nano-sized cores in this region (Martina et al., 2005) (Figure 2.6a). However, occupation of aqueous core by iron oxide nanoparticles leads to a drastic decrease in the available capacity for encapsulation of hydrophilic drugs. Therefore, the drugs must be hydrophobized in order to be encapsulated into the lipid bilayer or attached to the lipid surface (Figure 2.6a). Magnetic nanoparticles can also be hydrophobized in order to be incorporated within the lipid bilayer space (Qiu et al., 2013). Nevertheless, these strategies may slightly change the hydrodynamic diameter of the drug-loaded liposomes as well as the zeta potential of the entire system, leading to RES recognition and reduced circulation intervals (Soenen et al., 2009).

(e) Bubble-Generating Liposomes

Thermosensitive bubble-generating compounds such as ammonium bicarbonate could readily be incorporated into the aqueous core of TSLs and generate carbon dioxide bubbles through decomposition at temperatures above 42°C. The nucleation, growth, and collapse of these bubbles induce a disruptive force comparable to the cavitation effect produced by ultrasound beams (Figure 2.6b). Moreover, carbon dioxide bubbles exhibit hyperechogenic features and could thus enhance the contrast in MRI and ultrasound images (Chen et al., 2013b; Chung et al., 2012).

Incorporation of plasmonic compounds such as fullerenes (Babincova et al., 2003) or gold nanoparticles (Anderson et al., 2010b) could also result in bubble formation within the lipid bilayer. When the plasmonic nanoparticles are exposed to laser beams with specific wavelengths, produce significant amounts of heat and thus evaporate the surrounding aqueous medium. This vapour further generates nanobubbles, which cause mechanical disruption of bilayers due to their collapse after a rapid expansion.

2.1.2.2 Clinical Practice and Remaining Challenges

TSLs have received the most extensive research and development for thermal-triggered drug release, resulting in commercialization of a LTSL formulation loaded with doxorubicin (ThermoDOX®, Celsion Corp. Lawrenceville, NJ). This product is now undergoing clinical trials in phase III for the treatment of hepatocellular carcinoma using standardized radiofrequency (RF) ablation and phase I for treatment of primary or secondary liver tumours using high intensity focused ultrasound (HIFU).

Although TSL formulations exhibit a promising in vitro behaviour, their in vivo functionality may be negatively influenced by biomolecules such as plasma proteins and cellular membrane pools. Previous in vivo studies reported a 70% desorption of lysolipids from LTSL membrane in one hour after intravenous administration, which negatively influenced the thermal sensitivity of LTSLs (Banno et al., 2010). Moreover, lysolipids presumably undergo faster dissociation from the liposomal structure in diluted aqueous solutions (Sandström et al., 2005).

The undesired desorption of lysolipids upon administration in the bloodstream may negatively influence the thermal sensitivity of LTSLs and cause a premature outflow of entrapped drug at physiological temperature associated with systemic toxicity (Ta et al., 2014). For instance, near 50% drug leakage at 37°C was observed within 1 hour of in vivo injection (Chiu et al., 2005; De Smet et al., 2010). In contrast, PTSLs have shown a relatively higher stability in biological environments with increased drug accumulation in tumour site (Ta et al., 2010). However, further in vivo studies are required to verify their therapeutic efficacy in combination with various hyperthermia modalities.

2.1.3 Micellization

Aqueous solutions of some amphiphilic polymers exhibit thermal-triggered micellization by hydrophobic effect at temperatures and concentrations higher than their critical micellar temperature (CMT) and critical micellar concentration (CMC), respectively. In general, the hydrogels composed of polymer chains without covalent crosslinks may exhibit micellization behaviour rather than coil-globule transition.

Moreover, the content of hydrophilic moieties may favour the micellization behaviour. For instance, copolymerization of PNIPAM with specific amounts of hydrophilic moieties such as ethylene glycol or acrylic acid could result in micellization at temperatures near 37°C instead of coil-globule behaviour (You et al., 2007; Zhang et al., 2005). The produced micelles can further release their cargo by different mechanisms such as hydrophobic effect, or sol-gel-sol transition.

2.1.3.1 Triggering Mechanisms in Micelles

(a) Hydrophobic Effect

Micellar formulations are often synthesized using amphiphilic block copolymers which exhibit thermal-induced micellization/demicellization, controlled by their hydrophobic balance (Yu et al., 2008). The aqueous solutions containing particular concentrations of these amphiphilic block copolymers exhibit phase transition at temperatures above CMT and form micelles with hydrophobic inner cores surrounded by hydrophilic outer shells. Because of this phase separation in aqueous mixture, high concentrations of hydrophobic drugs (e.g. ibuprofen) could be dissolved within the medium in contrast to a pure aqueous solution (Anderson et al., 2001). Formation of hydrogen bonds between the hydrophilic corona and aqueous surrounding also reduces the risks of cellular adhesion, protein adsorption, and RES recognition (Rösler et al., 2012).

The conventional micellar formulations could not generally respond to the external thermal stimuli. However, substitution of the hydrophilic or hydrophobic moieties of

micelles by thermosensitive monomers such as PNIPAM to provide core-shell structures with thermosensitive outer shell or inner core, respectively (Rezaei et al., 2012; Wei et al., 2007). Upon heating, the collapse of thermosensitive moiety due to its reduced solubility and interaction with hydrophobic conjugate, results in micelle destabilization and burst-like release of entrapped drug.

(b) Sol-Gel-Sol Transition

The aqueous solution of some thermosensitive micelles shows thermal-triggered sol-gel behaviour at a particular micellar concentration. When the micellar volumetric fraction is above a specific threshold referred to as micelle gelation concentration (MGC), the micelles entangle together and further undergo three-dimensional and crystal-like packing, producing a hydrogel network (Mortensen et al., 1994; Yapar et al., 2013). In a similar manner to CST polymers, these hydrogels possess lower (LGTT) and upper gel transition temperatures (UGTT) (Vihola et al., 2008).

Poloxamers (trade name Pluronics®) are prominent thermosensitive gels which exhibit sol-gel-sol phase transition with inverse temperature-dependent volumetric change. Poloxamers are copolymers consisting of hydrophobic moieties symmetrically blocked by two hydrophilic chains (Chiappetta et al., 2007; Yapar et al., 2013). Polypropylene oxide (PPO) and polyethylene oxide (PEO) are the most frequently used hydrophobic and hydrophilic moieties for synthesis of poloxamers. Although both PEO and PPO, as well as the PEO–PPO–PEO block copolymers could exhibit LCST behaviour, poloxamers are often popular due to their sol–gel-sol transition rather than

LCST system. Thermal-triggered drug release from poloxamers probably occurs by spherical-to-cylindrical transition of micelles, or gel-sol behaviour.

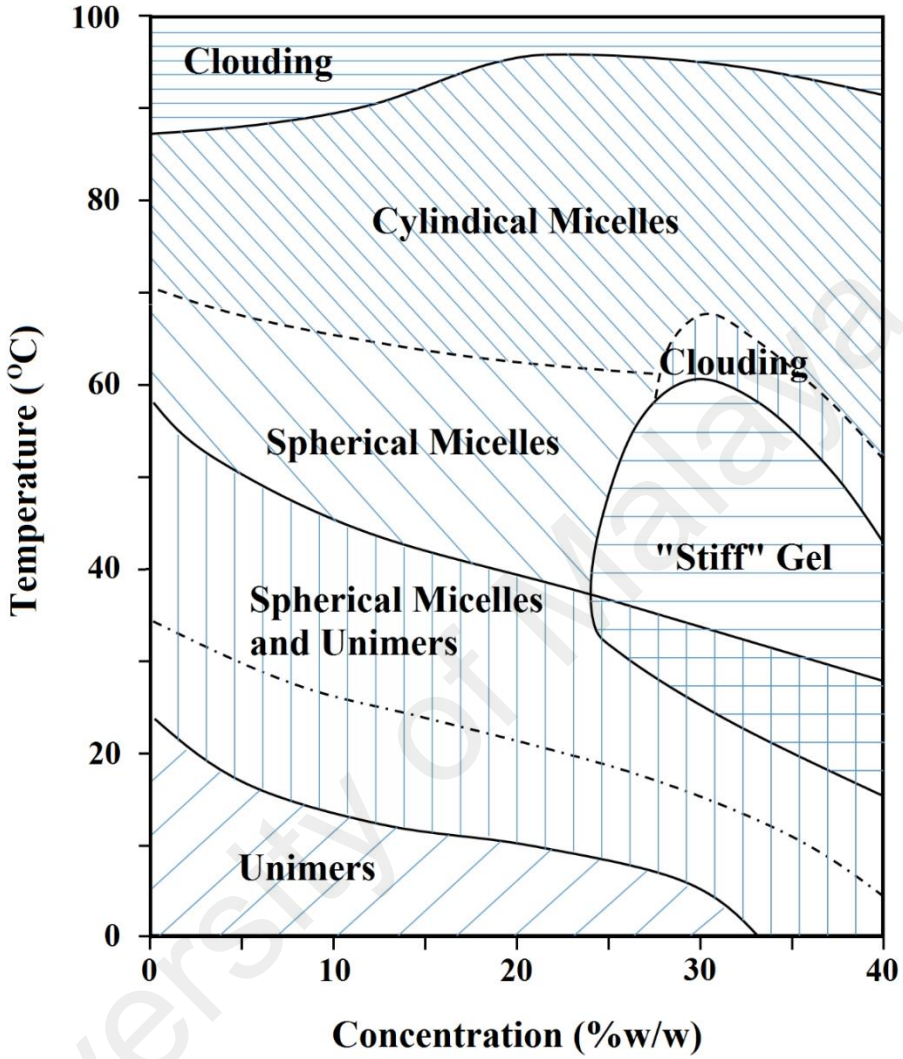

Figure 2.7: Phase transition diagram of a typical poloxamer (EO27-PO39-EO27) in aqueous solution. According to this diagram, two approaches including micellization (in dilute solutions) and "stiff-gel" formation (in polymer-enriched solutions) could be utilized for drug encapsulation. These carriers could further be heated to their corresponding "clouding" region to release their cargo (adapted from Glatter et al., 1994 with permission from American Chemical Society).

Figure 2.7 shows the phase diagram of a typical poloxamer formulation (EO_{27}-PO_{39}-EO_{27}, P-85) at temperatures and concentrations below 100°C and 40 %w/w, respectively (Glatter et al., 1994). When the copolymer concentration in aqueous solution is less than 24 %w/w, the temperature rise to above 60-70°C results in a micellar transition from spherical to cylindrical morphology, which is associated with release of the packing constraints (Glatter et al., 1994; Mortensen et al., 1994). Therefore at this temperature range, the release of encapsulated drug is favoured as a result of hydrogel shrinkage. However, heating of the solutions with higher poloxamer concentrations to above 40°C results in the formation of a stiff gel in the mixture.

Formation of the gel phase is probably because of the entanglements between PEO coronas, which cause strong intermicellar interactions without essential alteration of the structure arrangement. When heating is continued, dissociation of the stiff gel, regarded as "gel melting" or gel-to-sol transition, favours drug release from the polymer structure. This transition is relied on the shrinkage of PEO chains due to their decreased solubility and interaction with PPO moieties at higher temperatures (Glatter et al., 1994).

The chemical properties of hydrogels could be further modified to precisely control their thermal sensitivity, morphology, and biocompatibility. For instance, the hydrophobic PPO core could be substituted with more hydrophobic compounds such as poly(1,2-butylene oxide) (PBO) to decrease the CMC threshold (Li et al., 1997; Yang et al., 1996). PPO could also be replaced with poly(L-lactic acid) (PLA) (Saffer et al., 2011) or poly(lactic acid-co-glycolic acid) (PLGA) (Andhariya et al., 2011) to place biodegradable ester groups within the copolymer structure. Moreover, some metallic agents such as iron oxide (Andhariya et al., 2011) and gold (Bae et al., 2006) could be

incorporated into the poloxamers formulations to achieve improved thermal sensitivity and physical stability in biological environment.

2.1.3.2 Current Challenges and Perspective of Clinical Application

The interest in utilization of poloxamers as drug carriers has resulted in development of a micellar formulation comprised of Pluronics® L61 and F127 and loaded with doxorubicin (SP1049C, Supratek Pharma Inc., Montréal, Quebec, CA, USA). This product is currently undergoing clinical trials in phase III for treatment of relapsed patients with metastatic adenocarcinoma of the oesophagus and some other upper gastrointestinal tract cancers (Pitto Barry et al., 2014).

Although the gel-forming mechanism of poloxamers could provide an attractive solution in drug delivery, these gels may not remain stable for more than several hours because of weak physical crosslinking between the micelles. In vitro experiments reported a complete dissolution of a 25 %w/w poloxamer 407 and 50% dissolution of a 35 %w/w poloxamer 407 into phosphate buffered saline (PBS) medium after 4 hours (Bhardwaj et al., 1996). Therefore, more resilient hydrogel systems are required to attain a longer-term retention in blood circulation.

To overcome the limitations of poloxamers and obtain gels with improved durability and biocompatibility, graft copolymers of PEG-PLGA have been developed (Alexander et al., 2013; Piazza et al., 2014; Song et al., 2011; Yu et al., 2014). By altering the ratio of glycolic acid to lactic acid in the middle block, as well as the PLGA and PEG lengths, transition temperatures between 15°C to 45°C could be obtained in aqueous solution

(Jeong et al., 1999). In vivo experiments in rats reported a durability of above one month which makes them desirable for a long-term injectable drug delivery system (Jeong et al., 2000). However, owing to the molecular weight and degradation profile of the PEG–PLGA polymers, fabrication of triblock copolymers, which show the sol-to-gel phase transition in a desired range of 10°C to 30°C remains a challenge.

2.1.4 Superparamagnetic Behaviour

Magnetic hyperthermia is a treatment modality which employs external alternating magnetic fields (AMF) with appropriate frequency and strength to heat a magnetic nanofluid dispersed within the target tissue. The produced thermal energy is further transferred to the surrounding region whereby, maintaining the temperature within the therapeutic threshold (40-42˚C) for above 30 min could induce apoptosis and effectively killing of the tumour (Dobson, 2006; Pankhurst et al., 2003). This technique shows the potential to overcome the limitations of other hyperthermia modalities in targeting and heat deposition (Kim et al., 2008). Moreover, the dispersed magnetic nanofluids could enhance the contrast of MR images for better visualization of the tumour tissue and allow drug navigation and retention using an external magnetic field (Arruebo et al., 2007).

2.1.4.1 Mechanisms of Heat Generation in Magnetic Nanoparticles

Heat generation in the magnetic nanofluids during AMF exposure is mostly relied on hysteresis loss (Figure 2.8a), Néel relaxation, Brown relaxation (Figure 2.8b), and

frictional losses (Jeun et al., 2013). Hysteresis loss is resulted from irreversible magnetization due to the intrinsic parameters such as anisotropy in the magnetic behaviour of the crystalline structure as well as trapping of magnetic domain walls at grain boundaries or impurities (Pankhurst et al., 2003). Therefore, the magnetized material could not immediately relax back when the applied magnetizing field is removed. Demagnetization of the material or magnetization in opposite direction requires a certain amount of work to be carried out by AMF, which is further converted to heat within the material. The amount of energy needed for re-orientation of spontaneously magnetized domains depends on both intrinsic (e.g. particle size, shape, and magneto-crystalline anisotropy) and structural characteristics (e.g. grain boundaries, impurities, and vacancies) of the magnetic material. In general, substantial heating due to the hysteresis loss is observed in strongly anisotropic magnetic alloys such as neodymium-iron-boron and samarium-cobalt (Pankhurst et al., 2003).

Heat generation through Néel relaxation is due to the rapid changes in the direction of atomic magnetic moments within each particle, hindered by anisotropy energy that tends to turn the magnetic domains in a given direction according to their crystal lattice structure. Brown relaxation loss is resulted from the medium viscosity which tends to counter the physical rotation of the suspended magnetic particles. Frictional losses due to the fluid movement could also produce heat inside the medium. The heat generation in magnetic particles by eddy current induction is negligible because of their nanoscale size and low AMF frequencies (below 1.2 MHz) used to avoid nonspecific heating of healthy tissues, stimulation of skeletal or peripheral muscles, cardiac stimulation, and arrhythmia (Kim et al., 2008; Pankhurst et al., 2003).

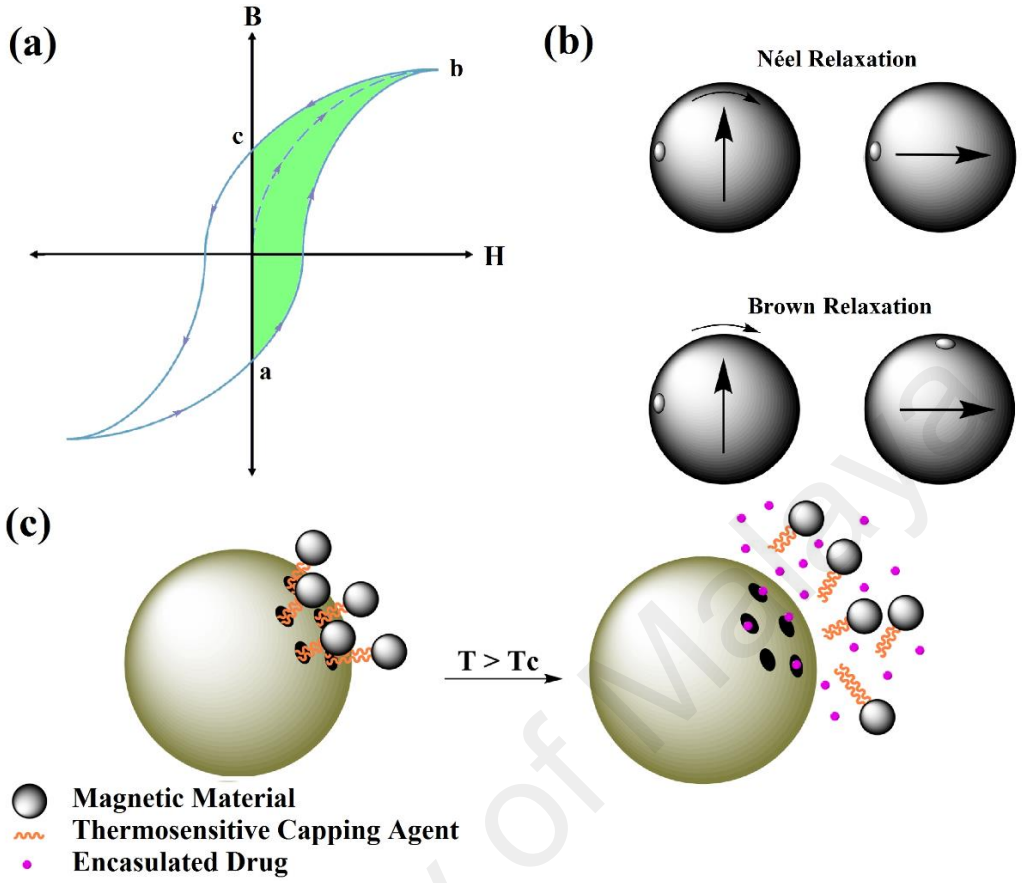

Figure 2.8: a) A typical hysteresis loop observed during magnetization/ demagnetization of magnetic nanoparticles. B and H are magnetic flux density, and magnetic field strength, respectively. A single magnetization/demagnetization cycle (a→b→c) produces a thermal energy proportional to the shaded area within the hysteresis loop. b) Illustration of the Néel, and Brown relaxation concepts. c) Drug release from the core nanopores after breakage of capping agent (e.g. DNA) at increased temperatures. Magnetic nanoparticles could enhance heat transfer efficacy to the capping agent, thus leading to faster drug release.

Superparamagnetic nanoparticles generally possess insufficient drug loading capacities; however, the heat produced in these materials under AMF exposure can be utilized to obtain "on-off" drug release. For this aim, a porous matrix (e.g. mesoporous silica nanoparticles) is blocked by superparamagnetic nanoparticles through capping agents such as double helix DNA (Derfus et al., 2007; Ruiz Hernandez et al., 2011), or pseudorotaxane-based nanovalves (Thomas et al., 2010), which undergo melting at hyperthermia temperature range. Upon AMF exposure, the heat generation by superparamagnetic nanoparticles results in dissociation of capping agent and "on-off" drug release from the porous structure (Figure 2.8c).

2.1.4.2 Current Challenges in Clinical Practice

Since the early utilization of magnetic materials for hyperthermia treatments, a number of investigations (Balivada et al., 2010; Gandhi et al., 2011; Jang et al., 2009; Sadhukha et al., 2013; Wilhelm et al., 2007) have shown both in vitro and in vivo potential of magnetic nanofluids in generating therapeutic heating levels. To date however, magnetic hyperthermia has not been successfully applied for treatment of human patients mostly due to the inadequate intratumoural accumulation of magnetic particles for generating therapeutic heat under low AMF frequencies. The majority of in vitro and in vivo studies have utilized field strengths or frequencies which exceed the harmless levels for human patients. Application of safer frequencies often results in drastic reduction of output heat, rendering this technique inappropriate for hyperthermia application. Furthermore, tissue cooling by bloodstream and perfusion complicates the calculation of the heat deposition rate needed to obtain sufficient temperature rise in target tissue. Therefore, tissue cooling

during magnetic hyperthermia is mostly avoided due to the mathematical complexity as well as difficulties in generalization of the results. Through a simple rule-of-thumb, heat deposition rate of 100 $mW.cm^{-3}$ and intratumoural particle concentrations of 5-10 $mg.cm^{-3}$ are considered adequate to generate therapeutic heat in most tissues (Pankhurst et al., 2003). However, further research is required to obtain these values in the clinical setting.

2.1.5 Photo-Absorbance

Photothermal therapy is an innovative modality in which the incident light beam absorbed by chromophoric molecules is converted to thermal energy (Huang et al., 2010; Pattani et al., 2012). This technique often employs the light beams with wavelengths in the near-infrared (NIR) window (650 to 900 nm) where the maximum tissue penetration is gained due to a moderate tissue transparency at this wavelength range (Weissleder, 2001). Scattering is the dominant light-tissue interaction in the NIR window which results in a rapid photon propagation and increased travelling distance (Peidaee et al., 2013).

When the photothermal therapy is carried out with irradiation of NIR light beams alone, the presence of endogenous absorbent molecules (e.g. haemoglobin, melanin, fat, and water) in the surrounding healthy tissues inflicts nonspecific damages and reduced heat deposition within the tumour (Pattani et al., 2012; Weissleder, 2001). Therefore, in order to improve the selective thermal destruction and reach the underlying tumour, exogenous organic light-absorbing molecules such as indocyanine green (Chen et al., 1996), naphthalocyanines (Busetti et al., 1999), and porphyrins (Soncin et al., 1999) are often administrated within the tumour tissue prior irradiation. However, rapid photo-

bleaching of these organic dyes may result in limited in vivo efficacy of photothermal therapy (Choi et al., 2009).

As alternative to the synthetic organic dyes, a range of metallic (e.g. gold nanoparticles (El-Sayed et al., 2013; Elliott et al., 2010; Jain et al., 2012; Ma et al., 2013; Mendoza Nava et al., 2013; Mocan et al., 2013), iron (Patel et al., 2015), iron-platinum (Chen et al., 2013a), copper (Bu et al., 2014), palladium (Zhao et al., 2014), and gadolinium (Mathew et al., 2013)) and carbon-based (Dewitt et al., 2014; Gollavelli et al., 2014; Maestro et al., 2013; Miyako et al., 2007; Wang et al., 2013; Zhang et al., 2011)) nanoparticles with enhanced NIR absorption efficacies and higher photo stabilities have recently been employed. The presence of delocalized mobile electrons in these nanoparticles results in effective absorption and scattering of NIR light. However, a superior heating effect is particularly observed when the beam energy is close to the plasmon frequency of the administrated nanocrystals (Govorov et al., 2007). Therefore, the noble metal nanoparticles such as gold that show surface plasmon resonance (SPR) behaviour in NIR range could be used as promising photo-absorbents for photothermal therapy. According to the Mie scattering theory, a million-fold increase in the absorption cross section could be observed when the gold nanoshells are used rather than the conventional NIR dyes such as indocyanine green (Loo et al., 2004).

2.1.5.1 Mechanism of Heat Generation by SPR Effect

Surface plasmons are coherent collective oscillations of delocalized electrons which propagate at the interface of two materials with negative (e.g. metals) and positive (e.g.

dielectrics) permittivity values (Pattani et al., 2012). The surface plasmon oscillations which are often excited by absorption of electromagnetic fields with specific wavelengths (Pattani et al., 2012), induce strong localized electric fields on the material surface (Huang et al., 2011). This SPR phenomenon significantly enhances the absorption and scattering cross sections of the material, which in turn make these particles promising for photothermal therapy and imaging purposes, respectively (El-Sayed et al., 2005; Huang et al., 2006).

Irradiation of the light beams with SPR wavelengths results in polarization of the delocalized electrons with respect to the heavy ionic nanoparticle cores (Link et al., 2003). The fast relaxation of these polarized electrons generates strong localized thermal energy through electron-electron and electron-phonon relaxations which respectively occur in femto- and pico- seconds (Huang et al., 2006; Huang et al., 2011). The generated heat is then dissipated into the surrounding tissues and cause necrosis in the tumour cells.

Although the SPR behaviour is observed in many compounds, the SPR wavelengths of these materials are often far from the NIR windows which make them inappropriate for photothermal therapy. However, the noble metals such as gold and silver which possess SPR wavelengths within the NIR region, could be used in photothermal therapy to achieve enhanced heat deposition efficacy in the tumour site. Gold nanoparticles particularly serve as excellent adjuvants for photothermal therapy in NIR range due to their tuneable SPR wavelength, strong optical absorption, photo-stability, anti-angiogenic properties, and flexible surface chemistry (Amato et al., 2013; Bartczak et al., 2013; El-Sayed et al., 2006; Kang et al., 2006; Sun et al., 2013; Vigderman et al., 2013). Although the spherical gold nanoparticles show the SPR behaviour in the visible spectral range

(approximately 520 nm) (El-Sayed et al., 2005), their SPR wavelength could be red-shifted to the NIR region by alteration of the particle morphology to nanoshells comprised of a dielectric core (e.g. silica) coated with an ultrathin gold shell (Loo et al., 2004; O'neal et al., 2004), or nanorods (El-Sayed et al., 2013). The absorption band of these nanostructures are respectively governed by the core diameter to the shell thickness (Loo et al., 2004; O'neal et al., 2004), and particle aspect ratio (El-Sayed et al., 2013).

2.1.5.2 Current Challenges and Future Perspective

Nonspecific heating and poor penetration of light source due to the absorption by various biomolecules are the major challenges which limit the clinical efficacy of photodynamic therapy (Zhou et al., 2009a). At near infrared window where the optical absorbance in tissues are minimal, the penetration depth of incident beams is limited to 1-2 cm beneath the skin (Smith et al., 2009). Therefore, plasmonic nanostructures have recently emerged as promising adjuvants in photothermal therapy to enhance the target selectivity and generate a lethal dose of thermal energy within the cancer tumours. In particular, gold nanoshells (Aurolase® by Nanospectra Biosciences Inc., Houston, TX) with high photo-to-thermal conversion efficacies and tuneable optical properties are in phase I clinical trials for treatment of superficial neck and head cancers (Hainfeld et al., 2014; Jabeen et al., 2014). However, crucial parameters such as treatment cost, biodegradation, blood retention time, and chemical interactions in physiological environments need further evaluation. Once the optimal conditions of these variables are obtained, the plasmonic nanostructures could be employed in clinical setting to improve the efficacy of photothermal therapy in human patients.

Table 2.1: A summary of advantages and limitations of various triggering mechanisms described in this study.

	Advantages	Limitations
CG	Sharp transition Controllable transition temperature Concentration-free response High loading capacity Facile construction Ease of functionalization Wide selection range	Low biocompatibility Low response rate High needed concentration Mechanical instability
MD	Approved for clinical use Biocompatibility Sharp transition Rapid response Concentration-free response High loading capacity Mechanical Strength Adjustable physical properties	In vivo dissociation Low drug availability High molecular weight
MI	Biocompatibility High loading capacity Thermal stability	Concentration-dependent threshold In vivo dissociation Low response rate
SP	Facile preparation High durability High heating efficiency	Insufficient loading capacity High needed concentrations Only applicable for IH
PA	Biocompatibility Long-term stability Ease of surface modification High loading capacity (in case of Carbon-based materials)	Inability to treat deep tumours High needed concentrations Complicated production Limited loading capacity (in case of metallic particles)

Abbreviations. CG: coil-globule, MD: membrane disruption, MI: micellization, SP: superparamagnetic behaviour, PA: photo absorbance.

Although all the reviewed triggering mechanisms are potentially attractive, several specific barriers for each mechanism must be overcome prior utilization in clinical setting. Table 2.1 provides an overview of the advantages and shortcomings of several triggering mechanisms described in this review. Understanding the features and limitations of triggering mechanisms in various thermosensitive nanoparticles allows in selection of appropriate compounds for particular experimental or clinical condition. In recent years, many studies have addressed these limitations in order to develop new

thermosensitive agents which could be reliably used in real clinical condition. However, few thermosensitive formulations have successfully fulfilled different clinical trial phases to become available in the pharmaceutical market. Hence, the present review could aid in better understanding of the limitations of each triggering mechanism in order to develop thermosensitive systems with tailored properties for real life application.

2.2 Tissue-Mimicking Gel Phantoms for Thermal Therapy Studies

Thermal therapy methods, similar to any other therapeutic or diagnostic technique, need assessment and verification in terms of their effectiveness and limitations prior to application in clinical setting. The ideal medium for experimental studies of temperature-based therapies is the real tissue of clinical interest due to the provision of the closest approximation to the clinical conditions. However, in vivo measurements as well as in vitro utilization of real tissues may cause substantial difficulties in preparation, handling, storage, and particularly, standardization of the results. Therefore, availability of artificial phantoms that closely mimic the physical and geometrical properties of target tissues plays an important role in pre-clinical evaluation of thermal modalities.

Although a number of phantoms are available commercially (e.g. from Computerized Imaging Reference Systems Inc., Gammex Inc., and ATS laboratories Inc.), these products are generally constructed for broad applications such as calibration of imaging devices as well as training purposes and may not be suitable for specific requirements. These phantoms may possess insufficient thermal stability or unfavourable physical properties at increased temperatures which would render them inappropriate for high-temperature experiments. Moreover, uniformity may not exist among laboratories in terms of fundamental properties of a specific tissue-mimicking media (Anderson et al., 2010a; Madsen et al., 1999; Wear et al., 2005); i.e., a tissue-mimicking phantom fabricated in a specific laboratory setup, may not exhibit similar characteristics when reproduced in a different experimental condition. Hence, many attempts have been made for development and customization of thermal phantoms to simulate biological tissues at desired experimental conditions (frequency (f), temperature (T), etc.). As a result, various

recipes have been suggested in liquid, solid, and gel (semi-solid) forms. However, gel phantoms have found more popularity because of representing a wide range of thermal, electrical, acoustic, and optical properties. Facile formability is another particular feature of gel phantoms which provides the ability to reproduce realistic irradiation geometries.

This section intends to review the advantages and limitations of the popular gel phantoms including agar, polyacrylamide, and gelatine which are widely employed for hyperthermia and thermal ablation applications.

2.2.1 Agar Phantoms

Agar is a gelatinous polysaccharide derived from the cell membranes of some species of seaweed and red algae. Due to the desirable physical and thermal properties, agar and agarose (the purified form) are widely used for fabrication of thermal phantoms. These phantoms are facilely fabricated by heating the agar aqueous solution above 85˚C and then cooling the liquid to the room temperature, resulting in a lightly opaque gelatinous substance (Huang et al., 2004).

2.2.1.1 Phantom Recipes

One of the early researches concerning the development and characterization of the agar-based phantoms was carried out by Ishida and Kato, 1980 for application at frequency of 13.56 MHz (Ishida et al., 1980). This recipe was later modified in further studies to reproduce the electrical properties of biological tissues at Industrial, Scientific

and Medical (ISM) frequencies including 435, 900, and 2450 MHz. The composition and various properties of these phantoms fabricated for radiofrequency (RF) and microwave (MW) modalities are compared in Table 2.2. The agar phantoms are mainly consisted of agar as gelling agent and water. However, v components such as sodium azide (NaN_3) (Ito et al., 2001; Kato et al., 1986; Kato et al., 1987) as preservative, NaCl (Ishida et al., 1980; Ito et al., 2001; Kato et al., 1986) or polyvinyl chloride (PVC) as electrical conductivity (σ) modifier (Kato et al., 1987), and polyethylene (PE) powder (with TX-151 to improve solubility) as dielectric constant (ε_r') regulator (Ito et al., 2001) are usually added to these recipes. The addition of NaN_3 may also result in a slight increase of electrical conductivity, while PVC powder could negatively affect the dielectric constant of agar phantoms (Kato et al., 1986; Kato et al., 1987).

Table 2.2: The composition (%w/w) and various properties of agar phantoms proposed for RF/MW studies. Some data are presented as mean ± standard deviation.

	Ishida & Kato, 1980	**Kato et al., 1986**	**Kato & Ishida, 1987**	**Ito et al., 2001**	
				Muscle	**Brain**
Agar	2	4	4	2.70	2.50
NaCl	0.43	0-0.60	-	0.90	0.50
NaN_3	-	0.10	0-0.80	0.05	0.05
PVC	-	-	0-44.40	-	-
PE	-	-	-	8.60	13.30
TX-151	-	-	-	2.10	1.40
Water	the rest	the rest	the rest	the rest	the rest
f(MHz)	13.56	1-40	5-40	430	900
T (ºC)	22	23.50	23.60	22	22
ρ ($kg.m^{-3}$)	-	1020	1020[b] (no PVC)	-	-
C ($kJ.kg^{-1}.K^{-1}$)	-	4.18	4.18±0.08[b] (no PVC)	-	-
σ ($S.m^{-1}$)	0.83	0.20-1.20	0.02-1.23	1.41	0.85
ε_r'	109	~81	35-80	53	43

[a]The target values were set to 2/3-muscle equivalent tissues, which corresponds to the electrical constants of muscle equivalent tissues times 2/3.
[b]The density (ρ) specific heat capacity (C) of PVC are 1380 $kg.m^{-3}$ and 1298 $J.kg^{-1}.K^{-1}$; Therefore, the ρ and C values of the final phantom can be calculated from the proportion of PVC in the phantom.

Agar phantoms usually provide small permittivity values compared to the biological tissues, making these gels inappropriate for MW studies. This shortcoming could be overcome by addition of some biological materials such as corn syrup (Zhou et al., 2009b). However, these additives may increase the perishability of agar phantoms and lead to difficulties in controlling or reproducing the electrical properties. Graphite is another additive that is used for adjustment of both electrical conductivity and permittivity. The graphite powder could also produce some "speckles" similar to those in biological tissues, resulting in more realistic ultrasound images (Kao et al., 2008). However, graphite is only suitable for adjustment of electrical conductivity and permittivity at microwave frequencies.

Agar phantoms have also been applied for high intensity focused ultrasound (HIFU) studies. The majority of these HIFU phantoms are developed according to a recipe proposed for diagnostic ultrasound application (Burlew et al., 1980). This recipe is composed of water, agar, graphite powder as scatterer, methyl paraben as preservative, and 1-propanol as sound speed (c) modifier. This recipe exhibits a thermal conductivity (k) in the range of biological tissues. However, the attenuation coefficient (α) of this phantom at 1 MHz is slightly higher than that of soft tissues, causing higher peak temperatures and smaller heated volumes in the phantoms compared to real tissues (Holt et al., 2001). The attenuation coefficient could be moderated by lowering the graphite ratio (Farny et al., 2010; Huang et al., 2004). Nylon threads are also suitable acoustic scatterers due to their high durability and oxidation resistance (Ortega et al., 2010). Glycerol (Rickey et al., 1995), cellulose (Rickey et al., 1995), evaporated milk (Madsen et al., 1998), glass beads (Anderson et al., 2010a; Madsen et al., 1998), silicon dioxide, and silicon carbide (Lai et al., 2010) are other materials which could be used as ultrasound

attenuating agents. On the other hand, thiomersal (Madsen et al., 1998) or formaldehyde (Poepping et al., 2002) could replace methyl paraben to protect the gel against deterioration. Formaldehyde also crosslinks the gel molecules, thus decreasing the compliance and increasing the melting point of agar phantoms (Poepping et al., 2002). It is important to note that the inertial cavitation threshold (P_{cav}) reported for the agar-based phantoms is significantly lower than that of biological tissues which thus results in a considerably higher bubble-enhanced heating during HIFU sonication (Farny et al., 2010; Holt et al., 2001). However, well-degassed agar phantoms containing increased ratios of gelling agent may provide improved P_{cav} values. The various properties of some popular recipes developed for HIFU experiments are summarized in Table 2.3.

Table 2.3: The composition and properties of agar-based phantoms developed for HIFU experiments. The amounts of ingredients are presented in %w/w, unless otherwise stated. Some data are given as mean ± standard deviation.

	Holt & Roy, 2001[a]	**Huang et al., 2004**	**Farny et al., 2010**	**Ortega et al., 2010**	
Agar	2.50	2.50	2.70	2.50	3
Graphite Powder	9.00	7.60	3.70	100 ($g.l^{-1}$)	-
Nylon	-	-	-	-	Threads[b]
1-propanol	5.30	5.60	1.90	-	-
Glycerol	-	-	-	5	5
Preservative	0.10	0.10	0.10	-	-
Water	the rest	the rest	the rest	the rest	the rest
f (MHz)	1	1	1	3.50	3.50
ρ ($kg.m^{-1}$)	1100±50	1045	1003	-	-
C ($kJ.kg^{-1}.K^{-1}$)	3.30±0.50	3.71	3.71	-	-
κ ($W.m^{-1}.K^{-1}$)	0.65	0.59	-	-	-
α ($dB.cm^{-1}.MHz^{-1}$)	1.60±0.1	0.88	0.44	0.31-0.68	0.48-0.62
c ($m.s^{-1}$)	1600±25	1551	1520	1519-1560	1601-1645
P_{cav} (MPa)	~1.42[c]	-	1.40[d]	-	-

[a]This phantom was made using 600 mL of water, 750 mg of methyl paraben, 18 g of agar, 65 g of graphite powder, and 48 mL of 1-propanol. These values are converted to %w/w in this table.
[b]Nylon threads formed a matrix of 7 x 7 parallel units, by regular distance of 5 mm between them.
[c]The Pulse repetition frequency (PRF) was not reported. Various sonication durations between 0.7 to 10.2 seconds were used. However, it was found that the P_{cav} value was constant at sonication durations above 1 second.
[d]The sonication duration was fixed at 5.5 seconds.

The optothermal properties of agar-based phantoms have also been characterized. Pure agar gel exhibits a very low turbidity and a negligible absorption. Therefore, its optical properties could easily be adjusted by addition of appropriate scattering (e.g. intralipid (Cubeddu et al., 1997), vasolipid (Elliott et al., 2010), and evaporated milk (Elliott et al., 2010)) and absorbing (e.g. India ink (Cubeddu et al., 1997), indocyanine green (Elliott et al., 2010), and naphthol green (Iizuka et al., 1999; Siddiqi et al., 2013)) agents.

The ability of agar gels to be quickly scanned under magnetic resonance imaging system (MRI) is an attractive incentive for clinical application (Siddiqi et al., 2013). Moreover, by incorporation of thermosensitive proteins such as albumen (a condensed form of egg white) (Iizuka et al., 1999) and bovine serum albumin (BSA) (Siddiqi et al., 2013), thermosensitive agar phantoms suitable for photocoagulation studies could be obtained. When these phantoms are heated at temperatures above 70°C, the added proteins undergo an irreversible coagulation which changes the optical and MR values of the gel, allowing to distinguish the heated region inside the phantom (Siddiqi et al., 2013).

2.2.1.2 Heterogeneous Agar-based Phantoms

Agar-based gels are promising candidates for construction of heterogeneous phantoms that simulate inner tumours surrounded by background tissue (Solazzo et al., 2005). Tumour-tissue phantom are mostly constructed by solidifying two solutions containing different ratios of agar. In a typical recipe, a solution containing 0.25 %w/w agar, 3 %w/w sucrose, and designated ratios of NaCl (0.3-36.0 %w/w) is used to form the tumour-mimicking compartment. The tissue-mimicking part is also fabricated by solidifying an

aqueous solution consisting of 5 %w/w agar, 3 %w/w sucrose, and different concentrations of NaCl (0.06-5.00 %w/w) (Solazzo et al., 2005). Designated amounts of a fat-saturated oil could be added to the outer compartment to reduce the thermal conductivity of this layer, causing a more heat deposition within the central tumour (Liu et al., 2006). The thermal conductivity of the outer part could be tuned by varying the concentration of the fat-saturated oil (10–90%) (Liu et al., 2006).

Due to the desirable mechanical strength, agar-based gels could be used for construction of tissue-mimicking phantoms that simulate the vascular system, surrounding tissue, and blood. These phantoms are typically composed of a latex or silicon rubber tube which represents the blood vessels and surrounded by a tissue-mimicking gel. In particular, the relatively high stiffness of agar gels allows the implementation of wall-less vessel phantoms to avoid the difficulties associated with vessel wall attenuation and acoustic impedance mismatches (Rickey et al., 1995). The wall-less vessel simulant is usually formed by placing a metallic mandrel into the solution prior to gelation and removing it after hardening (Rickey et al., 1995). An alternative method for construction of more complicated vessel geometries is the use of low-melting-point cores which are further removed by submersion of the solidified agar phantom in a water-bath at mild temperatures (approximately 50°C) (Poepping et al., 2002).

2.2.1.3 Advantages and Limitations

The high melting point of agar phantoms (approximately 80°C) is desirable for applications where high-temperature regimes are achieved (Ortega et al., 2010).

Moreover, agar phantoms exhibit a sufficient mechanical strength which permits the construction of large torsos (Kato et al., 1986). The critical properties of these phantoms can easily and independently be varied by altering the ratios of phantom ingredients. In particular, the sound speed can be adjusted by varying the percentage of 1-propanol, while the attenuation is controlled by addition of graphite powder. However, optical opacity is the crucial limitation of agar phantoms, causing difficulties in visual observation of the coagulated region (Huang et al., 2004). The agar phantoms also provide a low toughness, making them fragile during handling.

2.2.2 Acrylamide Phantoms

Acrylamide-based polymers are the most popular materials utilized for fabrication of thermal phantoms. Polyacrylamide (PAA) phantoms are fabricated by crosslinking of acrylamide monomer (AA) using N,N'-methylene bisacrylamide (MBAA) in aqueous solutions at room temperature in presence of an initiator usually ammonium persulphate (APS) and N,N,N',N'-tetramethyl ethylenediamine (TEMED) (Siddiqi et al., 2013).

2.2.2.1 Phantom Recipes

The PAA phantoms are widely used for simulation of human body in both RF and MW frequency ranges (Andreuccetti et al., 1988; Bini et al., 1984; Surowiec et al., 1992). The composition and various properties of the most popular recipes used for construction of RF/MW PAA phantoms are shown in Table 2.4.

Table 2.4: The ingredients and properties of different suggested PAA phantoms. The amounts of ingredients are presented in %w/v, unless otherwise stated.

	Bini et al., 1984		**Andreuccetti et al., 1988**	**Surowiec et al., 1992**	
	High-water	**Low-water**		**Muscle**	**Lung**
Acrylamide	15	40	27-32	26 (%w/w)	28 (%w/w)
MBAA	0.10	~0.27	0.18-0.21	0.196 (%w/w)	0.22 (%w/w)
TEMED	~0.39 (0.5 ml)	~1.03 (1.33 ml)	0.70-0.82	0.05 (%w/w)	0.05 (%w/w)
APS	0.13	0.07	0.13	1 (%w/w)	0.75 (%w/w)
NaCl	0.50[a]	0.58	0-1.75	1.05 (%w/w)	0.43 (%w/w)
Glycerine	-	-	-	-	15 (%w/w)
Water	the rest	-	the rest	the rest	the rest
Ethylene glycol	-	the rest	-	-	-
f (MHz)	27[a]	27	750-5500	500-3000	500-3000
T (ºC)	20[a]	20	20	37	37
ρ (kg.m^{-3})	1030	~ 1000	-	1070	-
C (kJ.kg^{-1}.K^{-1})	4.18	~ 4.18	-	3.47	-
κ (W.m^{-1}.K^{-1})	0.41	0.23	~ 0.40	0.40 (0.56[b])	-
σ (S.m^{-1})	0.61	0.01	-	-	-
ε_r'	-	21.80	44.50-52	63	38

[a]The authors proposed a formula to determine the needed NaCl based on temperature (20-40ºC) and frequency (13.56-40 MHz). However for brevity, only the base recipe for T=20ºC and f=27 MHz are presented here.
[b] Data was reported by Davidson & Sherar, 2003.

The dielectric properties of these phantoms drastically depend on the type and ratio of the gel constituents. For instance, in order to simulate a low-conductivity tissue, the NaCl content need be reduced. Lower levels of conductivity are also obtained by reducing the APS ratio. In fact, APS could be removed and the reaction is initiated by increasing the temperature near the melting point of acrylamide. Decreased permittivity values could be obtained using nonpolar or low-permittivity liquids (e.g. dioxane, pyridine, and ethylene glycol) instead of water. The AA concentration also exhibits a negative correlation with both electrical conductivity and relative permittivity as well as a positive correlation with mechanical strength (Bini et al., 1984). For application in HIFU experiments, the acoustic attenuation of PAA gels could be adjusted using evaporated milk, intralipid (Mcdonald et al., 2004) (or glycerol (Bu Lin et al., 2008) for enhanced transparency level), and corn syrup (Mcdonald et al., 2004; Park et al., 2010). The optothermal properties could also

be adjusted by addition of appropriate additives such as bovine haemoglobin (optical absorber), polyvinyl acetate (PVA; scattering particles), magnevist (T_1 contrast agent) and lumirem (T_2 contrast agent), in order to simulate biological tissues in laser studies (Bazrafshan et al., 2011).

2.2.2.2 Thermosensitive Acrylamide-Based Phantoms

The most crucial characteristic of PAA gels is their transparency in optical range, enabling visualization of the coagulation zone inside the phantoms by adding some thermosensitive ingredients including BSA, egg white (EW), non-ionic surface-active agents, and thermochromic dyes (NISAAs).

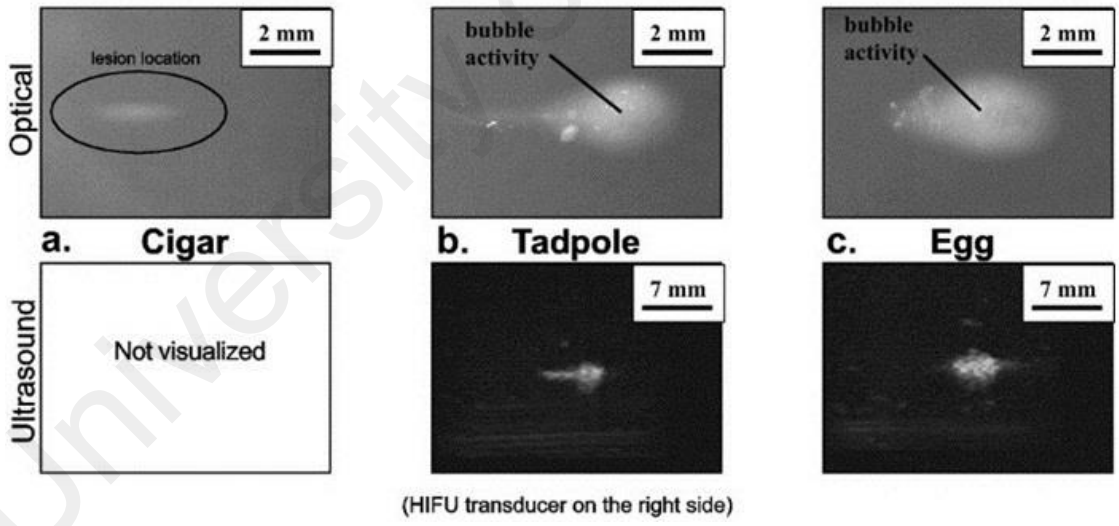

Figure 2.9: Thermal Lesions produced in a PAA phantom containing 6% BSA and their corresponding ultrasound images. (a) Cigar-shaped, (b) tadpole-shaped, and (c) egg-shaped lesions (Lafon et al., 2005). Reprinted with permission from Elsevier.

BSA is a popular thermosensitive protein which is widely used to capture the heat damage inside the phantoms (Bouchard et al., 2000). The thermal coagulation of BSA at temperatures between 60ºC to 70ºC, forms a white and opaque lesion in the phantom that represents the region where the temperature exceeded this threshold point. The thermal lesion also results in a reduced T_2 value which provides a contrast for observation of the heated region in T2-weighted MR images. These phantoms could be applied for determination of bubble activity during HIFU experiments. The gradual heating because of pure thermal effects results in a cigar-shaped lesion (Figure 2.9a) in PAA-BSA phantoms, while a combination of thermal and cavitational effects produces tadpole-shaped or egg-shaped lesions (Figure 2.9b-c) (Lafon et al., 2005).

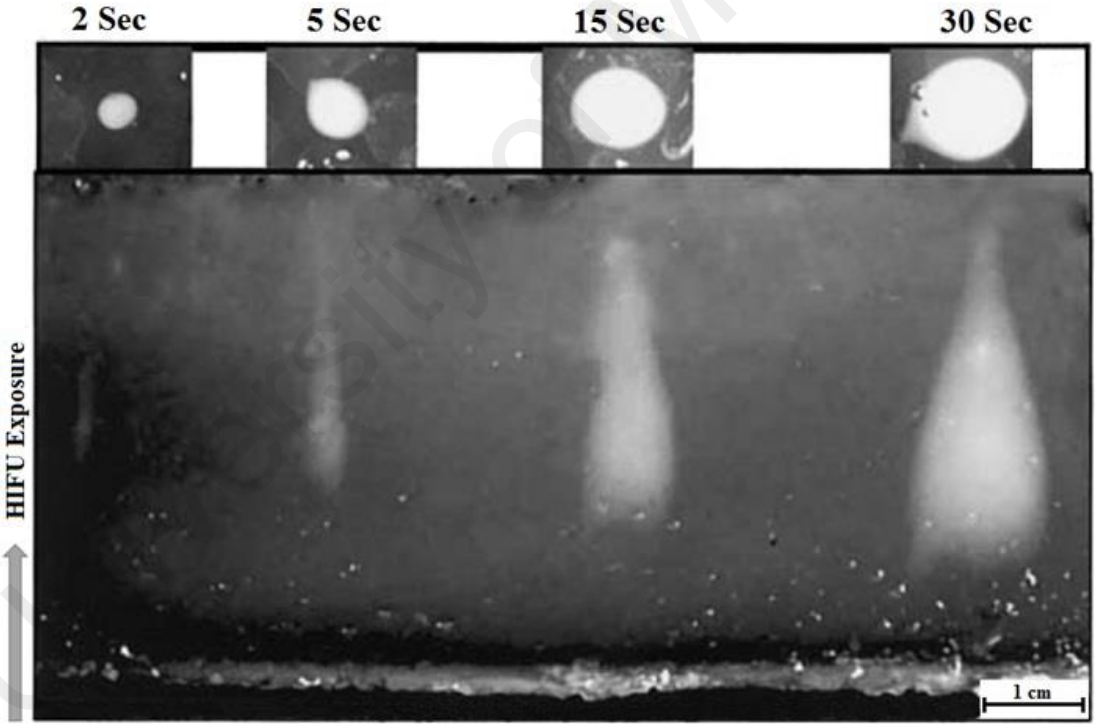

Figure 2.10: PAA phantom containing 30% EW sonicated with HIFU beams for 2, 5, 15 and 30 seconds. The cross and axial views of the coagulated lesion are shown at the top, and the bottom, respectively (Takegami et al., 2004). Reprinted with permission from Elsevier.

Table 2.5: The composition (%w/v) and various properties of PAA-BSA phantoms developed by researchers. Some data are presented as mean ± standard deviation.

	Lafon et al., 2005	**McDonald et al., 2004**	**Bu Lin et al., 2008[a]**
Acrylamide	7	7	9.50
MBAA	-	0.14	0.50
Initiators			
TEMED	~ 0.05[b]	-	-
APS	~0.07[b]	-	-
ascorbic acid	-	0.01	0.01
ferrous sulphate	-	0.0025	0.0025
H_2O_2	-	0.03	0.03
pH modifiers			
CCA	-	1.91	-
CAM	-	-	2.49
SCT	-	2.96	2.40
BSA	3-9	2	2 (lyophilized powder)
Sound Absorber			
Intralipid	-	6	-
Glycerol	-	-	~75 (60 ml)
Water	the rest	the rest	the rest
f (MHz)	1-5	5	0.47
T (ºC)	22	-	37
ρ ($kg.m^{-3}$)	1044	-	1069±3
T_{cog} (ºC)	>70	50-60	50-60
C ($kJ.kg^{-1}.K^{-1}$)	~5.1	-	3.68±0.20
κ ($W.m^{-1}.K^{-1}$)	0.70	-	-
α ($dB.cm^{-1}.MHz^{-1}$)	~0.08-0.18	0.52±0.03	-
c ($m.s^{-1}$)	1544	1556±4	-
P_{cav} (MPa)	~6[e] 8.67±0.44[f*] 0.94±0.13[f**]	-	-
σ ($S.m^{-1}$)	-	-	~0.12

Abbreviations: CAA, citric acid anhydrate; CAM, citric acid monohydrate; SCT, sodium citrate tribasic dehydrate.
[a]The authors examined the electrical properties of phantoms in three different pH phantoms (4.3, 4.5, and 4.7). However for brevity, only the data for the recipe with pH of 4.3 are presented in this table.
[b]0.01 ml TEMED per 15 ml Liqui-gel and 0.05 ml of 10 %APS solution per 15 ml Liqui-gel were used.
[c]Data are presented by Canney et al., 2010 for BSA ratio of 7 %w/v at f=2.158 MHz.
[d]The nonlinearity coefficient was measured by Lafon et al., 2005.
[e]The P_{cav} value was measured by Khokhlova et al., 2006 using a 200-cycle burst at f =2 MHz (7 %w/v BSA). The sonication duration and PRF were 4 seconds and 1 KHz, respectively.
[f]The values are reported by P. Zhang & Porter, 2010 using a 80-cycle pulse at f =2 MHz (7 %w/v BSA); [*]the recipe contains 0.3 %v/v albumin-coated dodecafluoropentane, [**]phantom contains 0.8 %v/v 2H, 3H-perfluoropentane.

The PAA-BSA phantoms provide an inertial cavitation threshold within a range similar to that of biological tissues (7-10 MPa) (Arora et al., 2008; Khokhlova et al., 2006; Zhang et al., 2010). The acoustic absorption and scattering of PAA-BSA phantoms could

be adjusted in the range of target tissues using evaporated milk, corn syrup, intralipid (Mcdonald et al., 2004), or glass beads (Choi et al., 2013). However, the coagulation temperature (T_{cog}) of these thermosensitive phantoms (approximately 60°C-70ºC) is relatively higher than that of biological tissues, resulting an inaccurate simulation of tissue coagulation during thermal therapies.

The coagulation temperature could be lowered to 50ºC by decreasing the pH from 4.7 to 4.3 using citrate buffer (Mcdonald et al., 2004). The pH level also shows a positive impact on specific heat capacity of the phantoms (Bu Lin et al., 2008). Another significant drawback of PAA-BSA phantoms is their low attenuation coefficient which could be 8 times smaller than that of real tissues (Lafon et al., 2005). Although the PAA-BSA phantoms are mostly used for HIFU experiment, their composition could be modified to present suitable dielectric properties for RF application (Bu Lin et al., 2008). The concentrations of AA and MBAA in RF phantoms must be higher compared to HIFU phantoms, enabling the gels to be hard enough for standing on the dispersive ground pad and tolerating insertion of electrodes without cracking. The composition and various properties of PAA-BSA phantoms are summarized in Table 2.5.

EW is another protein that is widely applied in construction of thermosensitive phantoms for HIFU experiments (Takegami et al., 2004). When a PAA-EW phantom is sonicated using HIFU beams, the EW protein in the focal point is heated and consequently coagulated (Figure 2.10). Using EW as a thermosensitive agent in the PAA phantoms results in similar benefits for lesion visualization as BSA, yet incurring a lower cost. An investigation on the influence of EW concentration on the acoustic properties of PAA phantoms demonstrated its positive impact on both sound speed and attenuation

coefficient. The attenuation coefficient could be adjusted between 0.1 and 1.3 $dB.cm^{-1}$ by varying the EW concentration (Takegami et al., 2004). Because of its high water content, EW could be used in construction of PAA-based thermosensitive phantoms without using additional water (Divkovic et al., 2007). Table 2.6 presents the composition and various properties of the PAA-EW phantoms developed in previous studies. The sound speed and attenuation coefficient of these phantoms exhibit positive and negative relationships with temperature, respectively. Studies also show an increased attenuation coefficient in the coagulated zone. However, the sound speed in the coagulated zone remains almost identical to that of non-coagulated material at constant temperatures (Divkovic et al., 2007).

Table 2.6: Various PAA-EW recipes suggested in the literature. The ratios are presented in %v/v.Some data are presented as mean ± standard deviation.

	Takegami et al., 2004	**Divkovic et al., 2007**	**Labuda & Church, 2011**
Acrylamide +MBAA[a]	24.80	~12.50	25
TEMED	0.20	~ 0.20	0.20
APS[b]	0.50	~ 0.50	0.50
Egg white	0-40	the rest	30
Water	the rest	-	the rest
f (MHz)	1.10-5.56	1-3	5
T (ºC)	25	26-55	25
ρ ($kg.m^{-3}$)	990-1000	1045±5	-
Tcog (ºC)	-	67	60
C ($kJ.kg^{-1}.K^{-1}$)	-	4.27±0.37	4.27
κ ($W.m^{-1}.K^{-1}$)	-	0.59±0.06	0.59
α ($dB.cm^{-1}.MHz^{-1}$)	0.14-1.29	0.14-0.67	1.04
c ($m.s^{-1}$)	1537-1544	1546±31	1541
Z (Mrayl)	-	-	1.50

[a]An aqueous solution containing 38 %w/w acrylamide and 2 %w/w bisacrylamide was used.
[b]A solution of 10 %w/w APS was used.

The crucial limitation of BSA and EW is their permanent coagulation process. Therefore, the phantom containing BSA or EW cannot be reused and need be discarded after coagulation occurs. To overcome this matter, non-ionic surface-active agents (NISAAs) have been proposed as alternatives for BSA and EW for construction of reusable thermal phantoms. NISAAs are a group of materials that undergo segregation when temperature exceeds a specific degree called "the clouding point (T_{CP})", resulting a white and opaque region. These materials return to their original transparency when cooled again below their clouding point. Several categories of NISAAs have been developed with different clouding points including polyoxyethylene-polypropylene condensates, polyoxyethylene-polypropylene condensates of ethylenediamine, second-class chained alcohol-ethoxylates, nonylphenol-ethoxylates, octhylphenol-ethoxylates, polyoxyethylene-cetylethers, and polyoxyethylene-alkylethers (Miyakawa et al., 1995). In general, T_{CP} depends on the NISAA type and ratio, the concentration of gelling and crosslinking agents, ratio of the ionization material (e.g. NaCl), and presence of some alcoholic compounds such as methanol, ethanol, 1-propanol (as T_{CP} boosters), and n-butanol (as T_{CP} moderator) (Miyakawa et al., 1995; Park et al., 2010). T_{CP} is also affected by the pH level and the type of buffer. In particular, acetate and tromethamine buffers show weaker suppression of T_{CP} than citrate and phosphate buffers (Park et al., 2010).

Various types of NISAAs with different clouding points ranging from 20ºC to above 100ºC have been examined for construction of thermosensitive phantoms in RF/MW (Miyakawa et al., 1995) and HIFU (Park et al., 2010) experiments (Table 2.7). The physical properties of the PAA phantoms may slightly be affected by addition of NISAAs. For instance, the addition of NISAAs results in small increases in both sound speed and acoustic impedance values, while the attenuation coefficients and densities

remain almost constant (Park et al., 2010). However, a significant drawback of NISAAs is a wide gap between the onset and ending temperatures of clouding. Using a NISSA from the polyoxyethylene-alkylether category could result a 17ºC and 20ºC difference between the onset and ending temperatures of clouding and clearing processes, respectively. Moreover, the onset temperature of clearing is approximately 5ºC lower than the ending temperature of clouding (Park et al., 2010). These results show the inability of NISAAs in precise estimation of temperature rise inside the phantom.

Table 2.7: The composition and properties of PAA-NISAA thermal phantoms. Data are reported in (%w/w), unless otherwise stated. Some data are presented as mean ± standard deviation.

	Miyakawa et al., 1995	**Miyakawa et al., 1998**		**Park et al., 2010**
Acrylamide + MBAA	3[a]	3[a]	13[a]	7.50 (v/v)[b]
TEMED	0.02-0.50[c]	0.02-0.50[c]	0.02-0.50[c]	0.05 (%v/v)
AMPS	0.03-0.14[c]	0.03-0.14[c]	0.03-0.14[c]	~0.80• (%v/v)
NISAA	1	1	0.5	5 (%w/v)
NaCl	0.29-0.83	2.5	2.5	-
Butanol	-	0.5	-	-
Sucrose	-	-	24	-
Corn syrup	-	-	-	40 (%w/v)
Water	the rest	the rest	the rest	58 (%v/v)
f (MHz)	27-860	430	850	1-5
T (ºC)	25	25	25	25
ρ ($kg.m^{-3}$)	-	1020	-	
T_{CP} (ºC)	30.70-31.60	30.10	18	48-57 (onset) 65-74 (ending)
C ($kJ.kg^{-1}.K^{-1}$)	-	4.25	-	-
κ ($W.m^{-1}.K^{-1}$)	-	6.45×10^{3}	-	-
α ($dB.cm^{-1}.MHz^{-1}$)	-	-	-	0.40±0.05
c ($m.s^{-1}$)	-	-	-	1568-1573
σ ($S.m^{-1}$)	-	1.21	1.69	-
ε_r'	72.50-79.80	73.50	51.60	-

[a]Containing 2 % MBAA.
[b]An aqueous solution containing 38 %w/w acrylamide and 2 %w/w bisacrylamide was used.
[c]The concentration varies according to the room temperature.

Due to their suitable mechanical properties, PAA-based gels also allow the construction of thermosensitive vasculature-mimicking phantoms (Jiang et al., 2012). In these phantoms, a thin-wall vessel compartment is produced using a thermal-sensitive powder and silicon-based gel. Due to the optical transparency of the surrounding PAA gel, the temperature changes of the vessel-mimicking component could be visually observed during HIFU sonication.

2.2.2.3 Advantages and Limitations

Acrylamide is the most widely used gelling agent for construction of thermosensitive phantoms, especially for HIFU application. These gels exhibit high melting points which provide a sufficient stability in thermal therapy experiments (Lazebnik et al., 2005). The optical transparency, formability into complex forms, gel-like mechanical properties, and the ability to represent a wide range of thermal, electrical, and acoustic properties are other attractive properties which make these gels promising candidates for simulation of both high-water-content, and low-permittivity, low-conductivity tissues (bone and fat) (Lazebnik et al., 2005).

In general, toxicity of the ingredients is the most critical limitation of the PAA-based phantoms. Acrylamide monomer is a severe neurotoxin that requires extreme precautionary measures during the fabrication process. These phantoms also show a limited shelf life –from several hours when exposed to air to few weeks when kept in an air-tight container (Bini et al., 1984). The polymerization of acrylamide is an exothermic reaction, causing a rapid temperature rise shortly after mixing the solutions. This

temperature rise may consequently cause an undesired coagulation of the thermosensitive proteins during the phantom preparation. Furthermore, due to a rapid polymerization reaction, a short time period (about 30 seconds) is available for stirring, casting, and degassing the unpolymerized solution. Continuous cooling of the mixture prior to polymerization may increase the available time for stirring and degassing of the solution.

2.2.3 Gelatine Phantoms

Gelatine is a mixture of peptides and proteins produced by physical, thermal, or chemical degradation of collagen extracted from the skin, tendon, cartilage, bone and some intestines of animals. Gelatine is widely used as a gelling agent in the medical and pharmaceutical fields due to its bio-compatibility, bio-degradability, non-immunogenicity, biological origin, and commercial availability at low cost (Bigi et al., 2002; Yamamoto et al., 2001; Zhang et al., 2006). The gelation process of this material that occurs at temperatures below 40°C, is due to a conformational disorder–order transition of the gelatine chains which form thermo-reversible networks by associating helices in junction zones stabilized by hydrogen bonds (Bigi et al., 2002).

2.2.3.1 Phantom Recipes

The first gelatine thermal phantom was developed to simulate the dielectric properties of human muscle at low frequencies (Marchal et al., 1989). This gel was composed of 20% gelatine with electrical conductivity of 0.27-0.48 $S.m^{-1}$ and relative permittivity of

90-93 at 27 MHz and temperature range of 15 to 50°C (Marchal et al., 1989). Examination of dielectric constant and electrical conductivity of this phantom in frequency range of 10-150 MHz showed the positive and negative impacts of applied frequency on electrical conductivity and dielectric constant, respectively (Nadi et al., 1992). Due to their appropriate dielectric, thermal, and physical properties, the gelatine-based phantoms are suitable for simulation of both high-water (muscle) and low-water (fat) tissues at different frequency ranges (Table 2.8) (Robinson et al., 1991; Yuan et al., 2012).

Table 2.8: The ingredients and various characteristics of gelatine-based phantoms. The concentration of ingredients are presented in (%w/w), unless otherwise is stated.

	Robinson et al., 1991		**Sunaga et al., 2003**	**Yuan et al., 2012**		
	Muscle	**Fat**		**Tumour[b]**	**Muscle[b]**	**Fat [b,c]**
Gelatine	10	5	13.50	95 (%v/v)[d]	90 (%v/v)[d]	15 (%v/v)[d]
Oil				5 (%v/v)	10 (%v/v)	85 (%v/v)
NaCl	2	-	1.70	0.75 (%w/v)	0.60 (%w/v)	0.024 (%w/v)
PE	-	40[a]	-	-	-	-
Honey	-	-	50.10	-	-	-
Ethanediol	48	55	-	-	-	-
Water	the rest	-	the rest	-	-	-
f (MHz)	50-2450	50-2450	64-400	100-433	100-433	100-433
T (ºC)	20	20	20	37	37	37
ρ ($kg.m^{-3}$)	1100	950	-	-	-	-
C ($kJ.kg^{-1}.K^{-1}$)	3.70	2.25	-	3.71	3.48	2.-17
κ ($W.m^{-1}.K^{-1}$)	0.43	0.29	-	0.49	0.42	0.20
σ ($S.m^{-1}$)	-	-	0.41-0.66	0.844-0.969	0.641-0.759	0.019-0.034
ε_r'	39.50-53.60	6.00-11.40	49.50-56.30	61.52-69.38	55.30-61.47	6.78-7.66

[a]A drop of detergent was also added to help wet the polythene powder which is then stirred in.
[b]The solution contains a small amount of surfactant to decrease the surface tension between oil and water.
[c]The fat and the bone marrow materials had same composition, since their dielectric properties were very similar in the studied frequency range.
[d]An aqueous gelatine solution was used in this recipe.

2.2.3.2 Heterogeneous Gelatine Phantoms

A crucial advantage of gelatines is their ability to fabricate heterogeneous structures with long-term stability of physical and mechanical properties (Madsen et al., 2003). Based on this fact, a stable heterogeneous breast phantoms for ultra-wide band frequencies (0.5-20 GHz) has been developed (Lazebnik et al., 2005). The dielectric properties of this phantom was adjusted using a varying ratio of an oil (a solution of 50% kerosene and 50% safflower oil). In this recipe, a component containing 10% oil was made to represent the hepatic tissue at both 915 and 2450 MHz, whereas the gels containing 80% and 10% oil were produced for mimicking the breast fat and cancerous lesions at frequency range of 1 to 11 GHz, respectively (Lazebnik et al., 2005).

The geometrical, thermal, and dielectric properties of human thigh with fat, muscle and deep-seated tumour could also be simulated using heterogeneous gelatine phantoms (Yuan et al., 2012). For this aim, the mixture of kerosene and safflower oil must be substituted by pure canola oil due to the closer thermal and MR properties of canola oil to human fat. A few drops of a surfactant need also be added to decrease the surface tension between the canola oil and water. At higher frequencies, due to a significant increase in water conductivity, both dielectric constant and electrical conductivity must be adjusted by increasing the oil ratio. The composition and properties of these phantoms at various frequency and temperature ranges are summarized in Table 2.8.

Because of suitable optical properties, the gelatine phantoms are also applicable in construction of heterogeneous tumour-tissue structures for optothermal studies. The normal tissue is simulated using gelatine and Liposyn II intralipid, while the tumour-mimicking sphere is prepared using same recipe with designated ratios of indocyanine

green. The indocyanine green results in a higher absorption coefficient and consequently, increased energy storage within the tumour-mimicking region. Similarly, gelatine has been used in construction of prostate phantoms incorporating tumour, rectum and urethra for laser ablation studies (Lindner et al., 2010).

2.2.3.3 Advantages and Limitations

The long-term stability, low cost, and facile production of gelatine-based phantoms make these materials suitable for serial studies. Despite the base phantoms are easily fabricated by mixing of gelatine in aqueous solutions, various additives including acrylamide/MBAA as coagulant (Baldock et al., 1998), ethanediol and PE powder as modifiers of electrical properties (Robinson et al., 1991), honey syrup as preservative (Sunaga et al., 2003), glutaraldehyde as gelation accelerator (Madsen et al., 2003), and graphite powder as controller of acoustic properties (Anderson et al., 2011) could be used in order to modify the physical and mechanical properties of these gels. On the other hand, the main limitation of gelatine phantoms is their low mechanical strength as well as low melting temperature which makes them impractical for application in temperature regimes above 50°C. Although both thermal and mechanical stability of these phantoms could be improved by addition of formaldehyde as a crosslinking agent (Lazebnik et al., 2005), the resulted phantoms may not provide favourable thermal and mechanical properties compared to acrylamide or agar phantoms.

Table 2.9 summarizes the various advantages and limitations of the thermal phantoms described in this chapter. It is important to note that a number of other gelling agents such

as TX-150, hydroxyethyl cellulose carrageenan, gellan gum, carrageenan, and alginate have also shown potential as thermal phantoms. The advantages and shortcomings as well as the various properties of these phantoms are comprehensively reviewed in our published article (Dabbagh et al., 2014). However, in spite of showing desirable physical properties, these materials have not been widely used in hyperthermia or thermal ablation studies and their critical properties have not been sufficiently established. Therefore, further studies are necessary for well characterization of these materials in various aspects which are crucial in thermal therapy experiments.

Table 2.9: A brief comparison of various gelling agents described in this study.

	Advantages	**Limitations**	**Suggested Use**
Agar	Thermal stability Mechanical Strength Applicable in a wide frequency range Adjustable physical properties Capability of producing hetero-geneous structures Useful for making Perfused phantoms	High opacity Low permittivity Low cavitation threshold	1) RF 2) MW 3) HIFU 4) LIT
Polyacryl-amide	Optical transparency Thermal stability Mechanical strength High formability Applicable for construction of heat sensitive phantoms Adjustable physical properties Thermosensitive Perfused phantoms Desirable cavitation threshold range	Toxic ingredients High cost of preparation Complicated construction process Limited shelf-life	1) HIFU 2) RF 3) MW 4) LIT
Gelatine	Ease of construction Low-cost ingredients Long-term stability Applicable in fabrication of hetero-geneous structures	Low melting point Insufficient mechanical strength High Opacity level	1) LIT 2) MW 3) RF

Abbreviations. RF: radiofrequency; MW: microwave; HIFU: high intensity focused ultrasound; LIT: laser-induced therapy

CHAPTER 3: REUSABLE THERMOSENSITIVE PHANTOM FOR PRECISE ESTIMATION OF TEMPERATURE IN HYPERTHERMIA APPLICATION

3.1 Introduction

With the rapid development of thermal therapies, there has been a growing interest on research concerning the influence of high temperatures on various properties of the biological tissues. However, due to substantial difficulties in the preparation, handling, maintenance, and standardization of the real tissues, the availability of effective phantoms with similar properties to target tissues is essential for these high temperature studies. A multitude of materials have been proposed in liquid, solid, and gel (semisolid) forms; but the gel phantoms have found more popularity among researchers due to their physical similarities to both soft and hard tissues, as well as their capability to represent a wide range of thermal, electrical, acoustic, and optical properties. One particular advantage of the gels is that they can easily be formed in different shapes so that realistic irradiation geometries are reproduced.

A number of gelling agents including TX-150 (Chou et al., 1984), agar/agarose (Gasselhuber et al., 2012a; Ito et al., 2001; Kato et al., 1987; Liu et al., 2006; Mylonopoulou et al., 2013; Ortega et al., 2010; Siddiqi et al., 2013), polyacrylamide (PAA) (Bazrafshan et al., 2011; Bini et al., 1984; Davidson et al., 2003; Surowiec et al., 1992), hydroxyethyl cellulose (HEC) (Ozen et al., 2005; Prakash et al., 2006; Stauffer et al., 2003), gelatin (Lazebnik et al., 2005; Lindner et al., 2010; Marchal et al., 1989; Yuan et al., 2012), gellan gum (Miyakawa et al., 1995), carrageenan (Kato et al., 2004; Yoshida et al., 2004), and sodium alginate (Sarkar et al., 2011a; Sarkar et al., 2011b) have been suggested so far for fabrication of thermal phantoms. However, PAA hydrogels are the

most popular materials for construction of the thermal phantoms. These gels are transparent in optical range, enabling the researchers to visualize the coagulation zone inside the phantoms by adding some thermosensitive ingredients. The added materials may cause a large change in magnetic resonance parameters (T_1 or T_2) or change the transparency level of PAA phantoms upon reaching the temperature range used in hyperthermia or thermal ablation procedures (Mcdonald et al., 2004). Bovine Serum Albumin (BSA) (Bu Lin et al., 2008; Choi et al., 2013; Mcdonald et al., 2004), and Egg white (EW) (Divkovic et al., 2007; Labuda et al., 2011; Takegami et al., 2004) are two popular thermosensitive agents proposed for visualization of the heated zone inside the PAA phantoms. The main drawback of PAA-BSA and PAA-EW phantoms is the irreversibility of coagulation process making the phantom useless for some routine applications such as calibration of thermal devices. Moreover, the exothermal nature of acrylamide polymerization may cause an unwanted coagulation of the thermosensitive agent during phantom preparation. Due to these shortcomings, Non-ionic surface-active agents (NISAAs) have been suggested to develop thermosensitive phantoms that have reversible reaction to the temperature changes (Park et al., 2010). NiSAAs are a group of materials that become segregated when temperature exceeds a specific threshold level called "the clouding point (T_{CP})", resulting a white and opaque region in the phantom and return to their original transparency when cooled again below the clouding point. However, similar to PAA-BSA and PAA-EW phantoms, the threshold temperature of these phantoms is inaccurate, making the researchers unable to precisely estimate the temperature profile inside the phantom. Park et al., 2010 evaluated the clouding and clearing (the temperature that NISAA recover its transparency) points of NISAAs and found that there was a 17ºC difference between the start and ending temperatures of

clouding process of a typical NISAA material. Moreover, the onset temperature of clearing process started at about 5ºC lower than the ending temperature of clouding process. Therefore, construction of reusable thermosensitive phantoms for accurate estimation of temperature distribution is still a challenge.

In the present study, we introduce a new thermosensitive PAA gel containing a thermochromic dye (TCD) of type N-(2-ethoxyphenyl)-N'-(2-ethylphenyl) ethanediamine as a new phantom for hyperthermia and thermal ablation studies. TCDs are usually coloured below a specified temperature and become colourless (transparent) above this temperature level. These dyes have a reversible thermal-sensitivity behaviour with a more accurate threshold temperature compared to that of BSA, EW and NISAAs. A number of TCDs with threshold temperatures ranging from -15°C up to 100°C are available. These materials are mainly composed of a dye as colour former, a weak organic acid as colour developer, and a solvent, which are microencapsulated to prevent the contents from undesired reactions. During the heating of the microcapsules, the solvent alteration between the solid and liquid states causes the colour-former component to be in contact below the transition temperature (coloured state) and separated above this temperature (discoloured state). This process could be repeated for a few thousand times (Kulčar et al., 2010).

The introduced thermosensitive phantom could be used for more accurate visualization of the temperature distribution during the heating and cooling stages in the high temperature experiments, evaluation of the heating and cooling rates, acoustic and electromagnetic dosimetry, and calibration of thermal devices. The low cost of preparation due to the low amount of required TCD as well as the ability to be made at

flexible temperatures, are the other advantages of these phantoms that make them attractive candidates for irradiation experiments including RF and magnetic resonance-guided focused ultrasound (MRgFUS) modalities.

3.2 Materials and Methods

3.2.1 Gel Fabrication

For preparation of the thermal phantom, acrylamide monomer (AA; gelling agent), N, N´-methylene bisacrylamide (MBAA; crosslinking agent), NaCl, N,N,N',N'-tetramethyl ethylenediamine (TEMED; catalyser), and ammonium persulphate (APS; polymerization primer) were purchased from Sigma-Aldrich (M) SDN. BHD. (Kuala Lumpur, Malaysia). The TCD was obtained from Thermographic Measurements Co. Ltd. (TMC, Flintshire, UK). Various types of TCDs with different colours and threshold temperatures (from -15 to 100ºC) are available; however, the selected dye for this study was blue at room temperature with threshold temperature of 47±2ºC. The rationale for the selection of this TCD was based on the proximity of its threshold temperature to the coagulation temperature of real tissues, making the phantom desirable for simulation of organic tissues in hyperthermia studies. It is noteworthy that the proposed recipe is merely valid for the ablative temperature ranges (45ºC to 55ºC) and it is not applicable for the mild hyperthermia application that applies a lower level of temperature (40ºC to 45ºC) (Partanen et al., 2012). Therefore, in order to construct an appropriate phantom for this temperature range, a TCD with lower threshold temperature must be used.

Table 3.1: Chemical Composition of the phantoms used in this study.

	AA (g)	MBAA (g)	TEMED (ml)	APS[a] (ml)	NaCl (g)	TCD (g)	Degassed Water (ml)
REP	7.5	0.05	0.25	5	0.25	-	45
TSP	7.5	0.05	0.25	5	0.25	0.03	45

[a]A 1.3 %w/v aqueous solution was used according to the recipe proposed by Bini et al., 1984.

The composition of the fabricated thermosensitive phantom (TSP) is presented in Table 3.1. A reference phantom (REP) with a same recipe (but without TCD) was also made to investigate the effects of the dye on acoustic and thermal properties of the phantom. This recipe was chosen due to its self-supporting ability that provides the possibility of being used outside the container for RF and MRgFUS studies. Meanwhile, the phantom has sufficient softness that allows the penetration of RF needle without cracking. The optimum concentration of the TCD was determined in preliminary experiments; while too much amount of dye results in a non-transparent gel, too little concentration of dye leads to low thermal-sensitivity and optical contrast.

In the present study, a cylindrical mould (60 ml, 4.0 cm diameter, and 5.0 cm height) was used. For preparation of a typical phantom, firstly the AA, MBAA, NaCl, TEMED, and TCD (for the TSP phantom) were mixed in-situ in designated amount of degassed water for 15 minutes. Secondly, APS solution was added and the mixture was homogenized using homogenizer (T25 Ultra-Turrax, IKA Works Inc., Wilmington, DE) for 30 seconds at 5000 rpm to initiate the polymerization. The higher rates of homogenization may cause the formation of microbubbles inside the phantom, whereas the lower rates may result in an inhomogeneous mixture. The solution was allowed to polymerize for 24 hours at room temperature before performing further experiments. After completion of polymerization, the phantom was removed from the container and

analysed by ultrasound imaging system to evaluate the homogeneity of its structure. It is important to note that the acrylamide monomer is a severe neurotoxin that causes severe health hazards. Therefore, the usage of this compound requires extreme precautionary measures (Siddiqi et al., 2013).

3.2.2 Experimental Procedures

In this study, the compositions of the REP and TSP phantoms were compared by Fourier transmission infrared spectrometry (FT-IR; Nicolet 6700, Thermo Scientific, Waltham, MA, USA). For determination of the onset (T_{od}) and ending (T_{ed}) temperatures of discolouration during heating, the spectrophotometry analysis (Dataflash 100, Datacolor International, Lawrenceville, NJ) was used. In these experiments, a number of 60 TSP discs (4.0 cm diameter and 1.0 cm thickness) were heated in a water-bath at twelve temperatures between 40°C to 53°C (5 discs for each temperature). Then, by assigning a REP disc as reference, the changes in the CIELAB values of the TSP discs including Db* (difference in yellow/blue values), DL* (difference in darkness/lightness values), and DE* (total colour difference) at different temperatures were measured. The obtained results were later analysed by analysis of variance (ANOVA) with 95% confidence interval using the Statistical Package for Social Sciences software (SPSS 20, SPSS Inc., Chicago, IL, USA); then, the first and last temperatures at which the CIELAB values were statistically different from the previous temperature points were considered as T_{od} and T_{ed}, respectively. A similar protocol was used for measurement of the onset (T_{oc}) and ending (T_{ec}) temperatures of colouration during cooling.

The acoustic and thermal parameters of the TSP were also measured and compared with that of REP phantom. The sound speed and the attenuation coefficient were measured by oscilloscope (GW-Instek GDS 2102, Good Will Instrument, New Taipei City, Taiwan) and Ultrasound Power Meter (UPM-DT-10AV, Ohmic Instruments Inc., Easton, MD, USA), respectively. The experiments were performed at room temperature and frequency of 1 MHz as the typical frequency in high intensity focused ultrasound (HIFU). Thermal conductivity and specific heat capacity values were calculated using a thermal analyser (KD2 Pro, Decagon Devices, Pullman, WA, USA). The latent heat of melting and melting point of the phantoms were measured by differential scanning calorimetry (DSC; DSC820 with TSO 801RO robot, Mettler-Toledo, Columbus, OH, USA). Thermogravimetric analysis (TGA; TGA/SDTA 851e, Mettler-Toledo, Columbus, OH, USA) was also conducted to investigate the physical stability of the phantoms at high temperature regimes. All the above experiments were repeated for at least five times and the results were evaluated by analysis of variance (ANOVA) technique with 95% confidence interval.

For heating of the TSP phantom, the RF and MRgFUS methods were applied. The RF procedure was performed by inserting the RF electrode (RITA Medical Systems, Mountain View, CA, USA) into the phantom with 1 cm above the bottom. The frequency and Power were set to 460 MHz and 50 W, respectively. The procedure was continued for 60 seconds with the target temperature of 100ºC. The development of the colourless region in the phantom was recorded by digital camera during the procedure. For experimental estimation of the Specific Absorption Rate (SAR) of electromagnetic power inside the TSP phantom, the obtained images were analysed using an image processing software (ImageJ 1.44P, National Institutes of Health, Bethesda, MD, USA). The

MRgFUS experiments were also conducted using clinical system (EX-ablate, Insightec, Haifa, Israel) available at University of Malaya Medical Centre. In these experiments, the phantom was placed in a water tank and sonicated for 20 seconds at frequency of 1.15 MHz with the acoustic energy and acoustic power of 2847 J and 142 W, respectively. The MR images of the TSP phantom were collected at different sonication times to visualize the propagation of coagulation zone during MRgFUS treatment.

3.3 Results and Discussion

Polymerization of acrylamide is an exothermic reaction causing a rapid temperature rise shortly after the addition of the initiator to the solution. Due to the rapid polymerization reaction, a short time period (about 30 seconds) is available for mixing the APS initiator in the solution and possibly pouring the liquid into a suitable mould. Therefore, inhomogeneity of the PAA phantoms is a common issue after the completion of polymerization. Therefore, a high-speed homogenizer was used in our experiments to rapidly mix the initiator into the mixture before polymerization occurs. Figure 3.1 shows the ultrasound images of REP and TSP phantoms that confirms the homogenous structure of both phantoms. This figure also shows that the phantoms have provided sufficient contrast to be distinguished in ultrasound images. The added TCD contains microcapsules with diameters ranging from 1-5 μm. As a result, the transparency of the phantom to ultrasound beam is slightly reduced due to addition of the TCD. The FT-IR spectra of the TCD and fabricated phantoms are also shown in Figure 3.2. This figure shows that the addition of thermochromic dye has negligible impact on the absorption spectra of the phantom due to low amount of dye used.

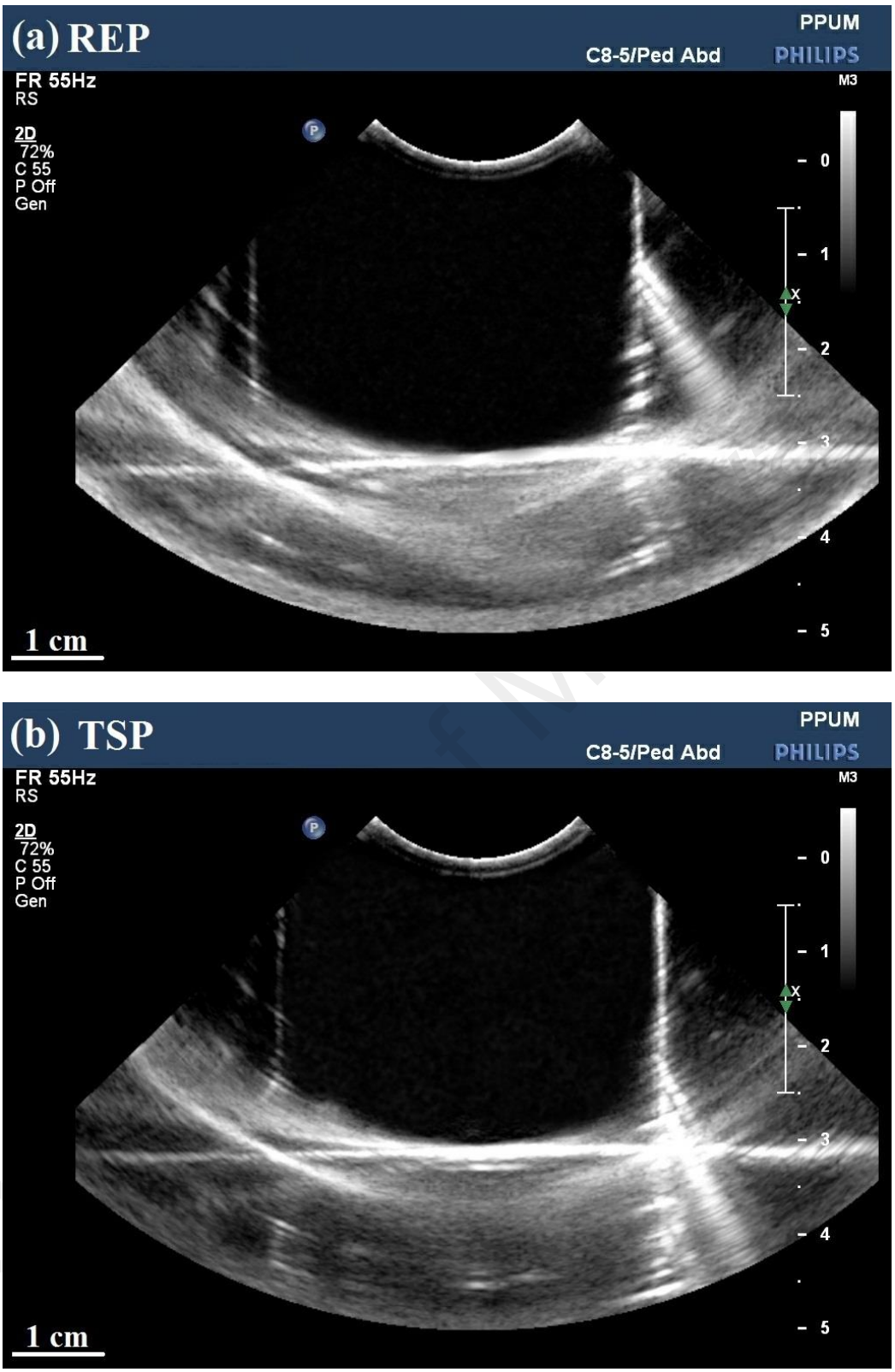

Figure 3.1: A typical ultrasound image of a) REP, and b) TSP. The bright lines at the margins are the optical reflection off the phantom surfaces.

The results of spectrophotometry analysis of the TSP phantom are plotted in Figure 3.3. For determination of the threshold temperature of the TSP phantom, the CIELAB values of the phantom were calculated during heating in temperature range of 40°C to 53°C and the point at which the temperatures of two CIELAB values (especially DE*) become statistically different was considered as threshold temperature.

According to the CIELAB spectra shown in Figure 3.3, the threshold temperature of the thermosensitive phantoms is 50±3ºC. This temperature is higher compared to the disclosed threshold temperature of the thermochromic dye (47±2°C) meaning that the threshold temperature of the TCD is increased after its addition to the phantom mixture.

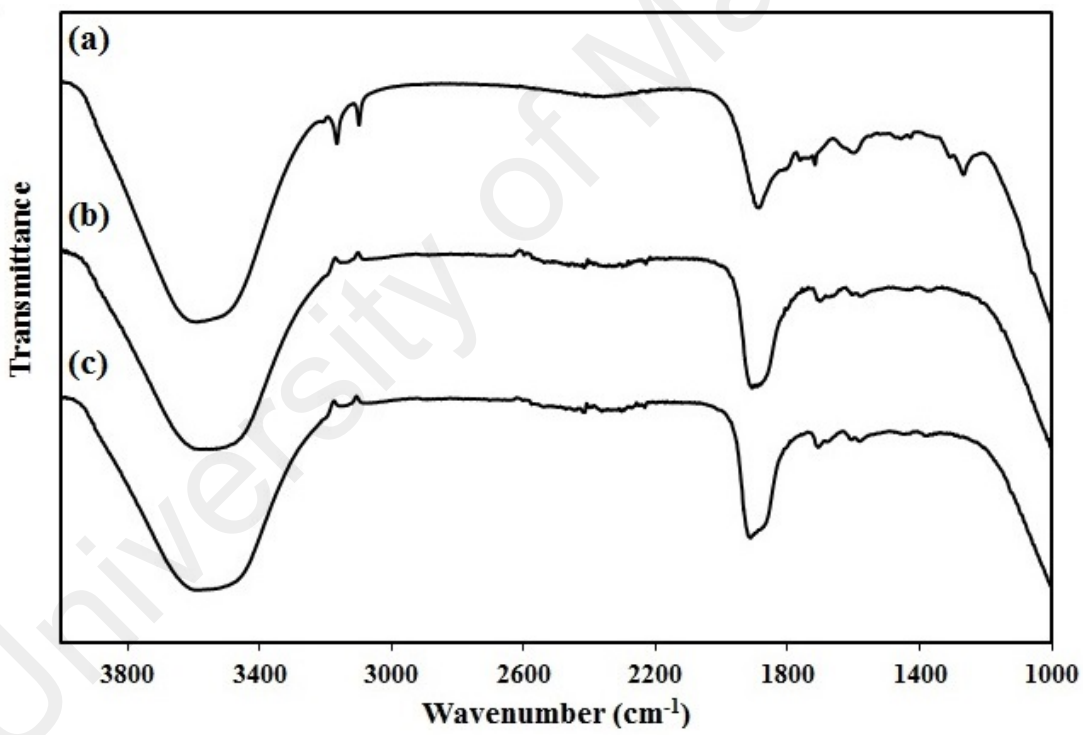

Figure 3.2: The FT-IR spectrum of a) TCD, b) REP, and c) TSP. Due to small quantity of TCD incorporated into the TSP formulation, no significant difference was observed between the FT-IR spectra of REP and TSP specimens.

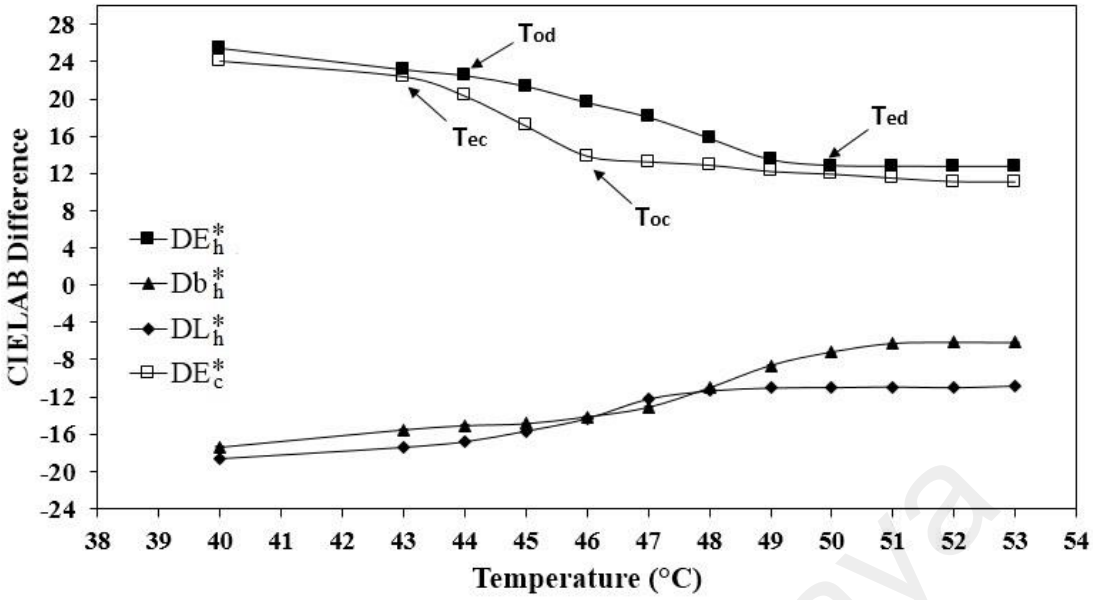

Figure 3.3: Different spectrophotometry spectra of a typical TSP specimen. Db*: The yellow/blue value; DL*: the darkness/lightness value; DE*: the total colour difference. The "h" and "c" subscripts represent the heating and cooling processes, respectively. T_{od}: onset temperature of discolouration; T_{ed}: ending temperature of discolouration; T_{oc}: onset temperature of colouration; T_{ec}: ending temperature of colouration.

Figure 3.3 also shows that the temperature interval between the onset and ending temperatures of discolouration is 6ºC. Moreover, the onset temperature of colouration during cooling is 4ºC lower than the ending temperature of discolouration during heating of the TSP phantom. However, the slopes of colouration are larger compared to discolouration, meaning that the colouration is completed faster than the discolouration process. Such a phenomena is occurring due to the effect of thermal history on colouration process of the TCD, i.e. the particular colour or temperature level reached during heating. This behaviour of the TCD ink is called "hysteresis". Therefore, colour hysteresis describes the interval between the T_{ed} and T_{oc} of a TCD as a function of thermal history.

In general, hysteresis is a characteristic of TCDs which may slightly depend on the TCD type used. For instance, the hysteresis in the phantoms containing a black-coloured TCD ink with threshold temperature of 55°C was measured about 5°C. In overall, the values measured in our study confirm that the TCD could provide a more accurate estimation of thermal profile than NISAA materials in spite of the comparable results for the hysteresis between the T_{oc} and T_{ed} in phantoms containing NISAAs (5°C) and TCD (4°C).

The thermal and acoustic properties of the REP and TSP phantoms are summarized in Table 3.2. The data presented in this table demonstrate that both sound speed and attenuation values are increased by addition of the dye. On the other hand, the specific heat and thermal conductivity are slightly smaller compared to those of REP phantom; although, the ANOVA results do not indicate a significant difference between the sound speed, attenuation, specific heat, and thermal conductivity values of the REP and TSP phantoms. It should be noted that the attenuation coefficient of the phantom has a positive correlation with the applied frequency and therefore, at frequency ranges which are regularly used in RF treatments (e.g. 460 MHz), the attenuation coefficient is drastically higher compared to the values measured at 1 MHz (Takegami et al., 2004). However, due to the independency of the RF modality on the acoustic parameters, the final result of the RF experiments is not affected by alteration of the attenuation coefficient.

Table 3.2: Acoustic and thermal properties of the REP and TSP specimens. Data are presented as mean ± standard deviation.

	Sound Speed ($m.s^{-1}$)	Attenuation (dB/cm)	Specific Heat ($kJ.kg^{-1}.K^{-1}$)	Thermal Conductivity ($W.m^{-1}.K^{-1}$)	Melting Point (ºC)	Latent Heat of Melting ($J.g^{-1}$)
REP	1571±5	0.12±0.01	3.68±0.22	0.60±0.02	113±7	1251±10
TSP	1579±6	0.14±0.01	3.59±0.21	0.59±0.02	112±9	1229±10

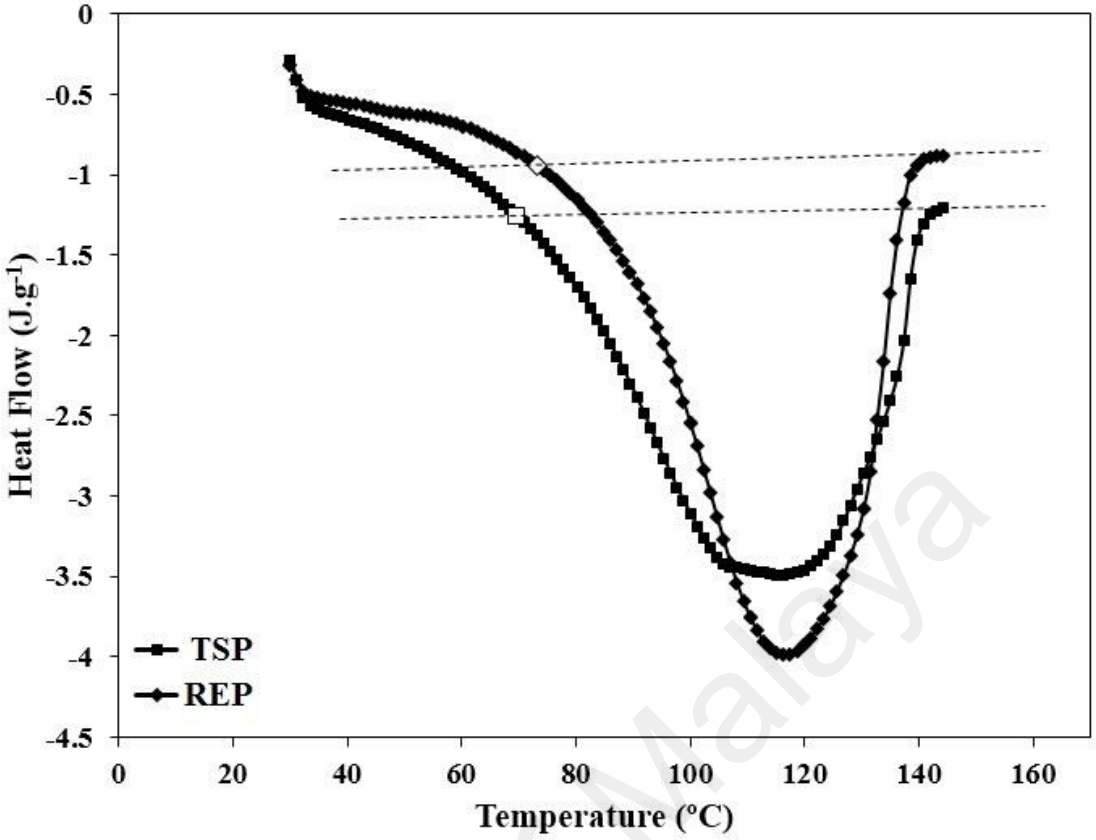

Figure 3.4: The DSC spectra of two typical REP and TSP specimens. The white markers represent the onset melting temperatures of these two typical phantoms.

Table 3.2 also shows that the melting point of the phantom is not affected by addition of the dye; whereas, the DSC spectra of the phantoms (Figure 3.4) illustrates a significant decrease in the onset temperature of melting (from 75ºC to 66ºC) of the TSP compared to the REP gel. Therefore, despite the negligible influence of the TCD on the melting point of the phantom, the transition interval between the gel and liquid phases is larger in phantoms containing TCD. Moreover, according to Table 3.2 and ANOVA analysis, the latent heat of melting of the TSP phantom is significantly lower than that of REP phantom. These facts reveal that, in spite of the similar melting points, deformation of TSP phantoms occurs at lower temperatures compared to that of REP phantoms and thus,

the thermal stability of the PAA phantoms is decreased by addition of the TCD. However, this concern is not of critical importance at hyperthermia temperature ranges and must only be considered in the experiments where the applied temperature is above 66ºC.

The TGA spectra of the REP and TSP phantoms are also shown in Figure 3.5. The thermal decomposition of both REP and TSP phantoms occurs at similar temperature ranges which is mostly corresponded to water evaporation from the phantom. Although the boiling point of water is around 100ºC, the evaporation of water also occurs with lower rates at mild temperatures such as room or hyperthermia temperature ranges. Therefore, due to the substantial influence of the water content on the physical properties of these phantoms, for a long-term usage, the water evaporation must be avoided during

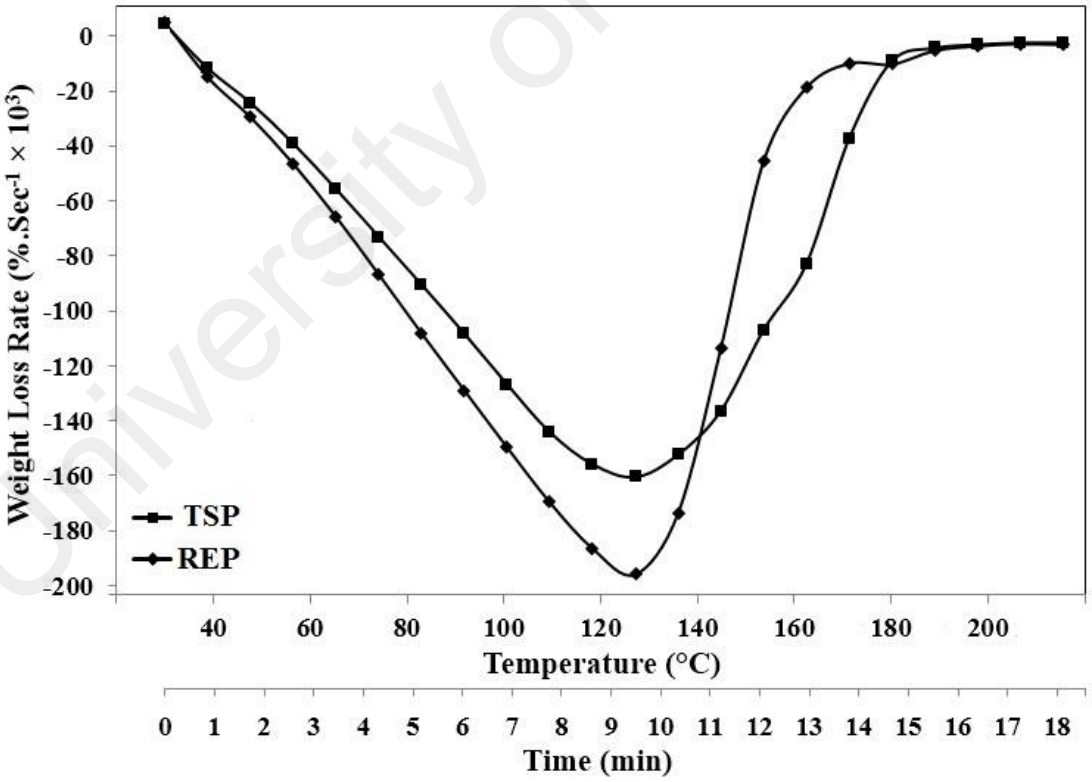

Figure 3.5: The TGA graphs of two typical REP and TSP specimens.

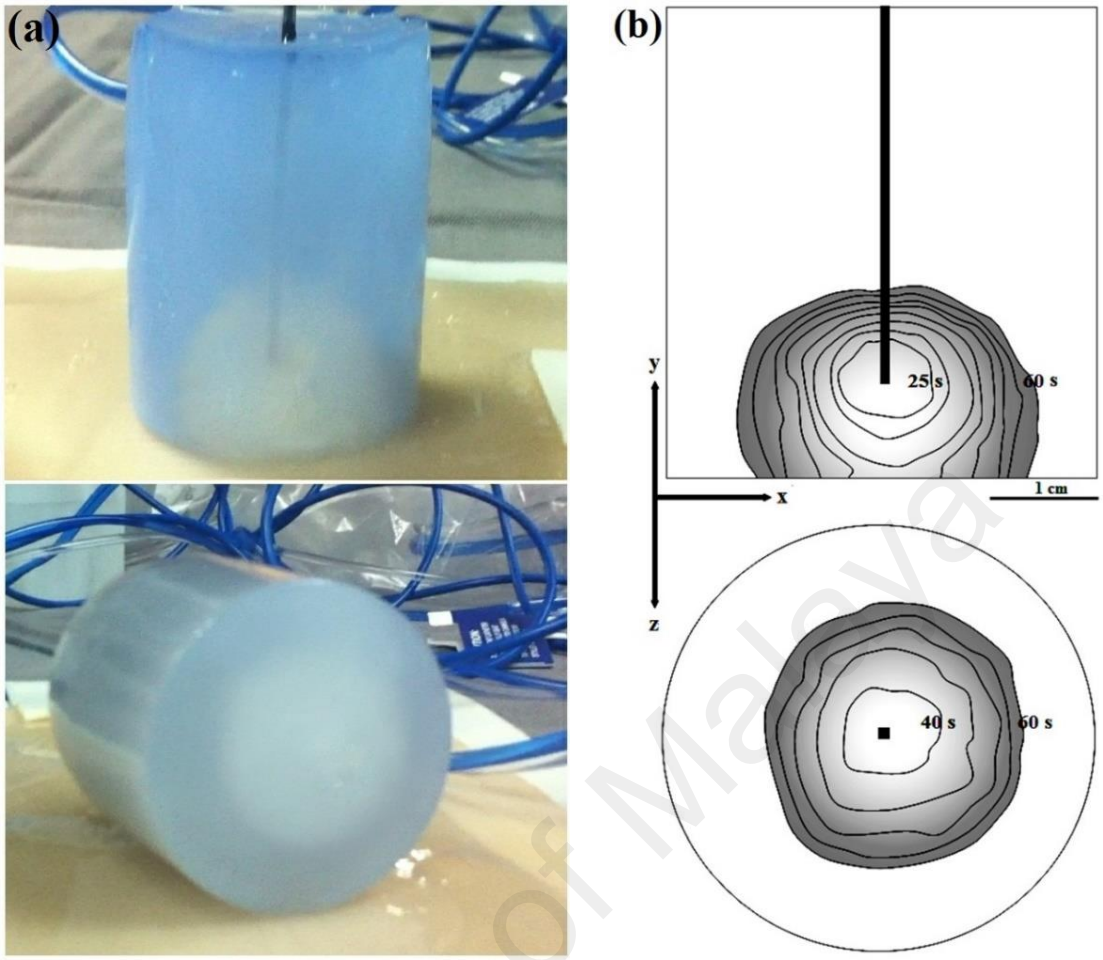

Figure 3.6: (a) The colourless region developed in TSP after RF irradiation for 60 seconds; (b) the estimated isothermal curves due to RF irradiation on X-Y and X-Z planes of TSP specimen.

maintenance and thermal experiments. At higher temperatures, the rate of weight loss is increased until the temperature rises to about 120ºC. The weight loss due to water evaporation continues until the temperature is reached to near 200ºC and then, no significant change in the weight-loss rate is observed. However, Figure 3.5 shows that the addition of TCD may decrease the water evaporation rate, most likely due to the small increase in the viscosity of the water.

Figure 3.6a shows the change in colour of the heated area in TSP gel after the exposure to RF beams for 60 seconds. Upon exposure of the TSP phantom to electromagnetic beams, a colourless region is created due to the power absorption, making the three-dimensional distribution of the temperature visible from outside. This feature of the TSP phantom could be useful in many applications where the accurate three-dimensional assessment of power absorption is required.

A typical application of the TSP phantom for measurement of local SAR inside the phantom is demonstrated in Figure 3.6b. SAR is defined as the time rate of energy deposition per unit mass in a lossy body and it is generally a measure of power density (Kanda et al., 2004; Paulides et al., 2013). In this figure, the area of the colourless region as a function of irradiation time is outlined using the image processing software. As mentioned previously, the discolouration of the phantom starts at 6°C below the threshold temperature. Based on this fact, the temperature on the boundary between the blue and colourless regions is assumed equal to the onset temperature of discolouration. This assumption could be confirmed by measurement of the colour values at boundary using the image processing software and comparing the obtained values with those of central area near the RF applicator that has a temperature above T_{ed}. The colour values at boundaries are lower (more close to dark) and gradually increase during the irradiation period, while the colour values at central area are relatively high (close to white) and stable over the irradiation time. Therefore, the surface of the colourless region at different irradiation times coincides with the isothermal layers with temperature of 44°C. These isothermal layers could be used for calculation of SAR on the boundary using the Pennes' bio-heat transfer equation (Arora et al., 2004; Paulides et al., 2013):

$$\rho C\frac{\partial T}{\partial t} = k\nabla^2 T + W_b C_b(T_b - T) + Q \quad (4.1)$$

Where, ρ, C, and k are the density, specific heat, and thermal conductivity of the phantom, respectively. W_b, C_b, and T_b are the flow rate, specific heat, and temperature of the blood. Q is also the heat deposited in the phantom due to RF irradiation (Paulides et al., 2013). It should be noted that this phantom has relatively small thermal conductivity compared to heat generation and the time period in which thermal conductivity can be negligible is longer than irradiation time used in this study. Moreover, there is no blood flow in the phantom. Therefore, the first and second terms on the right side are eliminated and the equation (4.1) is simplified as follows (Arora et al., 2004):

$$Q = \rho C\frac{(T_{od} - T_0)}{t} \qquad [W.m^{-3}] \quad (4.2)$$

And thus:

$$SAR = C\frac{(T_{od} - T_0)}{t} \qquad [W.kg^{-1}] \quad (4.3)$$

Where T_0 is the room temperature and t is the irradiation time. Since the specific heat capacity of the TSP phantom, the room temperature, T_{od}, and irradiation time are 3.59 $kJ.kg^{-1}.K^{-1}$, 25°C, 44°C, and 60 seconds, respectively, the local SAR is estimated as 1136.8 $W.kg^{-1}$. A similar protocol could be used for calculation of SAR at isothermal layers with temperature of 50°C by outlining the areas with stable colour values.

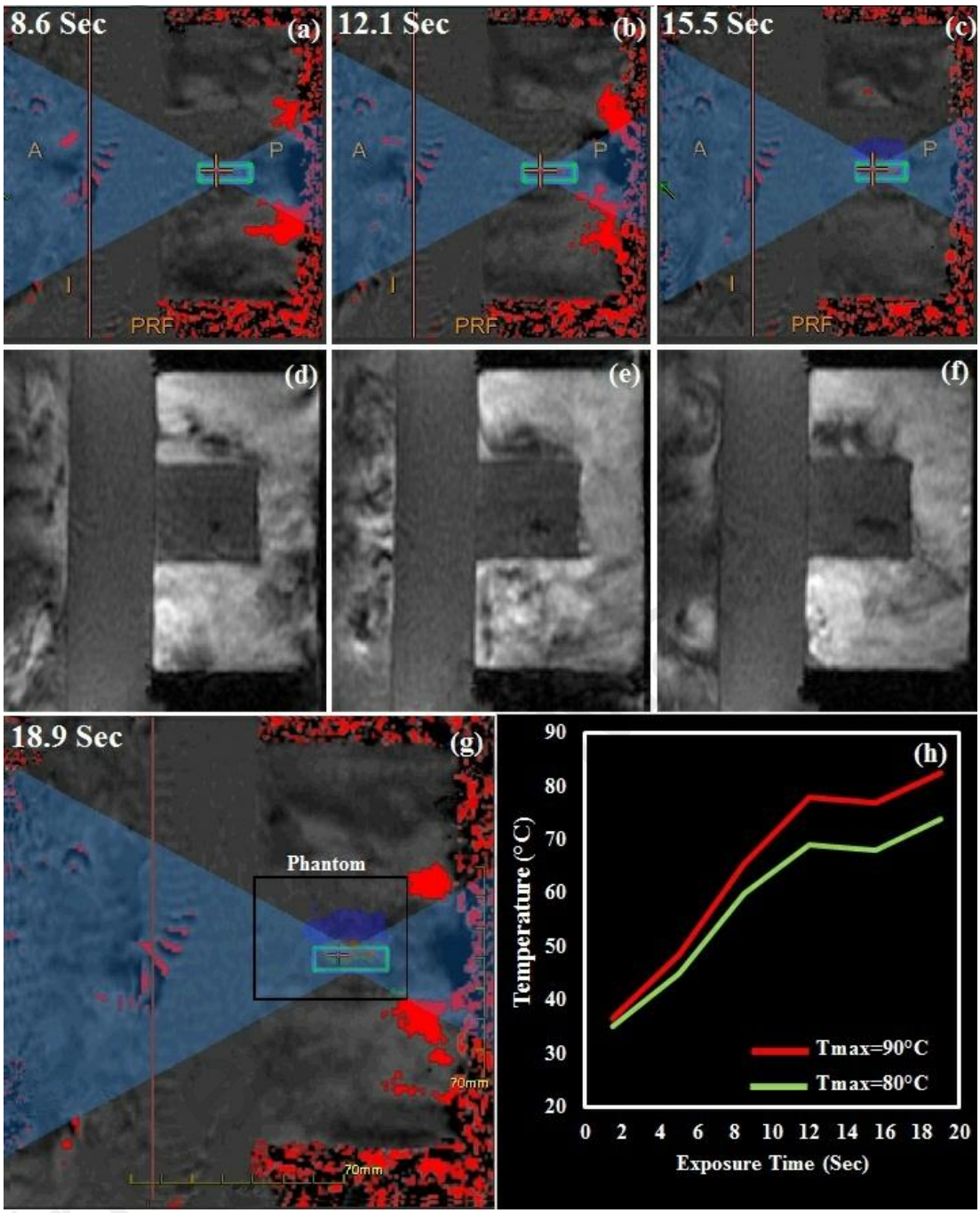

Figure 3.7: MR images of a typical TSP during MRgFUS heating. (a-c) the temperature patterns obtained during heating of the phantom, where higher temperatures are shown in red; (d-f) development of thermal lesion due to MRgFUS treatment; (g) the final temperature pattern after sonication for approximately 19 seconds; (h) the temperature plot of the focus point during sonication of the phantom.

The results of phantom sonication using MRgFUS system are shown in Figure 3.7. When the ultrasound pulses are propagated through the phantom, the MR images show a dark region with a slightly oval shape which is corresponded to the heated area at the focal point (Figure 3.7a-g). According to Figure 3.7h, the temperature of the focal point is increased to over 50°C after sonication for approximately 6 to 7 seconds; however, due to the small size and insufficient contrast at initial sonication times, the thermal lesion is not observed in MR images upon reaching the sonication time to about 8 seconds. After the FUS power is turned off, this region is disappeared again due to the diffusion of heat through the phantom. The reversibility of colour change is an effective feature for more effective focusing of the ultrasound beams to the desired point (e.g. tumour) during MRgFUS experiments.

The threshold temperature of the TSP phantom is close to the temperatures at which the true lesions are formed in real tissues. Therefore, the ability of TSP phantom to represent the thermal lesion at temperature of 50±3°C could be applied for more precise simulation of real tissues during MRgFUS experiments.

3.4 Conclusion

The thermal and acoustic properties of a Polyacrylamide gel containing thermochromic dye have been described. The acoustic properties of this gel were found to be similar to those of reference phantom, proving that the used dye may not have a significant impact on acoustic properties of the phantom. However, the thermochromic dye caused a decrease in specific heat capacity and latent heat of melting of the

Polyacrylamide phantom although other thermal parameters such as thermal conductivity and melting point were almost similar to that of reference phantom. The amount of dye used for preparation of phantom is much lower compared to other similar thermosensitive agents such as EW, BSA, and NISAAs which causes a negligible effect on various properties of the phantom. Moreover, due to the reversibility of the colour change, the phantom could be prepared without the need to decrease the temperature continuously; while temperature control is necessary for fabrication of PAA-BSA and PAA-EW phantoms because of irreversible coagulation of the thermosensitive agent. Another advantage of these dyes is the more precise estimation of temperature inside the phantom (error: 3ºC) compared to other thermosensitive phantoms (especially PAA-EW phantoms). The phantom is reusable for several experiments and the threshold temperature could be adjusted by choosing an appropriate thermochromic dye.

The new phantom model could be used in various modalities including RF, and MRgFUS. By use of this thermochromic dye, the local SAR value inside the phantom could be precisely estimated. This experimental method of SAR evaluation has many advantages in respect of the cost requirement for measurement or observation, availability of true 3-D pattern of the local SAR, and easiness of SAR estimation.

The main limitation of this phantom is the loss of transparency during the construction of sizeable phantoms. Therefore, this thermochromic dye is only suitable for construction of the phantoms with diameters smaller than 10 cm. However, the advantages of this thermosensitive phantom make it an attractive candidate as reusable tissue-mimicking material for various high-temperature modalities.

CHAPTER 4: A NEW MECHANISM OF THERMAL-SENSITIVITY FOR RAPID DRUG RELEASE AND LOW SYSTEMIC TOXICITY IN HYPERTHERMIA AND THERMAL ABLATION TEMPERATURE RANGES

4.1 Introduction

Utilization of thermosensitive carriers is an effective strategy to protect healthy tissues from the negative effects of chemotherapeutic drugs as well as to obtain a synergistic effect of hyperthermia and chemotherapy (Mcdaniel et al., 2013). These carriers transfer the chemotherapeutic drugs through the body and release them specifically in the desired region which is simultaneously heated by a thermal modality (Mcdaniel et al., 2013; Shao et al., 2011). In addition to a site-specific targeting and reduced side effects, encapsulation of free drugs in these nanoparticles could prolong their half-life and therapeutic efficacy (Parodi et al., 2013).

The active release of encapsulated drug from thermosensitive nanostructures is mostly relied on thermally triggered mechanisms including membrane disruption, coil-globule transition, and micellization (or sol-gel behaviour). The membrane disruption is the most investigated mechanism which is often seen in lipid-based drug-carriers such as traditional thermosensitive liposomes (TTSLs), lysolipid-containing thermosensitive liposomes (LTSLs), polymer-modified thermosensitive liposomes, magneto-liposomes, and bubble-generating thermosensitive liposomes. For instance, drug release from lysolipid-containing thermosensitive liposomes (LTSLs) occurs by generation of stabilized defects in lipid membrane due to the micellization of lysolipids at temperatures near 39-40°C. These defects further provide preferred routes for rapid release of encapsulated drug at hyperthermia temperatures (Gasselhuber et al., 2012b; Landon et

al., 2011; Li et al., 2013b; Needham et al., 2013; Ta et al., 2013). The LTSL formulations that have undergone pharmaceutical development and are currently under clinical development (i.e. ThermoDOX®) (Landon et al., 2011), can release their contents in few seconds after exposure to the increased temperatures and delay the tumour growth (Gasselhuber et al., 2012a; Viglianti et al., 2014). However, a number of studies demonstrated the rapid desorption of lysolipids from LTSLs when administrated in vivo, resulting in reduced thermal sensitivity and premature drug leakage at physiological conditions (Banno et al., 2010; Chiu et al., 2005; De Smet et al., 2010; Ta et al., 2010). There was also indirect evidence that lysolipids dissociate from LTSL upon dilution (Banno et al., 2010).

The coil-globule transition is mostly seen in polymers with lower critical solution temperature (LCST) such as isopropyl acrylamide-based polymers (Deshmukh et al., 2014; Ruiz et al., 2007; Scherzinger et al., 2014; Ward et al., 2011; Yan et al., 2011; Yang et al., 2011). The increased hydrophobicity of these polymers upon a slight heating above physiological temperatures, results in a thermo-induced conformational change from the swelled, hydrophilic coils to the shrunken, hydrophobic globules which provide a mechanical pressure to squeeze the encapsulated drug out of the particles (Bekhradnia et al., 2014; Li et al., 2013c). However, a relatively low mechanical strength and slow drug release due to their reliance on diffusion mechanism are two particular limitations of these phase-transitional polymers (Bekhradnia et al., 2014). Moreover, in the core-shell structures where a porous drug reservoir (e.g. mesoporous silica particles) is used, the shrinkage of polymer shell at temperatures above LCST may suppress the diffusion of encapsulated drug outward from the reservoir core (Yang et al., 2008).

Poloxamers (e.g. polyethylene oxide-polypropylene oxide-polyethylene oxide (PEO-PPO-PEO)) are typical examples of materials exhibiting micellization followed by sol-gel behaviour (Chen et al., 2007; Chiappetta et al., 2007; Yapar et al., 2013). At micellar volumetric fractions above a specific threshold, these micelles entangle together upon heating and undergo three-dimensional and crystal-like packing, producing a hydrogel network (Yapar et al., 2013). When heating is continued, phase separation and clouding due to the dissociation of the stiff gel network favours the release of entrapped drug. Although the gel-forming mechanism of poloxamers could provide an attractive solution in drug delivery, these gels may not remain stable more than several hours and thus, long-term delivery of these compounds remains a challenge. Moreover, the transition temperature of these materials is highly dependent on their concentration in aqueous solutions (Jeong et al., 2002).

In order to overcome the shortcomings of previously developed triggering mechanisms, a novel mechanism of drug release using thermosensitive capping agents have been recently proposed. In this mechanism, a porous matrix (e.g. mesoporous silica nanoparticles) is blocked by capping agents such as double helix DNA (Derfus et al., 2007; Ruiz Hernandez et al., 2011), and pseudorotaxane-based nanovalves (Thomas et al., 2010), which rapidly dissociate in the hyperthermia temperature range and allow an "on-off" drug release from the porous structure. The porous nanocore provides a high loading capacity as well as sufficient mechanical and chemical stability in physiological environment. However, considerable drug release from these nanocarriers at physiological temperature results in relatively high systemic toxicities and low therapeutic doses available at target tumour. For instance, in vitro drug release ratios

above 30% were observed in DNA-capped mesoporous silica nanoparticles incubated at 37°C for 15 minutes (Ruiz Hernandez et al., 2011).

In the present research, we have developed a polyacrylamide-mesoporous silica core-shell nanostructure (PAA-MSN) as a smart carrier of anticancer drugs. Polyacrylamide (PAA) has been used previously for delivery of photosensitizer agents in photodynamic therapy of cancer (Kuruppuarachchi et al., 2011); however, its potential as a thermosensitive capping agent for drug delivery has not been investigated. This study is an attempt to develop thermosensitive nanocarriers with a drug release mechanism based on the rapid dissociation of capping agent that provide higher loading capacity, better stability at physiological environment, and minimized drug release at body temperature. PAA possess a controllable gelation temperature that could be adjusted in the temperature range of thermal ablation by altering the crosslinker/monomer ratio. Therefore, we assumed that by irradiation of energy via the thermal ablation modalities, the PAA protective shell could be rapidly dissociated, facilitating the release of encapsulated drug. The onset gelation temperature of PAA is sufficiently higher than physiological temperature and within the therapeutic hyperthermia range, causing a minimal drug release in healthy tissues and consequently, lower systemic toxicity. To the best of our knowledge, this study is the first attempt to produce a thermosensitive polymeric drug carrier based on the gelation of the encapsulating shell. A schema of the synthesis procedure as well as the expected mechanism of drug release from the core-shell nanoparticles is presented in Figure 4.1.

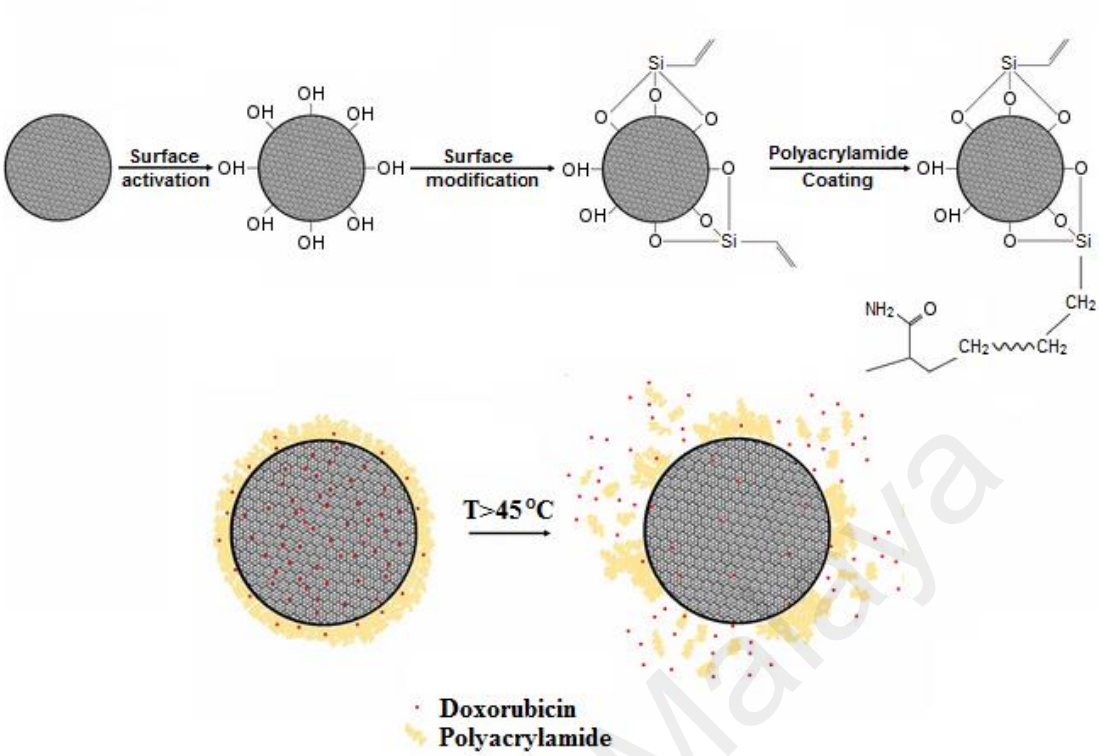

Figure 4.1: A schematic of the synthesis method and expected mechanism of drug release from the core-shell structure. Melting of protective shell provides preferred ways for drug discharge.

4.2 Materials and Methods

4.2.1 Synthesis of the Core-Shell Nanoparticles

The PAA-MSNs were synthesized using the following materials obtained from Sigma-Aldrich (M) SDN. BHD. (Kuala Lumpur, Malaysia). Tetraethyl orthosilicate (TEOS), cetyltrimethyl ammonium bromide (CTAB), ammonia solution (28 %w/w), ethanol, hydrochloric acid aqueous solution (HCl; 37 %w/w) triethoxy vinylsilane (TEVS), acrylamide (AA), N, N´-methylene bisacrylamide (MBAA), N,N,N',N'-tetramethyl ethylenediamine (TEMED), and ammonium persulphate (APS).

The mesoporous silica nanoparticles (MSNs) were produced by modification of the Stoëber method proposed in the literature (Rossi et al., 2005; Shin et al., 2008). In our modified recipe, CTAB was added as a template, resulting in a mesoporous structure in silica nanoparticles. In a typical process, two types of solutions were prepared. The first solution was a mixture of 16.75 ml TEOS, 3.3 g of CTAB, and 133.25 ml ethanol. The second solution contained 3.81 ml aqueous ammonia (28 %w/w), 40.78 ml deionized water, and 105.46 ml ethanol. Under stirring, the first solution was added to the second solution and the mixture was stirred for 210 minutes. Then, the mixture was centrifuged at 4,000 rcf for 15 minutes and the precipitate was rinsed with ultrapure water for three times followed by drying for 24 hours at 80°C. The CTAB template was later removed by incubation of the particles in a methanol solution containing 3 %v/v HCl for six hours. The MSNs were lastly obtained by another centrifuging, rinsing, and drying at 80°C for 24 hours.

In order to activate the surface of MSNs, the particles were dispersed in 100 ml of HCl solution and left stirring for an hour at room temperature. The solution was centrifuged (4,000 rcf for 15 minutes), washed three times in ultrapure water, and the activated mesoporous silica (AMSN) was obtained by drying the solution. Then, 1 g of AMSN was added to a beaker containing 40 mL of toluene and the mixture was dispersed using Ultra-Turrax homogenizer (T25, Ika Works Inc., Wilmington, DE) at 20,000 rpm. After 10 minutes, 600 µl of TEVS was slowly injected to the solution and the mixture was stirred for 24 hours at room temperature. The resulting suspension was later centrifuged (4,000 rcf for 15 minutes), washed, and dried at 80°C for 24 hours to obtain vinyl-modified MSNs (VMSNs).

Table 4.1: Materials needed for production of nanoparticles at different synthesis stages.

Particle Type	**Materials and Ratios**					
	Solution 1				*Solution 2*	
(1) Mesoporous silica (MSNs)	TEOS (ml)	CTAB (g)	Ethanol (ml)	Ethanol (ml)	NH_4OH (ml)	H_2O (ml)
	16.75	3.3	133.25	105.46	3.81	40.78
(2) Activated MSNs (AMSNs)	MSNs (g)	HCL (ml)				
	5	100				
(3) Vinyl-modified MSNs (VMSNs)	AMSNs (g)	Toluene (ml)	TEVS (µl)			
	1	40	600			
(4) Polyacrylamide-coated MSNs (PAA-MSN)	VMSN (mg)	AA (mg)	MBAA (mg)	TEMED (µl)	APS[a] (µl)	
	700	350	2.5	12	800	
		700	5	24		
		1050	7.5	36		

[a]An aqueous solution containing 1.3 %w/v APS was used.

PAA-MSNs were finally prepared by the graft polymerization method. As a typical procedure, 700 mg of VMSNs with varying amounts of AA (350, 700, and 1050 mg) were added to 50 ml of water, while the ratios of MBAA/AA and TEMED/AA in the solution were kept constant (3.2, and 16.1 mM per mole of AA, respectively). The mixture was stirred vigorously for 30 minutes using Ultra-Turrax at 20,000 rpm and then, 800 µl of an aqueous solution containing 1.3 %w/v APS was injected to initiate the polymerization. After 24 hours, the resulting suspension was centrifuged at 4,000 rcf for 15 minutes, washed for three times, and dried at 50°C for 48 hours. The overall procedure for preparation of PAA-MSNs is illustrated in Table 4.1. It is important to note that polyacrylamide has not been reported as a toxic material; however, its monomer is a severe neurotoxin which may be present in small amounts in the product. Therefore, a stringent washing process is needed to remove the unreacted monomer from the nanoparticles composition.

4.2.2 Material Characterization

The Fourier transform infrared spectroscopy (FT-IR) (Nicolet 6700, Thermo Scientific, Waltham, MA, USA) analysis was performed at wavenumber range of 600 to 4000 cm^{-1} to confirm the presence of hydroxyl, vinyl, and amide bonds in the nanoparticle structure. The structural morphology of the PAA-MSNs was observed using Scanning Electron Microscopy (SEM) (Hitachi S3400n, Hitachi, Tokyo, Japan), Transmission Electron Microscopy (TEM) (Libra 120 kV, Carl Zeiss AG, Oberkochen, Germany), and Atomic Force Microscopy (AFM) (Ambios AFP-200, Ambios Technology Inc., Santa Cruz, CA, USA). The average thickness of the polymer layer as well as the average size and volume of particles was estimated by analysis of at least 50 randomly-selected nanoparticles from TEM images using ImageJ software (v1.44 P, National Institutes of Health, Bethesda, MD, USA).

In order to calculate the polymer-to-silica weight ratio inside the nanostructure, Thermogravimetric Analysis (TGA) (TGA/SDTA 851e, Mettler-Toledo, Columbus, OH, USA) with scan rate of 5 $^{o}C.min^{-1}$ was used. The gelation temperature range of the polymer was also determined by Differential Scanning Calorimetry (DSC) (DSC820 with TSO 801RO robot, Mettler-Toledo, Columbus, OH, USA) with scan rate of 5 $^{o}C.min^{-1}$. The TGA and DSC experiments were repeated for at least five times and the obtained results were reported as mean±standard deviation using the Statistical Package for Social Sciences software (SPSS 20, SPSS Inc., Chicago, IL, USA).

4.2.3 Drug Loading Experiments

For the drug encapsulation, doxorubicin was dissolved in distilled water with a concentration of 2 $mg.ml^{-1}$. Then, 3 mg of PAA-MSNs was dispersed in 1.5 ml of this solution to adjust the drug/PAA-MSNs weight ratio to 1. The mixture was incubated at room temperature for three different intervals (24 h, 48 h, and 72 h) in order to determine the optimum incubation time which results in the statistically maximum encapsulation value (E_m). Drug loading procedure was performed at room temperature in 25 ml glass tubes without shaking during incubation. The dispersion was later centrifuged at 16,100 rcf for 60 minutes to separate the drug-loaded PAA-MSNs from the supernatant. Ultraviolet-Visible spectroscopy (UV-Vis) (Shimadzu UV-1800, Shimadzu Corporation, Kyoto, Japan) at wavelength range of 260 to 600 nm was used to determine the quantity of the drug in the aqueous supernatants. All the UV-Vis measurements were performed at room temperature and using distilled water as the baseline. An aqueous solution containing 2 $mg.ml^{-1}$ doxorubicin was prepared as the reference solution and the quantity of the encapsulated drug was calculated by comparing the obtained UV-Vis graphs with that of reference solution. UV-Vis analyses were all performed without dilution of the obtained supernatants. The amount of encapsulated drug within the PAA-MSNs was calculated from the difference in concentration of the drug in the supernatant after centrifugation and its concentration in the initial doxorubicin solution. The optimum incubation time calculated in this experiment was used in further stages to encapsulate doxorubicin in the PAA-MSNs.

4.2.4 Drug Release Experiments

In order to measure the amount of drug leakage from the polymer shell at physiological temperatures, the doxorubicin-loaded PAA-MSNs were incubated in an aqueous solution (2 $mg.ml^{-1}$) at 37ºC for 7 days. Then, the supernatants were separated and the amounts of released drug were quantified by comparing the UV-Vis spectra of the supernatants with that of a reference solution (an aqueous solution containing doxorubicin with concentration equal to E_m as reference solution for 100% drug release).

The release behaviour at increased temperatures was also studied by preparing ten similar aqueous solutions containing $2mg.ml^{-1}$ of doxorubicin-loaded nanoparticles. Each solution was heated separately at a specific temperature for 30 minutes using a water bath. Ten different temperature values ranging from 30 to 75°C (30, 37, 40, 45, 50. 55, 60, 65, 70, and 75°C) were used in these experiments to simulate the hyperthermia and thermal ablation conditions as well as to determine the effect of temperature on release ratio of the encapsulated drug. After heat treatments, the supernatants were separated from the PAA-MSNs and the amounts of released drug were quantified by comparing the UV-Vis spectrum of each sample with that of the reference solution. A similar protocol was also applied (except that the tests were performed only at 75-80°C) to calculate the ratio of drug release after sonication of nanoparticles using Magnetic resonance-guided focused ultrasound (MRgFUS) method (EX-ablate, Insightec, Haifa, Israel). For these experiments, a tube containing an aqueous solution of drug-loaded nanoparticles was placed in a thermosensitive tissue-mimicking phantom (TSP) which was developed in chapter 4. This phantom can mimic various acoustic properties of soft tissues (e.g.

attenuation, and sound speed) and precisely show the heated area by a reversible colour change as well as alteration of MR parameters.

The TSP was immediately sonicated for 5×20 seconds at frequency of 1.15 MHz with the acoustic energy and acoustic power of 5313 J and 266 W, respectively. Then, the drug release ratio due to heating by MRgFUS was measured by UV-Vis technique. The drug loading and release experiments were repeated for at least five times and the results were evaluated by analysis of variance (ANOVA) method with 95% confidence interval using the Statistical Package for Social Sciences software (SPSS 20, SPSS Inc., Chicago, IL, USA).

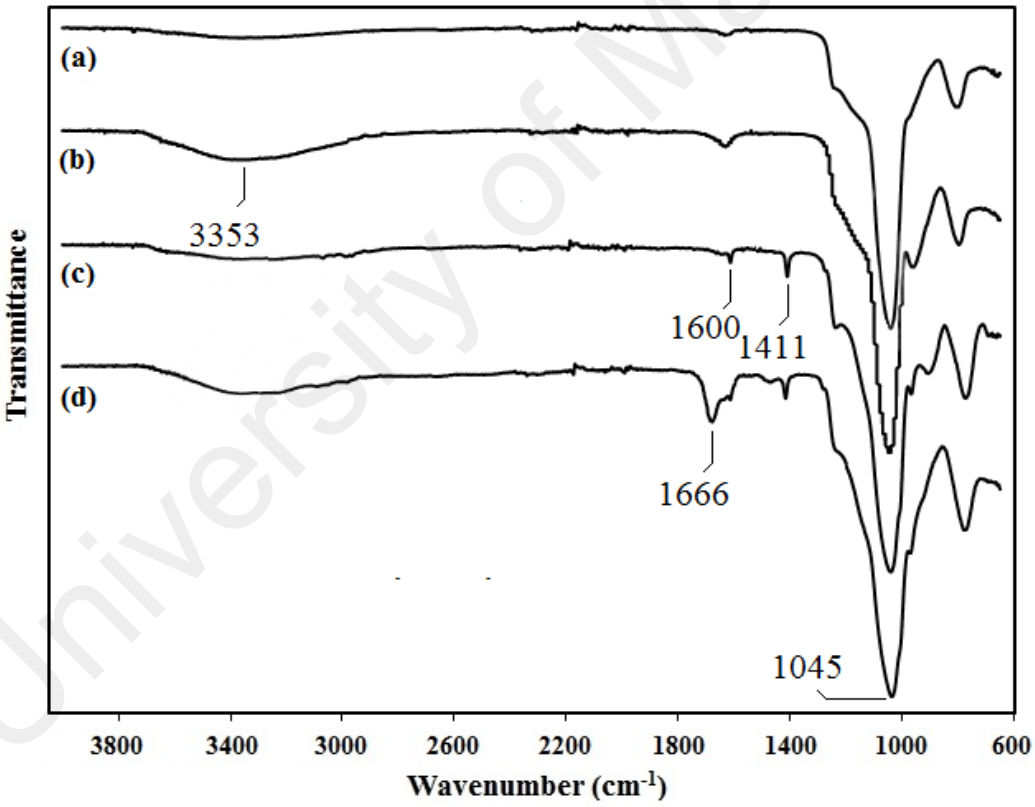

Figure 4.2: The FT-IR spectra of the particles at different synthesis stages. (a) MSN, (b) AMSN, (c) VMSN, and (d) PAA-MSN.

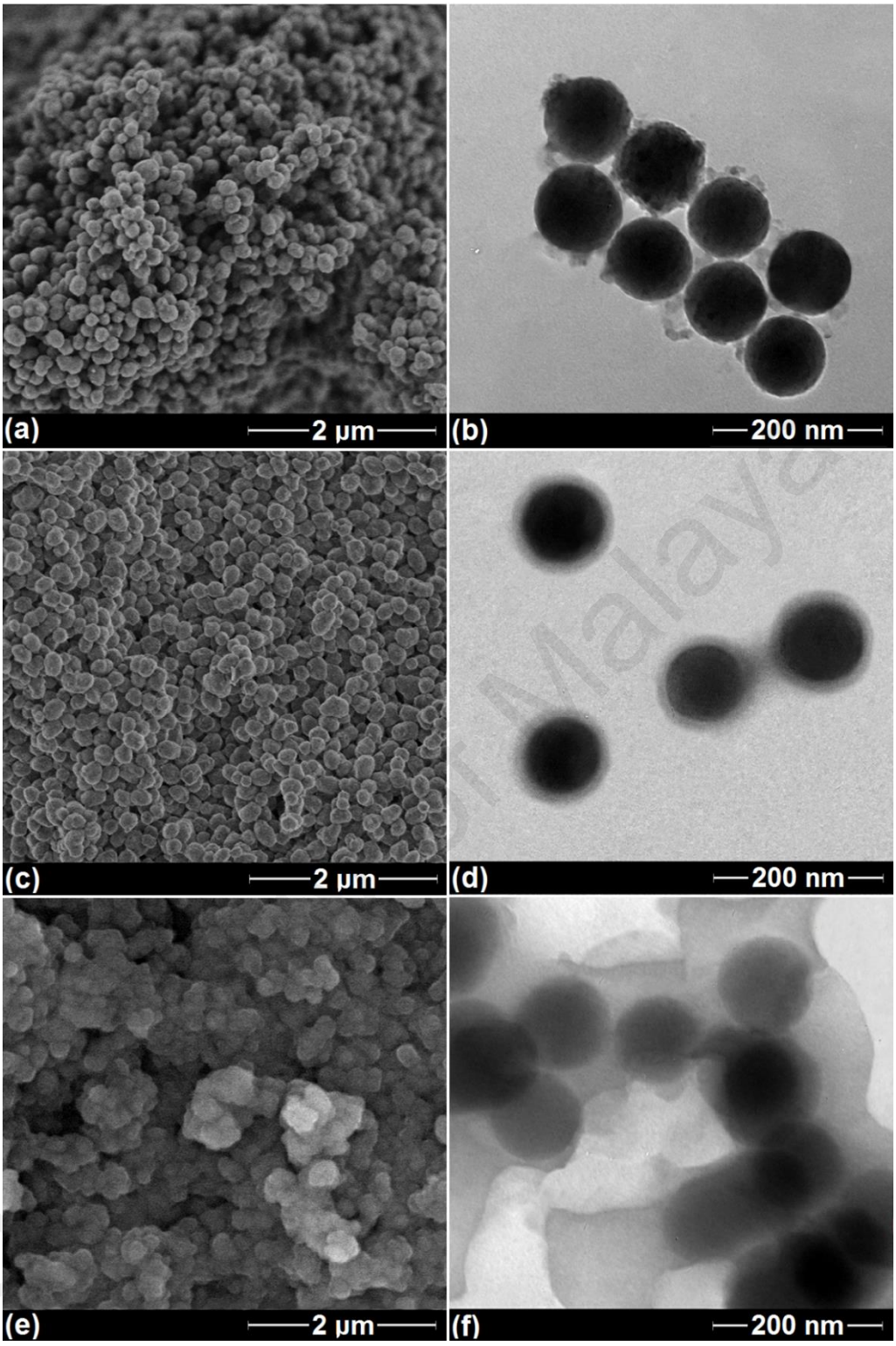

Figure 4.3: Microstructural images of synthesized nanoparticles. (a, c, e) SEM, and (b, d, f) TEM images of the specimens with AA/MSN weight ratios of 0.5, 1.0, and 1.5, respectively.

4.3 Results and Discussion

4.3.1 Material Characterization

The FT-IR spectra of the MSNs, AMSNs, VMSNs, and PAA-MSNs are shown in Figure 4.2. The strong peak observed at 1045 cm^{-1} in all samples represents the Si-O-Si vibration. In the FT-IR spectrum of the AMSNs, the peak of absorbed water is stretched at 3353 cm^{-1}. For the VMSN sample, one can clearly observe the peaks at 1411 cm^{-1} and 1600 cm^{-1} for vinyl and silane bonds, respectively. In the FT-IR spectrum of the PAA-MSNs, the peak at 1666 cm^{-1} is characteristic vibration of the amide group.

Figure 4.3 illustrates the SEM and TEM images of the PAA-MSNs with different weight ratios of acrylamide-to-mesoporous silica (AA/MSN: 0.5, 1.0, and 1.5). The dark spheres represent the mesoporous silica nanoparticles (MSNs) with a mean diameter of 90±20 nm and the thin grey shells imply the presence of polymer, covering the MSN cores. This figure clearly demonstrates that the AA/MSN ratio of 0.5 could not provide a uniform layer around the cores (Figure 4.3a-b), whereas the AA/MSN ratio of 1.0 results in a uniform polymer shell with thickness of 12±2 nm (Figure 4.3c-d). On the other hand, a particle aggregation is observed in the SEM and TEM images of the specimen with AA/MSN ratio of 1.5 (Figure 4.3e-f) due to a relatively large amount of monomer used in this specimen. Based on the obtained microstructures, the AA/MSN ratio of 1.0 was selected to synthesize core-shell nanoparticles for further experiments.

According to a typical curve obtained from TGA analysis (Figure 4.4a), a rapid weight loss occurs in PAA-MSNs at temperatures below 100°C that corresponds to the evaporation of water from the PAA structure. The second phase of weight loss begins at 200°C and continues until stabilization at the constant value of 67±3% (temperatures

above 630°C). Therefore, due to the thermal stability of silica at this temperature range, the amount of weight loss (~33±3%) might represent the weight ratio of the polymer shell in the PAA-MSN structure. The weight ratio of the polymer shell could also be calculated according to the following equation:

$$\%Wt_P = \frac{V_{PAA}\rho_{PAA}}{V_{MSN}\rho_{MSN} + V_{PAA}\rho_{PAA}} = \frac{({r_{PMSN}}^3 - {r_{MSN}}^3)\rho_{PAA}}{{r_{MSN}}^3\rho_{MSN} + ({r_{PMSN}}^3 - {r_{MSN}}^3)\rho_{PAA}} \quad (5.1)$$

Where V, ρ, and r values represent volume, density, and radius of nanoparticles, respectively. The densities of MSNs and PAA were respectively assumed equal to 2.648 $g.cm^{-3}$ and 1.13 $g.cm^{-3}$.

According to equation 5.1, the weight ratio of the PAA shell around the MSNs is around 31 %w/w that is slightly lower than the value obtained from the TGA analysis. This might be due to the availability of moisture in the nanoparticles as well as the presence of small amounts of polymer inside the MSN pores.

The DSC analysis was also performed to determine the gelation point of the PAA coating (Figure 4.4b). Although the melting point of PAA coating is 68.3±4.2°C (the minimal point in the DSC spectra), the wide DSC peak shows that the gelation of polymer shell initiates at 45.1±3.4°C. Therefore, a partial release of encapsulated drug from the MSN pores could also occur at hyperthermia temperature range. It is important to note that this temperature range is significantly higher than the physiological temperature which may minimize the ratio of drug release at the tissues surrounding target tumour.

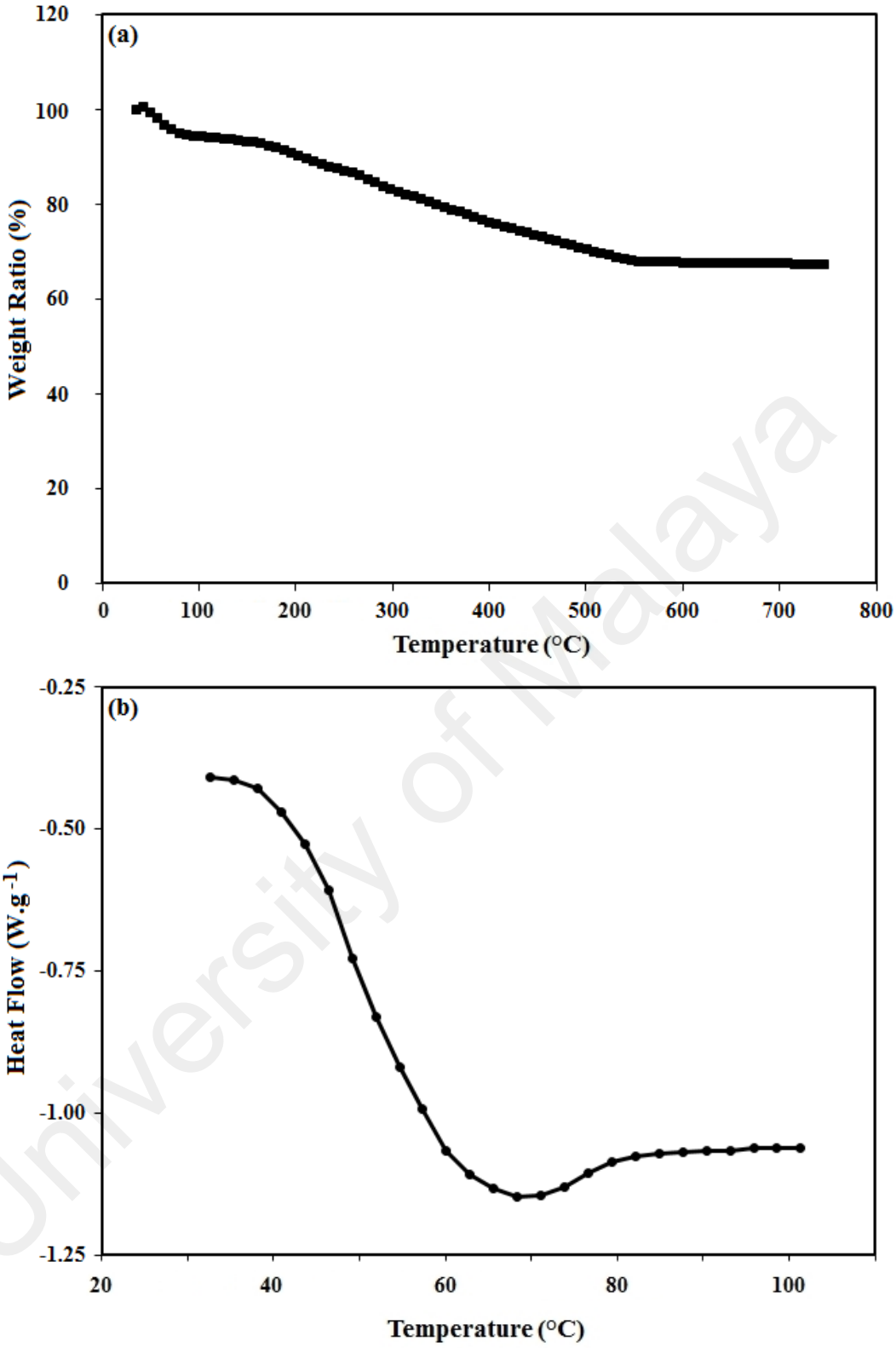

Figure 4.4: The thermal behaviour of core-shell nanoparticles. (a) The TGA, and (b) the DSC analysis of a typical specimen with AA/MSN weight ratio of 1.0.

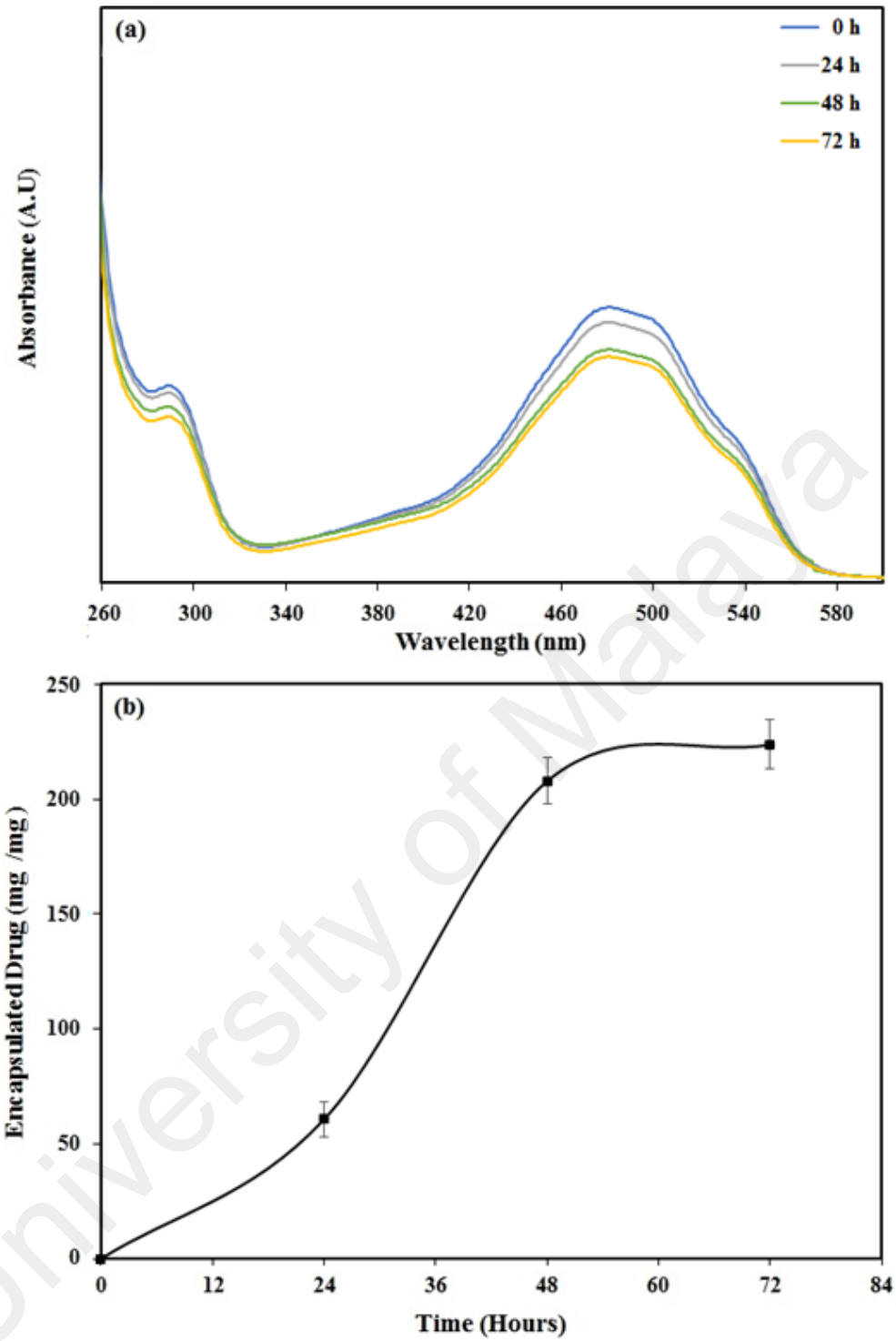

Figure 4.5: The nanoparticles ability in encapsulation of doxorubicin. (a) UV-Vis spectra of drug solution after separation of nanoparticles, which were incubated for 0, 24, 48, and 72 hours; (b) the amount of drug loaded in PAA-MSNs at different incubation times.

4.3.2 Drug Loading Behaviour

The optimal incubation time needed for encapsulation of doxorubicin in PAA-MSN structure was determined by UV-Vis spectroscopy. The UV-Vis spectra of the supernatants after centrifugal separation of PAA-MSNs from doxorubicin solution are illustrated in Figure 4.5a. The increase of incubation time results in reduced UV absorption intensity and thus, decreased doxorubicin concentration in the supernatant. The amounts of encapsulated doxorubicin in the PAA-MSNs after different incubation intervals are also plotted in Figure 4.5b. With the increase of incubation time up to 48 hours, the average ratio of encapsulated doxorubicin is increased (208±20 mg in 1 g of PAA-MSNs) and then, no significant change in its amount is observed.

Based on the obtained results, incubation time of 48 hours was used in all further experiments to prepare the drug-loaded nanoparticles. Moreover, an aqueous solution containing 416 $\mu g.ml^{-1}$ of doxorubicin (equal to the average amount of drug encapsulated in 2 mg of the PAA-MSNs) was prepared and its UV-Vis absorbance at wavelength range of 260-600 nm was recorded as reference for 100% drug release to quantify the ratio of drug release at ten different applied temperatures.

4.3.3 Drug Release Behaviour

Figure 4.6a shows the absorbance intensity of three specimens heated at 37, 45, and 60°C. The red spectrum gives an indication of the diffuse-type release of doxorubicin molecules from the PAA-MSNs at 37°C. The grey spectrum shows that a relatively higher quantity of drug molecules could be released at 45°C, possibly due to the partial melting

of the PAA shell at this temperature. However, a more intense absorbance is established by the specimens heated at 60°C. The similarity of absorbance spectra at different temperatures shows the stability of encapsulated doxorubicin during the experiments. Figure 4.6b also shows the percentage of drug release at different temperatures from 30 to 75°C. The percentage of drug release at physiological temperature (37°C) was about 11.5±2.4% which is not statistically higher than the released drug at 30°C ($P<0.05$). It is noteworthy that incubation of drug-loaded PAA-MSNs at physiological temperature for 7 days, resulted in a 14±3% drug leakage from the polymer shell. The obtained value was not statistically different from the leakage ratios after incubation at 30ºC and 37ºC for 30 minutes (Figure 4.6b). Therefore, it may be concluded that the entrapped drug inside the polymer shell could be rapidly released after incubation of the drug-loaded PAA-MSNs into the aqueous solution. According to Figure 4.6b, the maximum drug release ratio (67.6±2.5%) could be obtained at 60°C and then no significant increase in this value is observed.

The TEM image of typical PAA-MSNs after heating at 60°C (Figure 4.7a) illustrates a partial melting of the PAA shells that produces preferred routes for release of encapsulated drug at this temperature level. The partial elimination of polymer shells from the MSN surface provides the ability to visualize the silica mesopores in this figure. The melted shell may produce relatively large aggregates on the MSN surface or detach from the MSN surface and form small polymeric spheres in aqueous solution. According to the AFM images of the nanoparticles prior and after heating (Figure 4.7b-c), the partial melting of polymer shells may result in aggregation of PAA-MSNs in aqueous solutions containing high concentrations of PAA-MSNs.

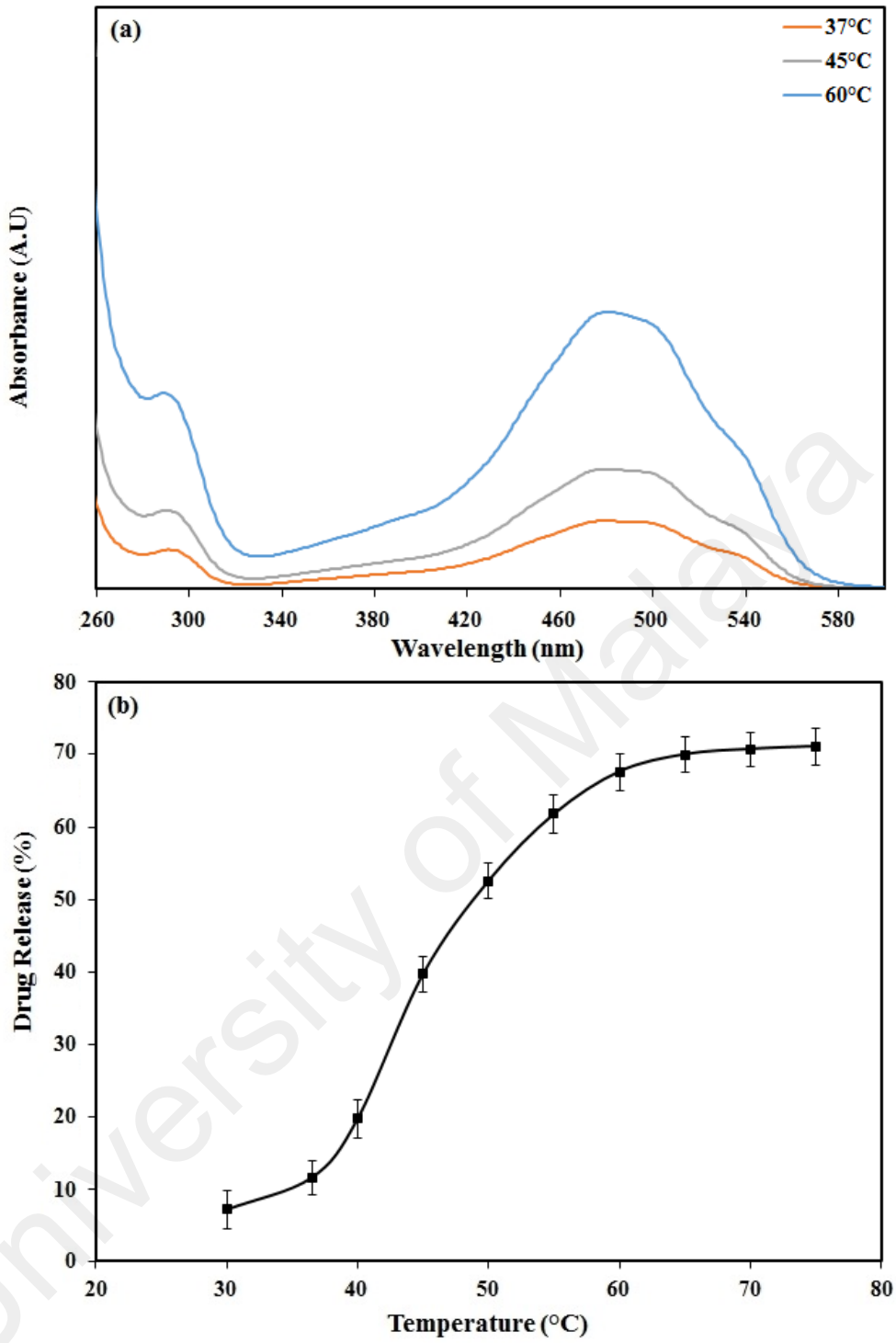

Figure 4.6: The ability of nanoparticles in release of doxorubicin. (a) UV-Vis spectra of supernatants after separation of PAA-MSNs, which were heated at 37, 50, and 60°C; (b) the percentage of drug release from the PAA-MSNs after heating at various temperatures for a period of 30 minutes.

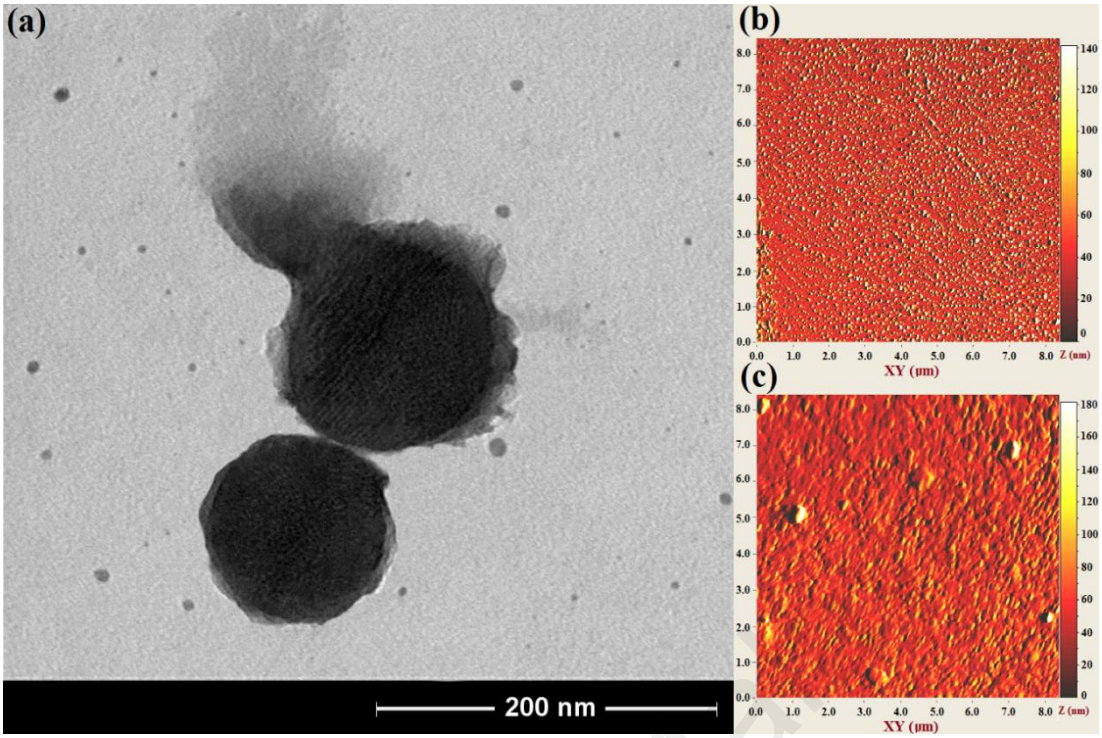

Figure 4.7: (a) TEM image of PAA-MSNs after heating at 60°C. The PAA shell is partially removed because of melting at this temperature range. (b, c) AFM image of PAA-MSNs before, and after heating at 60°C, respectively.

The procedure applied for sonication of drug-loaded PAA-MSNs using MRgFUS system is shown in Figure 4.8. When the ultrasound pulses are propagated through the TSP, the magnetic resonance (MR) images show a dark oval region corresponded to the heated area at the focal point (Figure 4.8a-c). The temperature patterns of the focal region at different sonication times are also illustrated in Figure 4.8d-g. The region with maximum temperature was initially produced at bottom of the container (where PAA-MSNs are precipitated) and gradually propagated through the container until all the aqueous solution reached the maximum temperature at 19 seconds. According to Figure 4.8h, the temperature of the focal point was increased to over 50°C and 70°C after sonication for approximately 4 and 16 seconds, respectively, producing sufficient thermal energy for gelation of the polymer shell.

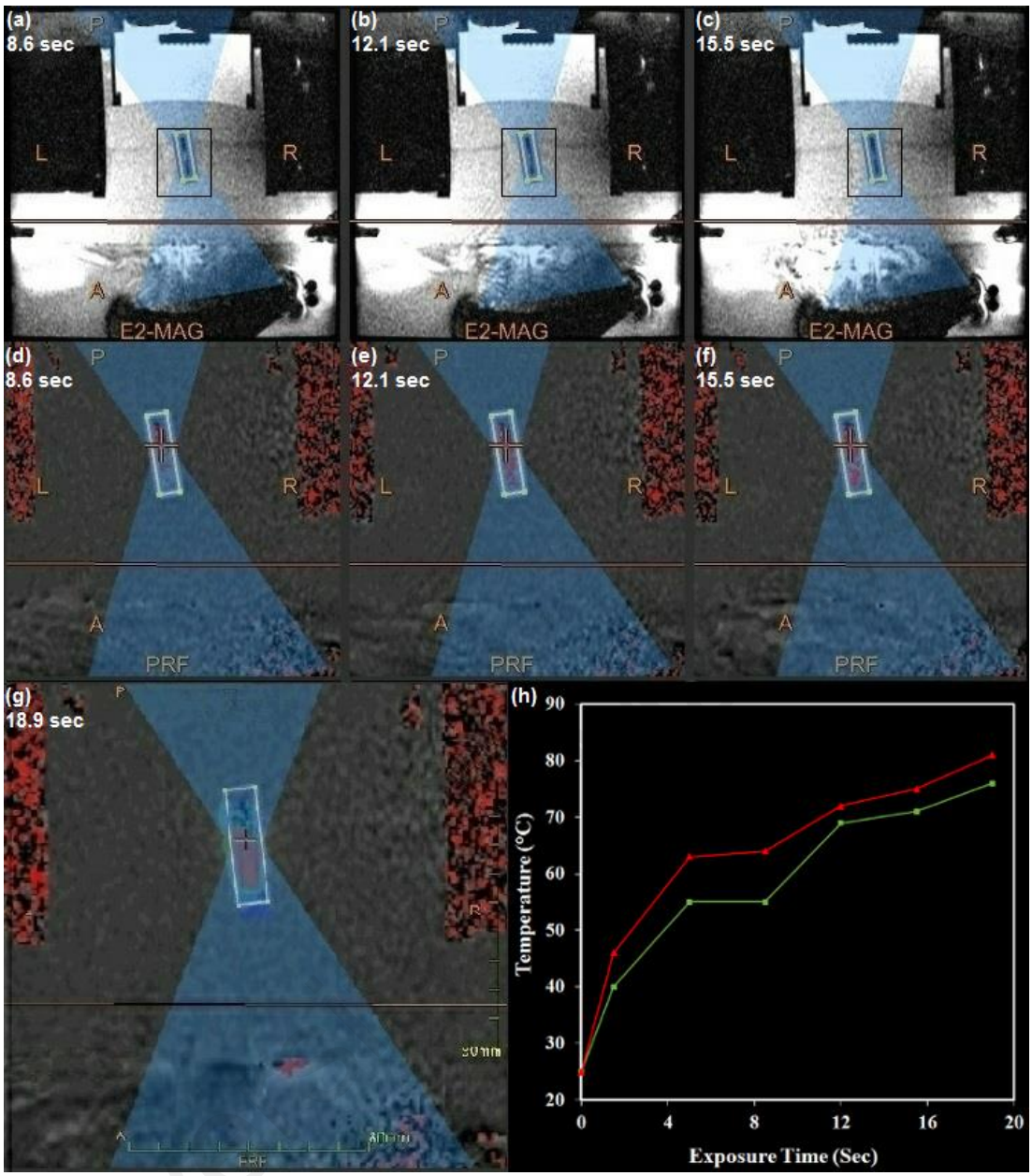

Figure 4.8: The procedure applied for MRgFUS sonication of nanoparticles. (a-c) Magnetic resonance phase images of a typical TSP containing drug-loaded PAA-MSNs during MRgFUS heating; (d-g) the temperature patterns obtained during the heating process, where the maximum temperatures are shown in red; (h) the minimum (green) and maximum (red) temperature plots of the focal point during sonication of the phantom.

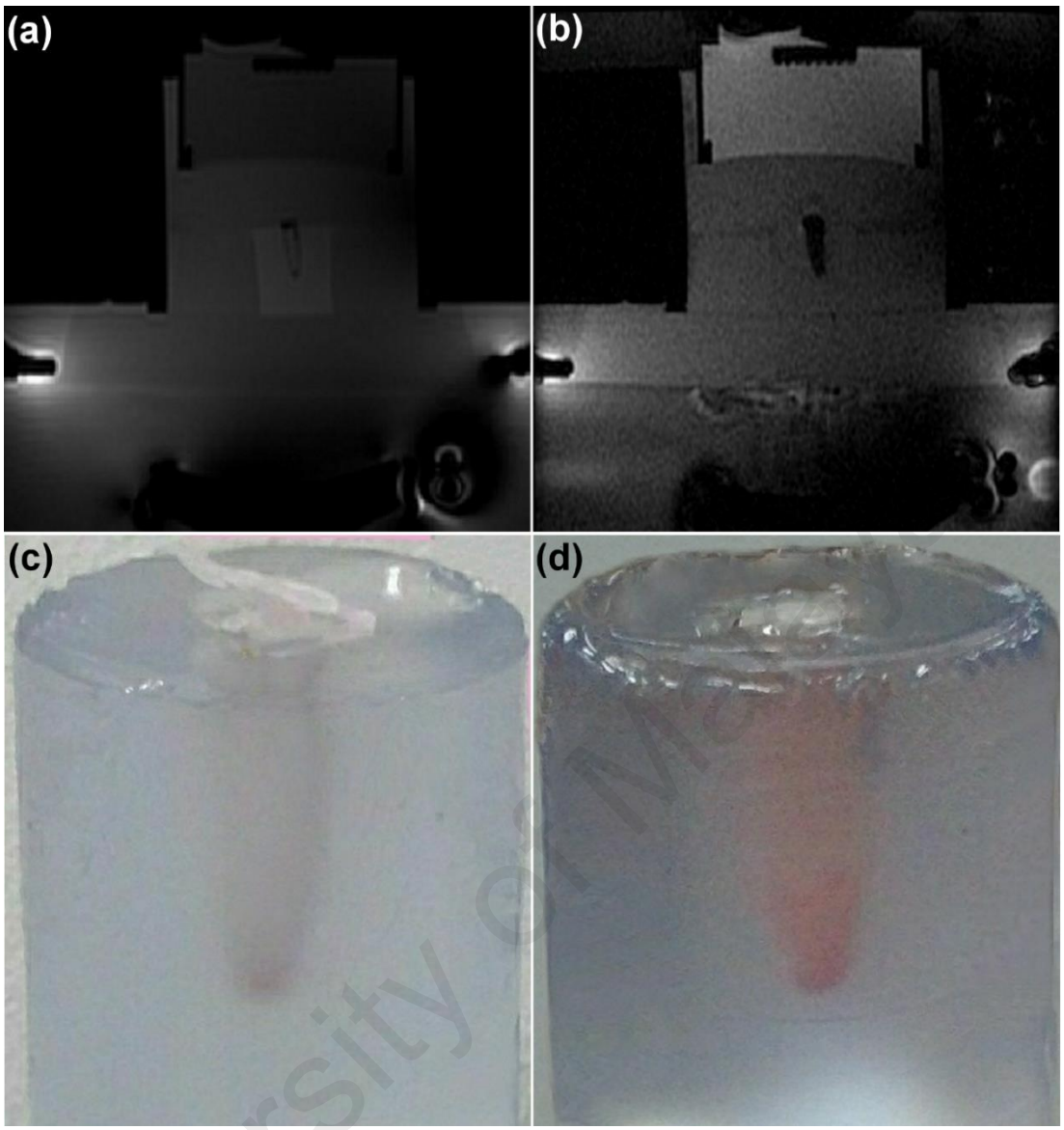

Figure 4.9: Influence of MRgFUS sonication on drug-loaded nanoparticles. (a,b) MR phase images of a TSP containing drug-loaded PAA-MSNs before and after sonication, respectively; (c,d) The colour change of the aqueous solution containing drug-loaded PAA-MSNs after sonication, confirming the partials release of encapsulated drug.

The MR images of a typical TSP containing drug-loaded PAA-MSN solution before and during heat treatment using focused ultrasound are shown in Figure 4.9a-b. The

temperature rise in the surrounding TSP provides suitable contrast in MR images which also confirms that all the container has been heated during the sonication. Figure 4.8c-d also illustrates a phantom before and after sonication using focused ultrasound. A colour change in the aqueous solution is clearly observed due to the partial leakage of red-coloured doxorubicin from the core-shell nanostructure. The measurement of drug release ratio using UV-Vis technique indicates that 39.2±2.2% of encapsulated doxorubicin is released from PAA-MSNs due to the sonication by focused ultrasound. This fact shows the capability of these nanoparticles for fast and effective release of encapsulated therapeutic agent when applied in clinical setting.

4.4 Conclusion

In this research, we developed a mesoporous silica-polyacrylamide core-shell nanostructure that showed thermal sensitivity in the temperature range of 40°C to 60°C. The nanoparticles were synthesized in average particle size range of 102±22 nm which is within the optimum particle size range (80-120 nm) for effective delivery of drug preferentially to the tumours through the enhanced permeability and retention (EPR) effect (Hon et al., 2012).

Doxorubicin was used as a typical guest hydrophilic drug to test the encapsulation ability of the synthesized nanoparticles. The mesoporous silica in this structure acted as a drug reservoir while the polyacrylamide shell prevented the entrapped drug from rapid diffusion outward the structure. Mesoporous silica nanoparticles are known as efficient carriers of diagnostic and therapeutic agents. Among various characteristics, the

biodegradability of these carriers is of particular interest which has been confirmed in a number of studies (Hon et al., 2012; Rosenholm et al., 2012). Silica nanoparticles (especially mesoporous silica) readily degrade in biological medium to form silicic acid, which is a natural trace compound in human. The in vivo degradation of these nanoparticles is often excessively fast (<12 h) for optimal drug delivery efficacy and thus, surface modifications are needed to increase their circulation time (Hon et al., 2012). Therefore, the polyacrylamide coating not only provides a sufficient degree of thermal sensitivity in the drug carrier, this polymeric layer could also protect the silica nanoparticles from rapid degradation within biological environments.

The toxicity, biocompatibility, and biodegradation of polyacrylamide have also been evaluated in a number of studies and no obvious evidence of toxicity, but even some degrees of biodegradability has been observed (Caulfield et al., 2002). However, more investigations are needed to confirm the safety of this polymer for application in drug delivery.

During the heating of these nanoparticles, the gelation of polymer shell at temperatures above 40°C provided preferred routes for facile diffusion of entrapped drug outside the nanoparticles. The obtained value of drug release at physiological temperature was obviously smaller than the reported value for hollow PNIPAM hydrogel (around 60%) (Xing et al., 2011) and DNA-capped mesoporous silica nanoparticles (approximately 30%) (Ruiz Hernandez et al., 2011). The release of doxorubicin at temperatures lower than 40°C might be due to the diffusion of the drug molecules which are entrapped in the PAA shell outward the nanostructure. By increase of the temperature above 40°C, the ratio of drug release from the PAA-MSNs was significantly increased due to the gradual

gelation of the polymer shell. Although the maximum drug release was obtained at temperatures above the clinically applicable temperature range, the nanoparticles could release over 50% of their loading at temperatures near 50ºC which could still be sufficient for an effective targeted drug delivery.

This thermosensitive behaviour makes these nanoparticles suitable for hyperthermia and thermal ablation temperatures range (45°C to 55ºC) which is mostly applied in thermal modalities such as high intensity focused ultrasound and radiofrequency. By targeted delivery of these carriers, a significantly higher local release of the encapsulated could be obtained with lower systemic toxicity levels compared to the current similar products. However, in spite of a significant decrease, the amount of drug release at physiological temperatures is still challenging which could be addressed in further studies. A wide and continuous transition range is another limitation of these nanoparticles that must be improved to obtain polymer layers with discontinuous gel-to-liquid transition temperatures. The stability tests in complete serum as well as in vivo comparative studies at both hyperthermia and thermal ablation ranges must also be conducted to determine the in vivo efficacy of the newly synthesized product.

CHAPTER 5: LOW-MELTING-POINT POLYMER SHELLS FOR THERMAL-TRIGGERED DRUG RELEASE UNDER HYPERTHERMIA CONDITION

5.1 Introduction

Thermosensitive nanocarriers of therapeutic drugs are increasingly combined with hyperthermia modalities to achieve improved drug delivery condition with minimized systemic toxicity and enhanced local drug dosage at tumour region (Ganta et al., 2008). Thermal sensitivity is often governed by a non-continuous alteration in at least one physical characteristic of the material during temperature change accompanied by structural defects which result in facilitated drug release from the nanostructure. The therapeutic drugs need be entrapped within the thermosensitive carrier at physiological temperature and rapidly released within the locally heated tumour to counteract quick clearance by the bloodstream (Mura et al., 2013).

Thermosensitive nanocarriers can be synthesized using a variety of organic and inorganic biomaterials such as lipids (Dicheva et al., 2014; Kneidl et al., 2014; Ta et al., 2013), self-assembling amphiphilic micelles (Croy et al., 2006; Kedar et al., 2010; Talelli et al., 2011), and biocompatible polymers (Gong et al., 2013; Qiu et al., 2001; Ward et al., 2011) which exhibit thermal-triggered drug release due to the gel-liquid, micellization, and coil-globule phase transitions, respectively. In addition to a number of general parameters such as biocompatibility and biodegradability, the clinical efficacy of these thermosensitive nanocarriers in hyperthermia application is mainly relied on the temperature range and discontinuity of their physical phase transition mechanisms.

In the previous chapter, we introduced a new mechanism of thermal sensitivity by employing polyacrylamide (PAA) nanoshells which exhibit gelation behaviour at increased temperatures. The gelation temperature of this polymer could be adjusted in the ablation temperature range by controlling the crosslinker/monomer ratio. Therefore, during exposure to the thermal ablation modalities, the encapsulating PAA nanoshell could quickly dissociate and thus facilitate drug release from the nanostructure. However, the crucial limitation of these polymers was their continuous phase transition occurring in a wide temperature range which required relatively high temperatures and irradiation energies to provide the maximum drug release value.

In the current chapter, we aim to achieve sharper gel-liquid transition temperatures by replacing the PAA layer with a polyethylene glycol (PEG) nanoshell. PEGs are hydrophilic and biocompatible polymers which have been widely employed to improve the stealth behaviour of various nanocarriers and decrease their clearance by the reticuloendothelial system (RES) (Jokerst et al., 2011; Li et al., 2014; Otsuka et al., 2012; Salmaso et al., 2013). However, the potential of these polymers for application as low-melting-point encapsulating shells has not been evaluated.

The phase transition temperature of PEG polymers could be adjusted within the hyperthermia range by controlling their molecular weight. Therefore, different molecular weights of PEG were examined to determine the optimal formulation which offers a melting temperature within the hyperthermia range. The selected PEG was then employed to encapsulate doxorubicin within a mesoporous silica core. It was assumed that the gel-liquid phase transition of PEG shell under hyperthermia condition could facilitate diffusion of the physically entrapped drugs into the surrounding environment. Figure 5.1

illustrates a schematic of the expected release mechanism from the PEG-coated mesoporous silica nanoparticles (PEG-MSNs) at hyperthermia temperatures.

5.2 Materials and Methods

5.2.1 Calculation of the Optimal PEG Molecular Weight

Three PEG formulations with molecular weights of 1000 Da (PEG1000), 1500 Da (PEG1500), and 2000 Da (PEG2000) were purchased from Sigma-Aldrich (M) SDN. BHD. (Kuala Lumpur, Malaysia) in order to determine a formulation which shows the gel-liquid phase transition close to the hyperthermia temperature range. The phase transition behaviours of these polymers were evaluated using differential scanning calorimetry (DSC; DSC820 with TSO 801RO robot, Mettler-Toledo, Columbus, OH, USA) with scan rate of 5 $^{o}C.min^{-1}$. The recipe with the desired range of phase transition temperature was then chosen for synthesis of PEG-MSNs.

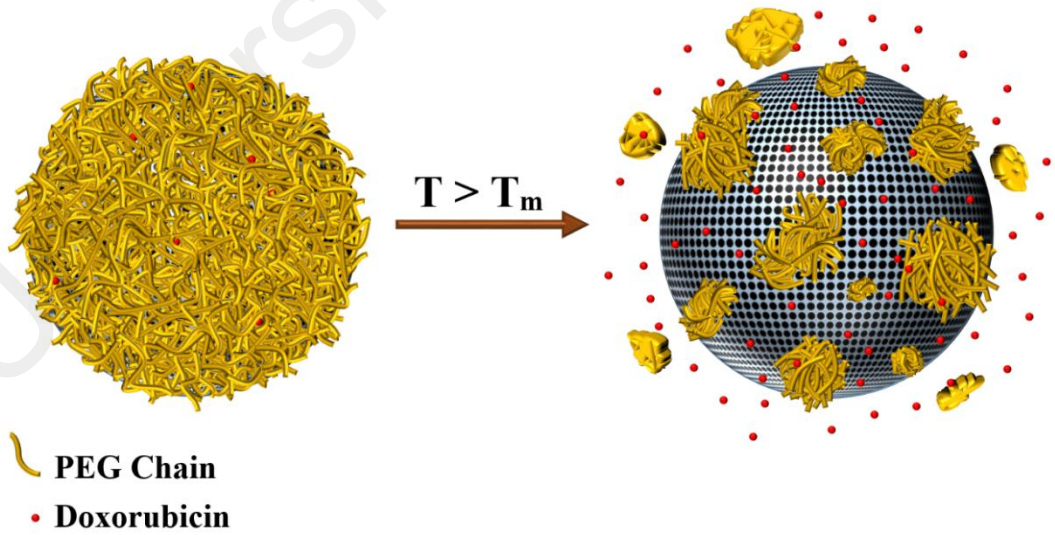

Figure 5.1: A schematic of the expected release mechanism from the synthesized core-shell structures at hyperthermia temperatures. Tm = PEG melting point.

5.2.2 Synthesis of Core-shell Nanoparticles

The PEG-MSNs were synthesized using diamine-terminated PEG, toluene, tetraethyl orthosilicate (TEOS), cetyltrimethyl ammonium bromide (CTAB), ammonia solution (28 %w/w), ethanol, and hydrochloric acid aqueous solution (HCl; 37 %w/w) obtained from Sigma-Aldrich (M) SDN. BHD. (Kuala Lumpur, Malaysia).

The mesoporous silica nanoparticles (MSNs) were firstly activated according to the method proposed in chapter 4. The activated particles (AMSNs) were further coated by a PEG shell using a facile graft-to technique. In a typical procedure, equal weight ratios of the MSNs and diamine-terminated PEG (1 g each) were added to 50 ml of toluene. The solution was heated to 80°C and vigorously stirred for 24 hours. The resulting suspension was then centrifuged at 4,000 rcf for 15 minutes, washed for three times with ethanol and distilled water, and freeze dried for 24 hours to obtain the PEG-MSN core-shell nanoparticles.

5.2.3 Material Characterization

The presence of hydroxyl and amine bonds in the AMSNs and diamine-terminated PEG structures as well as the formation of PEG-MSN nanoparticles were confirmed by Fourier transform infrared spectroscopy (FT-IR; Nicolet 6700, Thermo Scientific, Waltham, MA, USA) at wavenumber range of 600 to 4000 cm^{-1}. The particle size distribution was analysed by dynamic light scattering (DLS) technique using Malvern Zetasizer Nano ZSP instrument (Malvern Instruments, Worcestershire, UK). This instrument was also employed to determine the zeta potential of the synthesized

nanoparticles in an aqueous medium with pH 7.0. Transmission electron microscopy (TEM; Libra 120 kV, Carl Zeiss AG, Oberkochen, Germany), and atomic force microscopy (AFM; Ambios AFP-200, Ambios Technology Inc., Santa Cruz, CA, USA) were also employed to visualize the structural morphology of the PEG-MSNs. DSC analysis was again applied on PEG-MSNs to determine the probable changes in the phase transition temperature of the PEG compartment after formation of the core-shell structure.

5.2.4 Drug Loading Experiments

The drug loading experiments were performed according to the protocol described in chapter 4. In brief, the PEG-MSNs were immersed in an aqueous solution containing 2 $mg.ml^{-1}$ doxorubicin in three different intervals (24, 48, and 72 hours) to determine the optimal incubation time which results in the statistically maximum encapsulation value (E_m). Drug loading procedure was performed at room temperature in 25 ml glass tubes without shaking during incubation. The drug-loaded PEG-MSNs were then separated from the supernatant by centrifuging at 16,100 rcf for 60 minutes. The drug quantity in the aqueous supernatants was further determined using Ultraviolet-Visible spectroscopy (UV-Vis) (Shimadzu UV-1800, Shimadzu Corporation, Kyoto, Japan) at wavelength range of 260 to 600 nm. The drug loading quantities were calculated by comparing the obtained UV-Vis spectra with that of a reference solution containing 2 $mg.ml^{-1}$ doxorubicin. The optimal incubation time determined in these experiments was applied in further steps to encapsulate doxorubicin within the PEG-MSNs structure.

5.2.5 Drug Release Experiments

The drug release studies were also followed our procedure described in chapter 4. The drug-loaded PEG-MSNs were firstly stabilized in an aqueous solution (2 $mg.ml^{-1}$) at 37ºC for 7 days. The supernatants were then separated and the ratio of drug leakage was quantified by comparing the UV-Vis spectra of the supernatants with that of a reference solution containing E_m $mg.ml^{-1}$ doxorubicin.

The drug release ratios at increased temperatures were also quantified by preparation of ten similar aqueous solutions containing 2 $mg.ml^{-1}$ of drug-loaded PEG-MSNs. Each solution was heated in a water bath for 30 minutes at a designated temperature. Ten temperature values of 30, 37, 40, 45, 50. 55, 60, 65, 70, and 75°C were chosen in this study to simulate the hyperthermia and thermal ablation conditions as well as to determine the drug release ratios at different temperatures.

After heat treatments, the PEG-MSNs were separated from the supernatants and the drug release percentages were measured by comparing the obtained UV-Vis spectra with that of the reference solution.

5.2.6 Magnetic Resonance-Guided Focused Ultrasound (MRgFUS) Tests

The PEG-MSNs were also sonicated using MRgFUS method (EX-ablate, Insightec, Haifa, Israel) as a typical thermal modality to evaluate the rate of drug release from their structure. In these experiments, a tube containing an aqueous solution of doxorubicin-loaded PEG-MSNs was placed in a thermosensitive tissue-mimicking phantom (TSP)

developed in chapter 4. The phantom was then sonicated for 5×20 seconds at frequency of 1.15 MHz with the acoustic energy and acoustic power of 5313 J and 266 W, respectively. The drug release ratios after sonication were further measured by UV-Vis technique.

5.2.7 Data Analysis

All the thermal analyses, drug loading/release tests, and MRgFUS experiments were carried out for at least five times and the results were reported as mean ± standard deviation using the Statistical Package for Social Sciences software (SPSS 20, SPSS Inc., Chicago, IL, USA). The confidence interval value of 95% was also chosen for performing the comparative studies.

5.3 Results and Discussion

5.3.1 Selection of the Optimal PEG Molecular Weight

The DSC spectra of PEG formulations with different molecular weights are shown in Figure 5.2 and their critical temperatures of phase transition are summarized in Table 5.1. By increase of the molecular weight from 1000 Da to 2000 Da, the onset (T_O) and peak (T_P) phase transitions temperatures were respectively increased from 25.3±2.5°C and 37.1±2.3°C to 45.4±1.5°C and 50.0±1.3°C, whereas the phase transition intervals decreased from 11.8°C to 4.6°C. Therefore, heavier PEG formulations provided a sharper phase transition in contrast to those with lower molecular weights. However, the optimal

range of phase transition temperature for hyperthermia application was observed in PEG1500. Although the T_P value of PEG1500 was approximately 48.3±1.7°C, the phase transition initiated at 40.4±1.8°C which was appropriate for drug release under hyperthermia condition. Therefore, PEG1500 was selected in order to synthesize the PEG-MSNs for thermal-triggered drug release at hyperthermia temperature range.

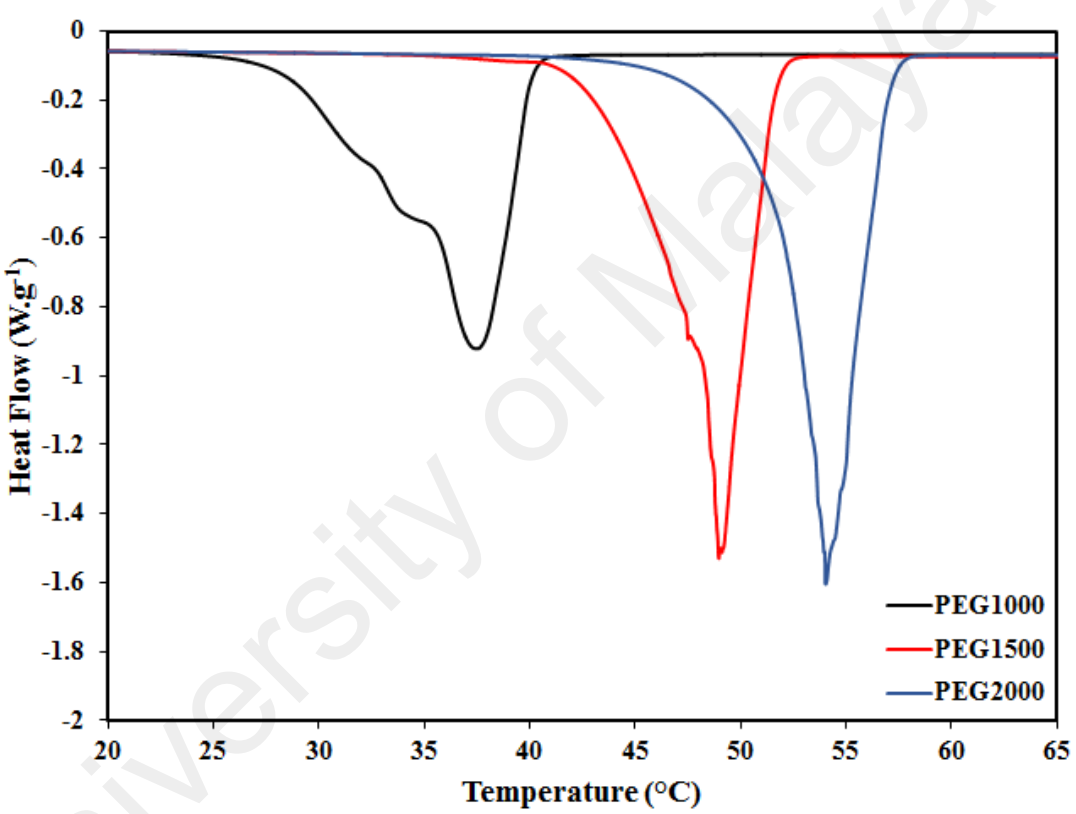

Figure 5.2: The DSC analyses of PEG formulations with molecular weights of (a) 1000 Da, (b) 1500 Da, and (c) 2000 Da. Increase of the molecular weight results in higher phase transition temperatures.

Table 5.1: The phase transition properties of various PEG molecular weights examined for synthesis of PEG-MSNs. Data are presented as mean ± standard deviation

	PEG1000	**PEG1500**	**PEG2000**
Molecular Weight (Da)	1000	1500	2000
Onset Temperature of Phase Transition (°C)	25.3±2.5	40.4±1.8	45.4±1.5
Peak Temperature of Phase Transition (°C)	37.1±2.3°C	48.3±1.7	50.0±1.3
Phase Transition Interval (°C)	11.8	7.9	4.6

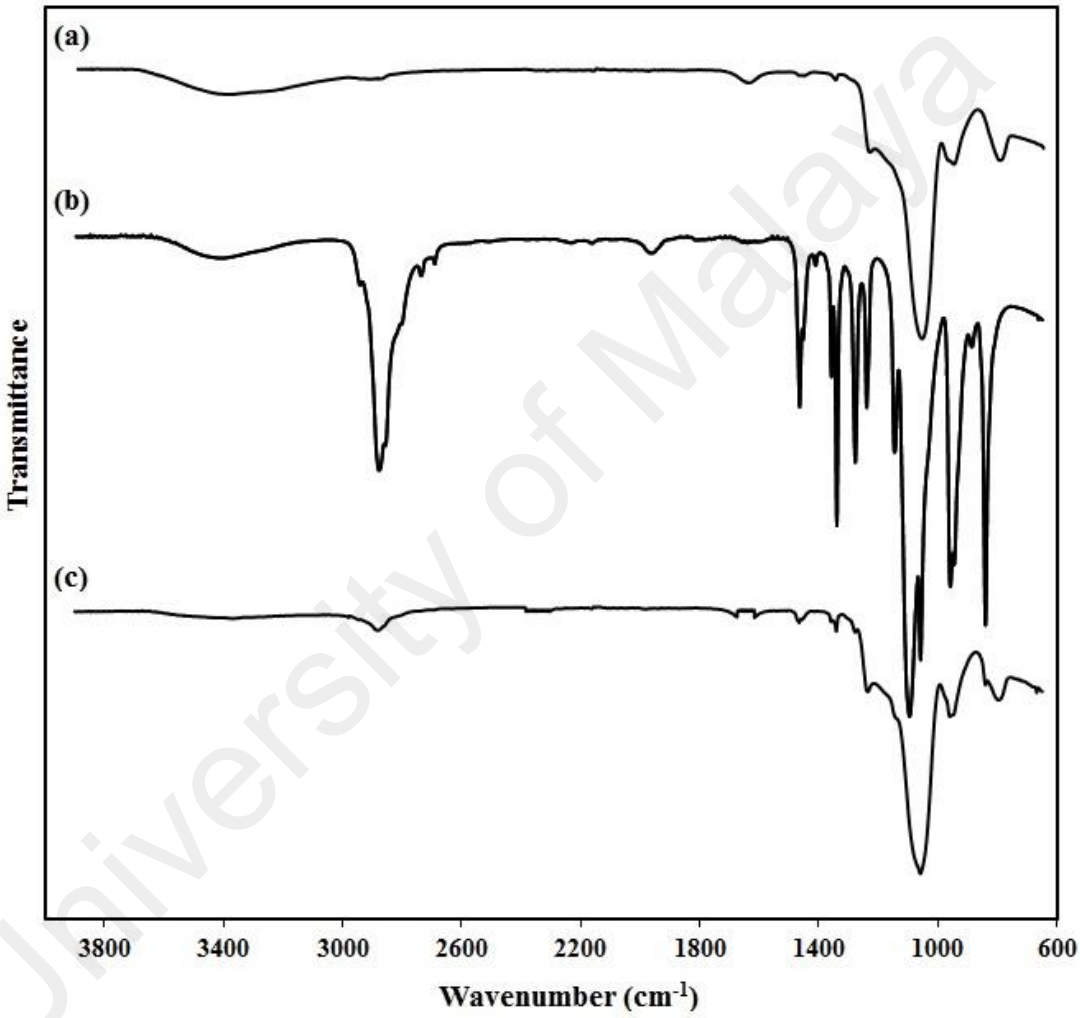

Figure 5.3: The FT-IR spectra of the particles at different synthesis stages. (a) AMSN, (b) diamine-terminated PEG, and (c) PEG-MSNs.

5.3.2 Material Characterization

The FT-IR spectra of the AMSNs, diamine-terminated PEG, and PEG-MSNs are presented in Figure 5.3. The strong peak observed at 1045 cm^{-1} in AMSNs represents the Si-O-Si vibration, whereas the wide stretch at wavenumber range of 3200-3600 cm^{-1} belongs to the absorbed water. A wide stretch was also observed in the FT-IR spectrum of diamine-terminated PEG which probably represents the amine bonds in this polymer. In FT-IR spectrum of the PEG-MSNs, the characteristic peaks of both MSNs and PEG were observed, which proved the presence of both these materials within the synthesized nanoparticles. However, the peak intensities of the MSNs were significantly higher, indicating the dominance of MSNs weigh ratio in the core-shell nanostructure.

Figure 5.4 shows typical DLS spectra of MSNs prior, and after PEGylation. Formation of a thin PEG layer on the MSN surfaces resulted in slight increase of the particle size from 95±2 nm to 102±4 nm. Moreover, the zeta potential of the particles was decreased from 8.48±0.33 mV to 4.14±0.42 mV at pH 7.0, probably due to the coverage of surface reactive groups, which act as anchors for PEG conjugation (Andreani et al., 2014).

A typical TEM image of the core-shell nanostructures synthesized using PEG1500 is illustrated in Figure 5.5. The MSNs were uniformly covered with a thin PEG layer which not only acted as an encapsulating shell, could also minimize the particle agglomeration in the aqueous solution. However, a relatively low nanoshell thickness was obtained, probably due to the short length of the PEG1500 chains. Although the shell thickness may be increased by utilization of PEG formulations with higher molecular weights, a significant change in the phase transition temperature makes the heavier polymers impractical for hyperthermia application.

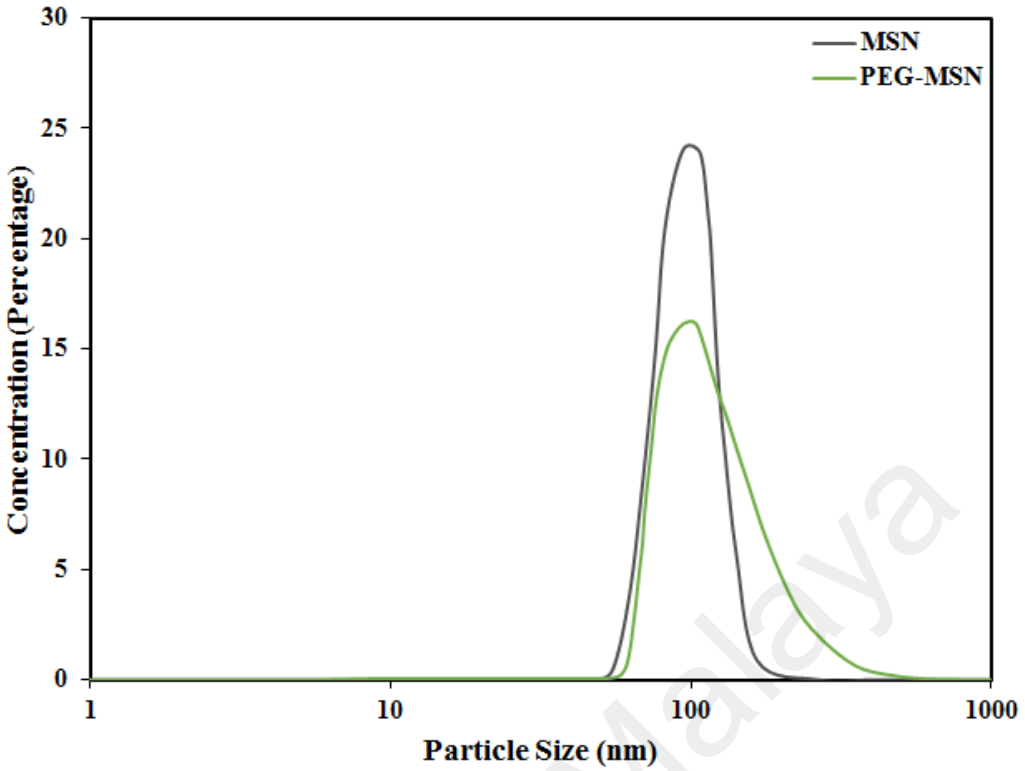

Figure 5.4: Particle size distribution of the MSNs prior, and after PEGylation.

The PEG-MSN nanoparticles were again subjected to the DSC analysis in order to determine the probable alteration of the PEG phase transition temperature after formation of the core-shell nanostructure (Figure 5.6). The results indicated that interaction with the MSN core had negligible influence on the phase transition temperature of the PEG nanoshell. Although small increases were observed in the mean T_O (43.5±2.5°C) and T_P (49.3±2.7°C) values of the PEG nanoshell, these values were not significantly different from those of pure PEG1500 polymer. The wide peak in the DSC graph of the PEG-MSNs at temperatures above 100°C might be corresponded to evaporation of the water absorbed by the MSN cores. The T_O value of the PEG nanoshell was comparable to that of PAA obtained in our previous study which may minimize the polymer dissociation at

physiological temperature. However, the PEG1500 nanoshell presented a significantly narrower transition temperature range as well as a lower T_P value in contrast to the PAA shell (Table 5.2), which may lead to higher drug release rates and quantities and less amounts of thermal energy required for achieving the maximum drug release.

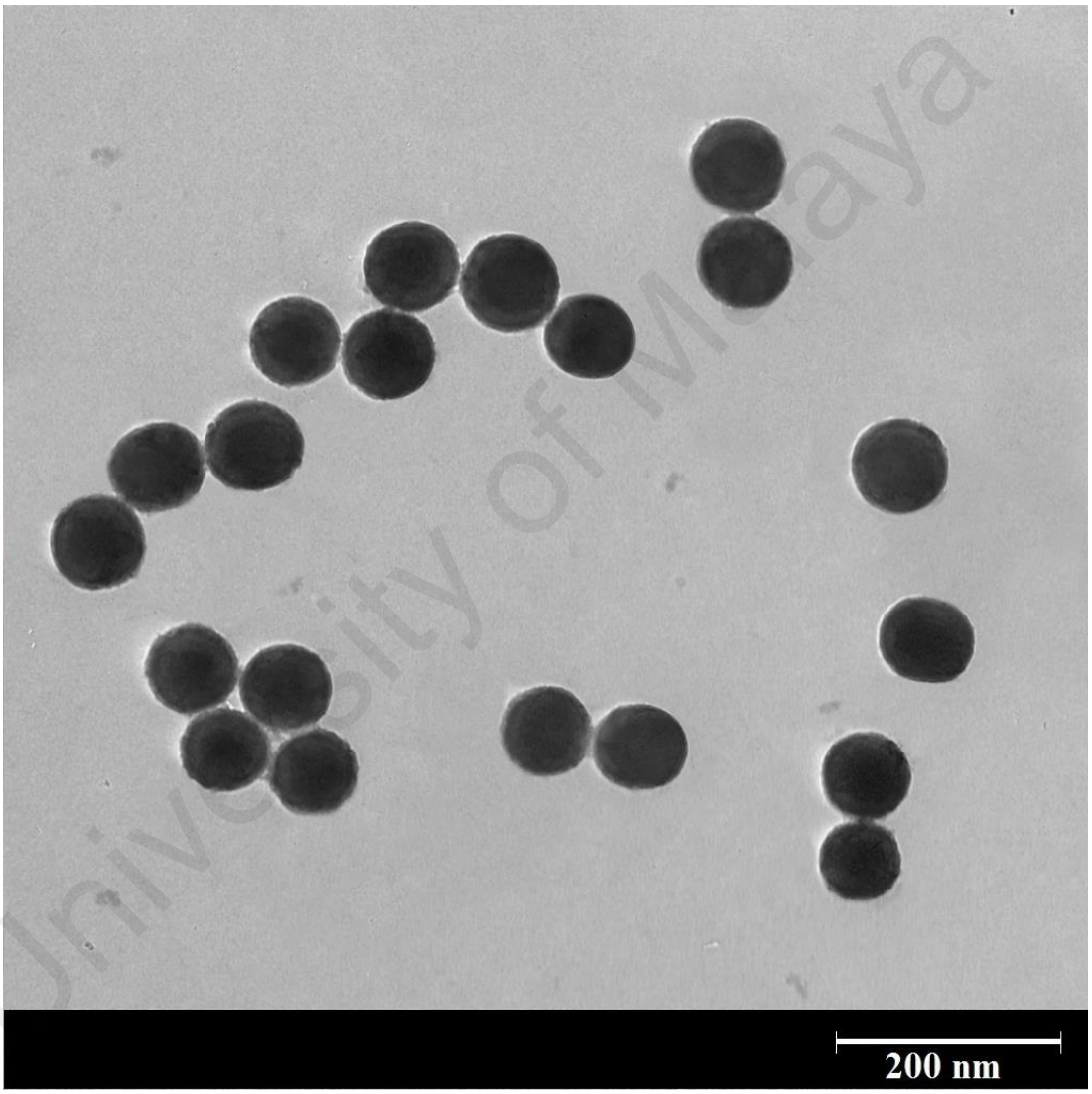

Figure 5.5: A typical TEM image of the synthesized nanostructure. An ultrathin PEG shell is formed on the surface of mesoporous silica nanoparticles.

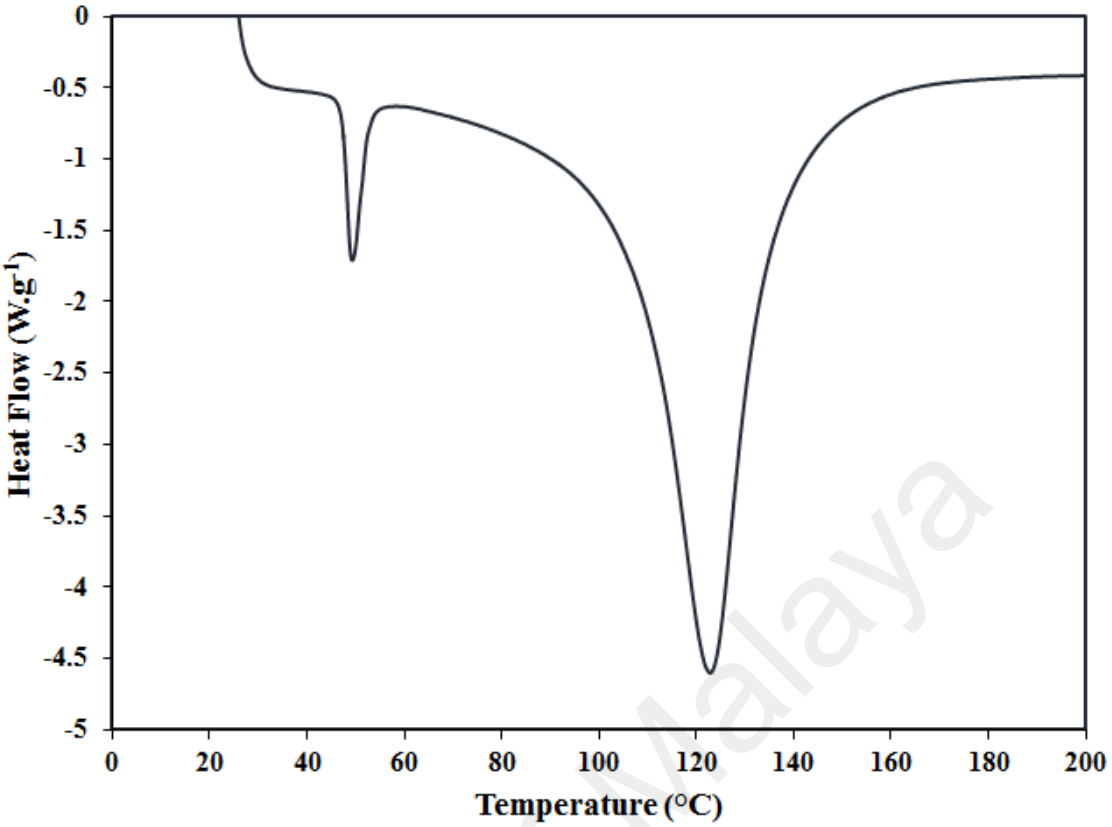

Figure 5.6: The DSC analysis of the core-shell nanoparticles prepared using PEG1500. The phase transition temperature of PEG remained unaltered after formation of the core-shell structure.

Table 5.2: A comparison between the drug loading and release characteristics of PEG-MSNs and PAA-MSNs. Data are presented as mean ± standard deviation.

	PAA-MSNs	**PEG-MSNs**
Coating Thickness	~12	~7
Optimal Drug Loading Interval (hours)	48	48
Drug loading amount (mg per g of nanoparticles)	208±20	183±14
Onset Temperature of Phase Transition (°C)	45.1±3.4	43.5±2.5
Peak temperature Phase Transition (°C)	68.3±4.2	49.3±2.7
Phase Transition Interval (°C)	23.2	5.8
Drug Leakage Ratio (%)	11.5±2.4	20.2±4.3
Maximum Drug Release Ratio (%)	67.6±2.5	68.2±3.7
Maximum Drug Release Temperature (°C)	60	50
Drug Release by 5×20 s MRgFUS Sonication (%)	39.2±2.2	45.5±3.1

5.3.3 Drug Loading Behaviour

The optimal incubation time needed for encapsulation of doxorubicin in PEG-MSN structure was determined by UV-Vis spectroscopy. The UV-Vis spectra of the supernatants after centrifugal separation of the PEG-MSNs from the doxorubicin solution are illustrated in Figure 5.7a. The increase of incubation time resulted in reduced UV absorption intensities and thus, decreased doxorubicin concentrations in the supernatant. The amounts of encapsulated doxorubicin in the PEG-MSNs at different intervals are also plotted in Figure 5.7b.

With the increase of incubation time up to 48 hours, the average ratio of encapsulated doxorubicin in the nanoparticles was increased (183±14 mg in 1 g of PEG-MSNs) and then, no significant change in this quantity was observed. Although the optimal incubation time was identical to that observed in the PAA-coated MSNs (PAA-MSNs), however the amount of encapsulated drug in PEG-MSNs was significantly lower than that of PAA-MSNs (Table 5.2). This might be due to the lower thickness of the PEG shell in contrast to that of PAA which resulted in less amounts of drug entrapped within the polymer shell.

Based on the obtained results, incubation time of 48 hours was used in further experiments to prepare the drug-loaded nanoparticles. Moreover, an aqueous solution containing 366 $\mu g.ml^{-1}$ (the average quantity of drug encapsulated in 2 mg of the PEG-MSNs) doxorubicin was prepared and its UV-Vis absorbance at wavelength range of 260-600 nm was recorded as reference for 100% drug release to quantify the ratio of drug release at ten different applied temperatures.

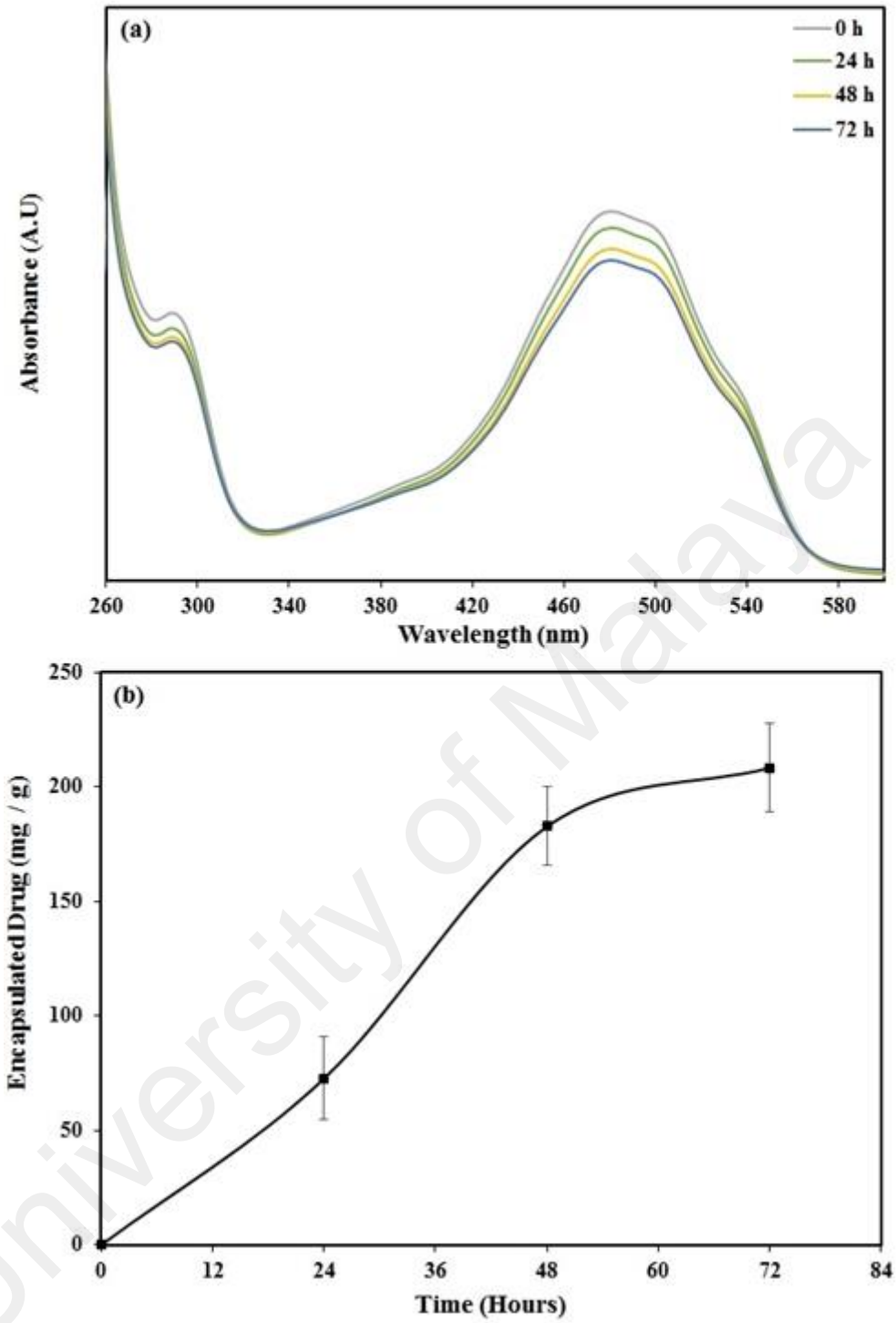

Figure 5.7: The ability of nanoparticles in encapsulation of doxorubicin. (a) UV-Vis spectra of drug solution after separation of PEG-MSNs which were incubated for 0, 24, 48, and 72 hours; (b) the quantity of doxorubicin encapsulated in the nanoparticles at various incubation intervals.

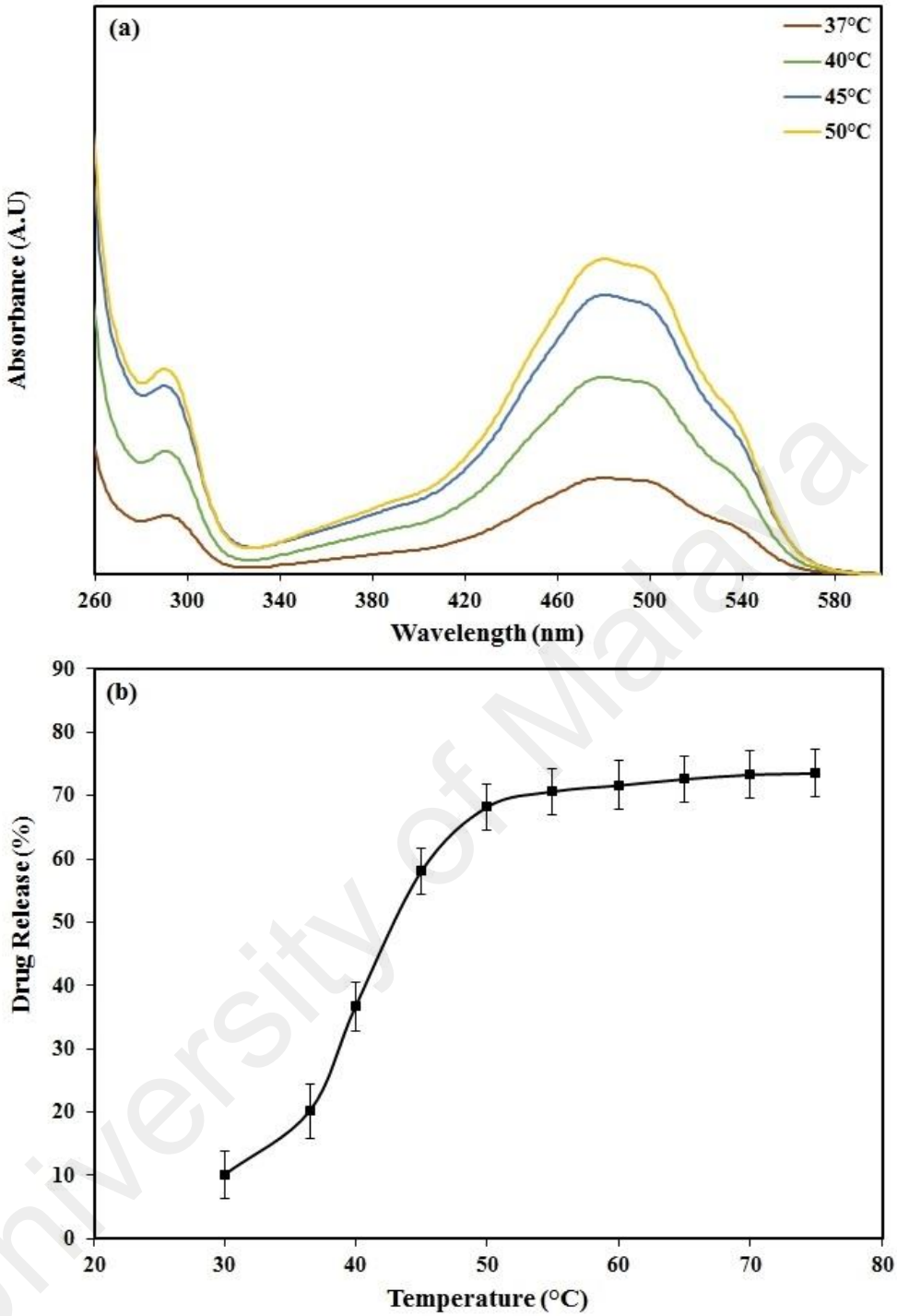

Figure 5.8: The ability of nanoparticles in release of doxorubicin. (a) UV-Vis spectra of supernatants after separation of drug-loaded PEG-MSNs which were heated at 37, 40, 45, and 50°C; (b) the ratio of drug release from the PEG-MSNs after heating at different temperatures for a period of 30 minutes.

5.3.4 Drug Release Behaviour

Figure 5.8a shows the typical absorbance intensities of three specimens heated at 37, 40, 45, and 50°C. The similarity of absorbance spectra at different temperatures indicated the stability of encapsulated doxorubicin during the experiments. The brown spectrum gives an indication of the diffuse-type release of doxorubicin molecules from the PEG-MSNs at 37°C. The green and blue spectra respectively show that relatively higher amounts of drug molecules could be released at 40°C and 45°C, probably due to a partial melting of the PEG1500 shell at these temperatures. However, the most intense absorbance was established by the specimens heated at 50°C. Figure 5.8b also shows the percentage of drug release at different temperatures from 30 to 75°C.

Incubation of PEG-MSNs at 37°C resulted in a 20.2±4.3% drug leakage which was not statistically different from that obtained after immersion at similar temperature for 7 days (23.1±4.5%). Therefore, it may be concluded that the entrapped drug inside the polymer shell could be rapidly released after incubation of the drug-loaded PAA-MSNs into the aqueous solution. According to Figure 5.8b, the maximum ratio of drug release (68.2±3.7%) was obtained at 50°C and then no significant increase in this value was observed.

The TEM images of typical PEG-MSNs after heating at 50°C (Figure 5.9a) illustrated some small polymer masses detached from the particle surfaces. Therefore, a number of preferred routes could be generated which facilitate the diffusion of therapeutic agent. Moreover, the TEM and AFM images in Figure 5.9 indicated that in contrast to the PAA-MSNs, the gel-liquid phase transition of the PEG shell might not result in agglomeration of the nanoparticles, probably due to the low thickness of the polymer shell.

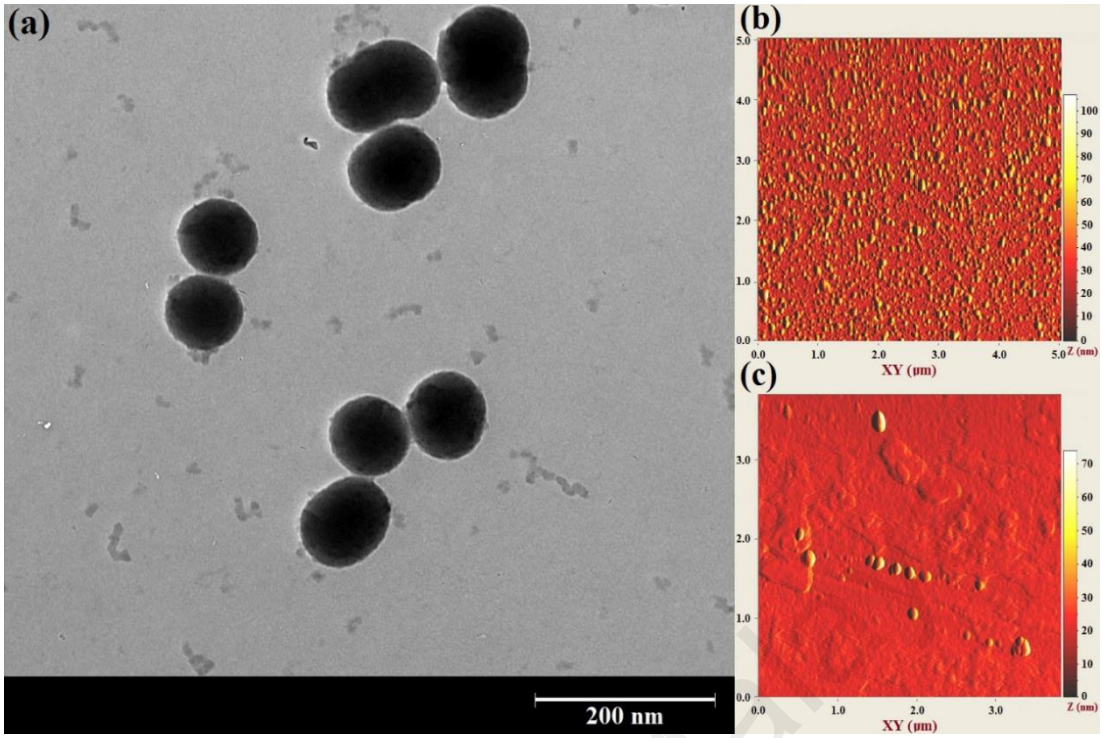

Figure 5.9: (a) TEM image of PEG-MSNs after heating at 50°C. The PEG nanoshell is partially removed because of gel-liquid phase transition at this temperature range. (b, c) AFM image of PEG-MSNs prior, and after heating at 50°C, respectively.

5.3.5 Drug Release under MRgFUS Exposure

The technique employed for sonication of the doxorubicin-loaded PEG-MSNs with MRgFUS modality is presented in Figure 5.10. Heating of the TSP by the ultrasound pulses resulted in a dark oval area in the magnetic resonance (MR) images shown in Figures 5.10a-c. The temperature patterns of the focal region at different sonication times (Figure 5.10d-g) also showed a gradual propagation of the heated volume until the entire container reached the maximum temperature at 19 seconds. In a typical MRgFUS procedure, the temperature of the focal point was raised to over 50°C and 70°C after sonication for approximately 2 and 5 seconds, respectively (Figure 5.10h), generating enough thermal energy for initiating the gel-liquid phase transition of the PEG nanoshell.

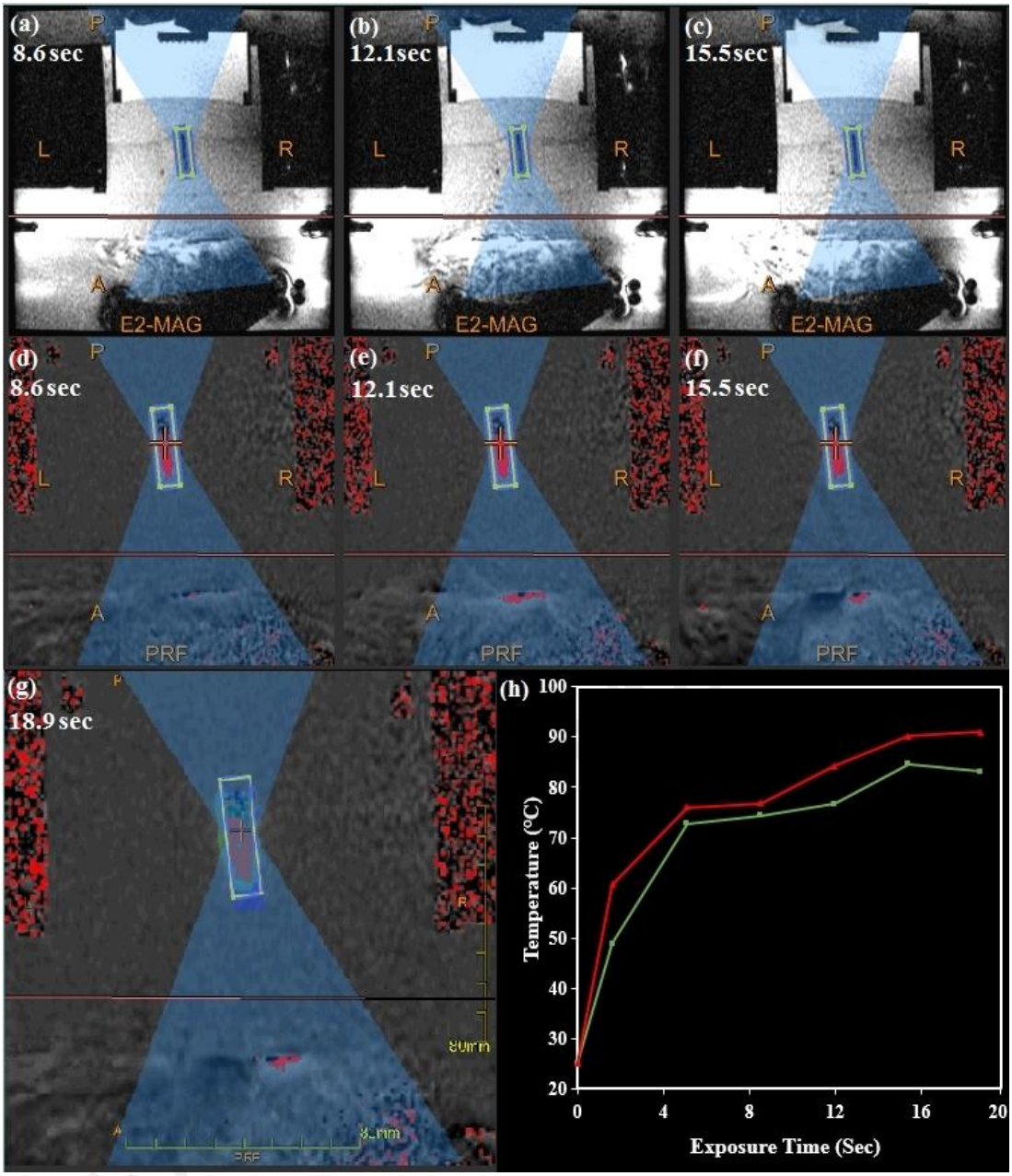

Figure 5.10: The protocol employed in MRgFUS sonication of PEG-MSNs. (a-c) Typical magnetic resonance phase images of a TSP containing doxorubicin-loaded PEG-MSNs during MRgFUS experiments; (d-g) the changes in temperature patterns during heating process, where maximum temperatures are illustrated in red; (h) a typical temperature pattern showing the minimum (green) and maximum (red) rates of temperature change in the focal region during sonication.

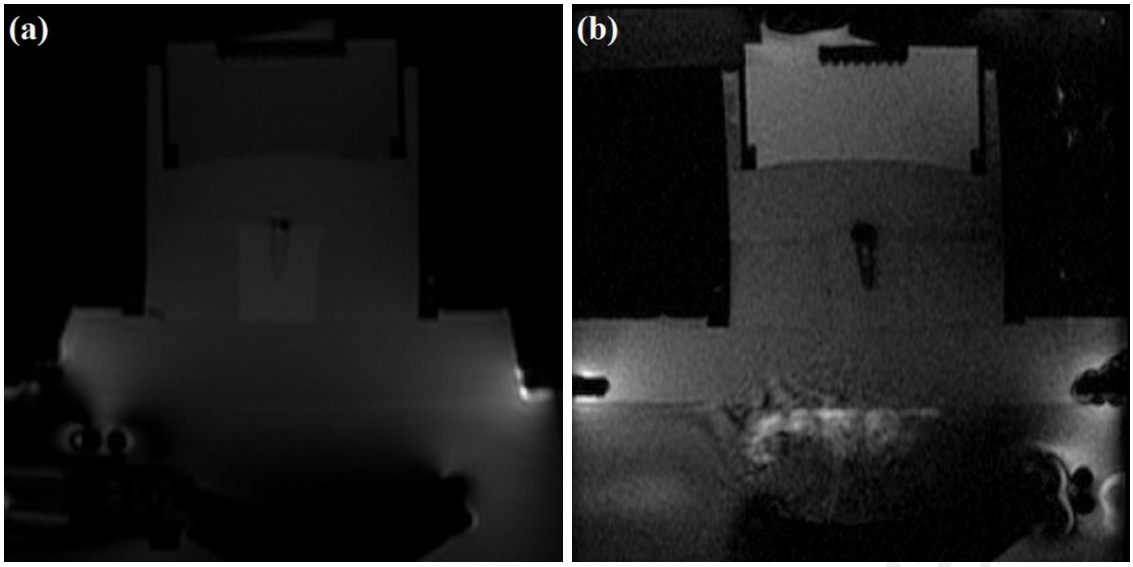

Figure 5.11: Magnetic resonance phase images of a typical TSP containing drug-loaded PEG-MSNs (a) prior and (b) during sonication. Formation of a dark region around the container shows the uniform heat distribution within the container.

The MR images of a typical TSP containing an aqueous solution of doxorubicin-loaded PEG-MSNs prior and during sonication are illustrated in Figure 5.11a-b. The change in the MR contrast parameters of the surrounding TSP during sonication proved the uniform distribution of thermal energy within the container. The UV-Vis analysis indicated a 45.5±3.1% drug release from the PEG-MSNs after MRgFUS sonication for 5×20 seconds. This result showed the potential of these nanoparticles for rapid release of encapsulated therapeutic drugs when used in clinical practice.

5.4 Conclusion

Thermal-triggered drug release in polymer-based nanoparticles is mostly achieved by coil-globule or micellization phase transitions at their lower critical solution temperatures

(LCSTs). However, most of the polymers which exhibit coil-globule transition possess dubious biocompatibility and biodegradation (Patenaude et al., 2012). Moreover, the LCST of these polymers are often not appropriate for hyperthermia application and must be adjusted by copolymerization with other hydrophilic or hydrophobic moieties, which may negatively affect their thermosensitive behaviour (Kaneko et al., 1998).

The LCST may also depend on the nature and molar concentration of the comonomers (Kujawa et al., 2006), solvent quality (Lien et al., 2008), and co-solvents or additives present in the solution (Lutz et al., 2006). For instance, substitution of water with deuterated water results in a 1-2°C increase in the LCST of poly(N-isopropyl acrylamide) (PNIPAM) thermosensitive polymers (Wang et al., 1999).

Polymers with micellization behaviour such as poloxamers have also shown potential for application in drug delivery systems and one particular formulation comprised of Pluronics® L61 and F127 is currently undergoing clinical trials in phase III for treatment of metastatic esophageal adenocarcinoma and other upper gastrointestinal tract cancers (Pitto Barry et al., 2014). However, weakness of the physical crosslinking between the micelles may cause insufficient in vivo stability for passive targeting of nanocarriers by the enhanced permeability and retention (EPR) effect, which requires a long-term circulation in the bloodstream. In vitro experiments reported a complete dissolution of a 25 %w/w poloxamer 407 and 50% dissolution of a 35 %w/w poloxamer 407 into phosphate buffered saline (PBS) medium after 4 hours (Bhardwaj et al., 1996). Therefore, resilience of these hydrogels need be improved to achieve long-term retention of the therapeutic drug in the blood circulation.

In order to address the limitations of these thermosensitive polymers, we previously introduced a new mechanism of thermal-triggered drug release based on the polymer gelation and dissociation at temperature range of 40°C to 60°C which result in facilitated drug flow into the surrounding environment. The obtained value of drug leakage at physiological temperature was significantly less than that of hollow PNIPAM hydrogel (Xing et al., 2011) and DNA-capped mesoporous silica nanoparticles (Ruiz Hernandez et al., 2011) (approximately 60% and 30%, respectively). However, because of a wide and continuous transition temperature range, the maximum ratio of drug release in these nanoparticles occurred at temperatures inapplicable in clinical practice.

In the current research, the PAA shell was replaced with PEG in order to achieve a sharper phase transition and obtain the maximum drug release value at temperatures more close to the clinical hyperthermia range. The biocompatibility and biodegradability of PEG has been demonstrated in a number of studies (Chen et al., 2014; Mahoney et al., 2006). Moreover, the short- and long-term influence of PEGylation on biodegradability of MSNs in different media including aqueous solutions (Lin et al., 2011), simulated body fluids (SBF) (Cauda et al., 2010), phosphate buffered saline (PBS) (Rytkönen et al., 2012), and Dulbecco's modified eagle's medium (DMEM) with fetal bovine serum (FBS) (Lin et al., 2011) has been evaluated. Although the biodegradability of these nanoparticles in complex environments is relatively lower than that in aqueous solutions, however PEGylation shows an overall enhancing effect on MSNs biostability, yielding to a decreased loss of mesoporous parameters such as surface area and pore volume (Cauda et al., 2010; Lin et al., 2011).

The PEG coating could also improve the colloidal stability of MSNs by increasing their hydrophilicity as well as the steric distances, which in turn reduces the attraction forces between the nanoparticles (Jokerst et al., 2011). Moreover, decreased surface charge due to the coverage of active groups by the PEG layer results in decreased protein adsorption (opsonization) on the particles surfaces (Lin et al., 2011; Rytkönen et al., 2012). Therefore, the PEG shell can endow the nanoparticles with stealth properties, decreasing their clearance by the RES system.

The gel-liquid phase transition temperature of PEG is significantly influenced by its molecular weight. Therefore, various PEG molecular weights were firstly examined to determine the formulation with optimal phase transition temperature. The results indicated that the phase transition of PEG1500 which initiated at 40.4±1.8°C and reached its peak at 48.3±1.7°C, could be appropriate for hyperthermia application. The phase transition interval of core-shell nanoparticles synthesized using MSNs and PEG1500 (5.8°C) was significantly narrower than that of PAA-MSNs (23.2°C). As a result, despite the maximum ratios of drug release were not statistically different in both PAA-MSNs and PEG-MSNs (67.6±2.5% and 68.2±3.7%, respectively), this amount in PEG-MSNs was achieved at approximately 10°C lower than PAA-MSNs (Table 5.2). However, the ratio of drug release at physiological temperatures was significantly higher in PEG-MSNs in contrast to PAA-MSNs, probably because of the low thickness of the PEG nanoshell which resulted in faster leakage of encapsulated drug at lower temperatures.

The gel-liquid phase transition of PEG-MSNs allowed a rapid drug release when these nanoparticles were exposed to MRgFUS sonication for 100 seconds. Therefore, these nanocarriers show potential for rapid supply of the encapsulated anticancer drugs in a

locally heated tumour. However, a relatively high drug release ratio at body temperatures must be addressed in further studies to minimize the systemic toxicity of these carriers.

It is also important to note that replacement of the MSN core with superparamagnetic compounds could enhance the contrast properties in MR images and allow nanoparticle navigation using external magnetic fields with appropriate intensities. Moreover, the high thermal conductivity of superparamagnetic cores could increase the melting rate of polymeric shells and lead to higher drug release rates under hyperthermia condition. However, limited loading capacity for encapsulation of therapeutic agents is the crucial limitation of superparamagnetic materials which may inflict insufficient drug dosage at tumour site. In a preliminary study, drug-loading values below 50 mg were observed in 1 g of PEG-coated maghemite nanoparticles. Synthesis of maghemite nanoparticles with porous structure could be a particular solution to achieve higher drug loadings combined with intrinsic advantages of these superparamagnetic materials.

CHAPTER 6: CONCLUSION AND RECOMMENDATION FOR FURTHER RESEARCH

6.1 Conclusion

Temperature-based drug delivery has been extensively investigated to achieve the synergistic effect of chemotherapy and hyperthermia and overcome the intrinsic limitations of each approach such as high systemic toxicity and low ablation efficiency of large tumours, respectively. However, the majority of developed thermosensitive nanocarriers remain far from clinical application due to a number of shortcomings such as low dosage delivery, immature drug release, rapid degradation or clearance by the reticuloendothelial system, and low mechanical stability in physiological environment.

In the current research, we introduced a new triggering mechanism in thermosensitive nanocarriers comprised of mesoporous silica nanoparticles (MSNs) and two low-melting-point polymer nanoshells including polyacrylamide (PAA) and polyethylene glycol (PEG). The drug loading and release behaviours of these nanocarriers at hyperthermia and thermal ablation temperature ranges were investigated using doxorubicin as a hydrophilic model drug. The drug release ratios at short exposure intervals were also evaluated using magnetic resonance-guided focused ultrasound (MRgFUS) technique. Both PAA and PEG have been previously utilized to synthesize core-shell nanostructures with different core materials. In particular, PEG is extensively employed to improve the stealth characteristic of nanoparticles and increase their circulation time. However, the potential of these polymers as thermosensitive nanoshells for localized delivery of therapeutic agents under hyperthermia and thermal ablation conditions has not been investigated.

In vitro investigation of the synthesized nanocarriers required a tissue-mimicking phantom with high thermal stability and accurate acoustic simulation of the soft tissues. Therefore, a novel thermosensitive phantom was also developed to allow visual detection of the thermal lesion via a reversible discolouration at hyperthermia temperature. Moreover, the contrast changes at increased temperature resulted in an easier detection of the focal point during MRgFUS sonication.

According to the project objectives defined in chapter 1, the obtained results could be categorized in three parts including thermosensitive phantom studies, proof-of-concept study, and PEG-MSN synthesis which are summarized in the following sections.

6.1.1 Thermosensitive Phantom Studies

1. In chapter 3, we developed a thermosensitive phantom using a thermochromic dye (TCD) of type N-(2-ethoxyphenyl)-N'-(2-ethylphenyl) ethanediamine. The incorporated TCD was blue-coloured at room temperature and colourless (transparent) above a specific temperature level. Therefore upon heating, a colourless region was generated inside the phantom, allowing an accurate three-dimensional assessment of the thermal profile during power absorption.
2. Due to the reversibility of TCD discolouration, the exothermic nature of the polymerization reaction could not inflict undesired phantom response during the preparation process. This reversible discolouration also made phantoms reusable for several experiments.

3. The threshold temperature of the incorporated TCD was measured 50±3ºC with a 6ºC temperature interval between the onset and ending temperatures of discolouration. Therefore, the developed phantom could provide a more predictable estimation of temperature profile inside the phantom in contrast to most previously-developed thermosensitive phantoms. Moreover, this threshold temperature was close to the temperature ranges at which the thermal lesions are generated in tumour tissue.

4. The quantity of dye required for preparation of this phantom was significantly lower than that of other thermosensitive agents, causing a negligible effect on various acoustic and thermal properties of the phantom.

5. This phantom was employed to calculate the local specific absorption rate (SAR) during heating by radiofrequency technique. The surface of the colourless area at different irradiation intervals coincided with the isothermal layers with temperature of 44°C. These isothermal layers were further utilized for calculation of SAR by the Pennes' bio-heat transfer equation. This method of SAR measurement shows a number of advantages in terms of cost requirement, provision of a true three-dimensional pattern, and ease of SAR estimation.

6. In addition to their visible discolouration transition, when these phantoms were exposed to the MRgFUS sonication, a contrast change in the focal point generated a dark region in the magnetic resonance (MR) images. This dark region was diminished again after elimination of the ultrasound beams and dissipation of thermal energy within the phantom. The visibility of focal point in MR images as

well as the reversibility of this phenomenon could be effectively employed to accurately focus the ultrasound beams to the desired region (e.g. tumour simulation) during MRgFUS experiments.

7. The main limitation of these phantoms is their transparency loss during fabrication of large phantoms. Therefore, this preparation technique was only applicable in fabrication of phantoms with diameters smaller than 10 cm. However, the reusability of these thermosensitive phantoms as well as their accuracy in representation of the thermal lesion makes them prominent for three-dimensional investigation of thermal profile in various high-temperature studies.

6.1.2 Proof-of-Concept Study on the PAA-MSNs

1. In chapter 4, we synthesized PAA-MSNs using graft-from method to assess the feasibility of employing a new mechanism for thermal-triggered drug release at hyperthermia and thermal ablation temperature ranges.

2. It was assumed that the gelation and dissociation of PAA protective nanoshells at increased temperatures could provide preferred trajectories for facilitated diffusion of the encapsulated drug into the surrounding region. The onset gelation temperature of PAA was sufficiently higher than physiological temperature and within the therapeutic hyperthermia range, causing a minimal drug release in healthy tissues and consequently, lower systemic toxicity.

3. In order to synthesize the core-shell nanostructures, different monomer-to-MSN ratios were examined and the ratio of 1.0 was found to provide a uniform polymer nanoshell with approximate weight ratio of 31-33% around the MSN cores.

4. The melting temperature of PAA nanoshell was measured 68.3±4.2°C. However, the gelation of this polymer initiated at 45.1±3.4°C which was significantly higher than the physiological temperature and thus could result in minimized immature at physiological temperatures.

5. The optimal incubation time needed for encapsulation of doxorubicin in PAA-MSN structure was around 48 hours, resulting in encapsulation of 208±20 mg doxorubicin within 1 g of the core-shell nanocarriers. Therefore, this incubation interval was applied in further steps to prepare the drug-loaded nanoparticles.

6. Incubation of the drug-loaded PAA-MSNs at physiological temperature for 30 minutes resulted in 11.5±2.4% drug leakage. This ratio was not statistically different from that obtained at 30°C, indicating the nonthermal-based leakage.

7. Increasing the temperature to above 45°C resulted in partial melting of the PAA shells and thus produced preferred routes for release of the encapsulated drug. The maximum ratio of drug release (67.6±2.5%) was obtained at 60°C and then no significant increase in this ratio was observed.

8. The molten polymer could produce relatively large aggregates on the MSN surface or detach from the MSN surface and form small masses in the aqueous solution. Partial melting of the polymer shells could result in aggregation of PAA-MSNs in aqueous solutions which contain high concentrations of these nanocarriers.

9. Measurement of drug release ratio under MRgFUS sonication indicated a 39.2±2.2% drug release from the core-shell nanocarriers. This fact shows the capability of this triggering mechanism for fast and effective release of encapsulated therapeutic agent when applied in clinical setting.
10. The crucial limitation of these polymers was their continuous phase transition occurring in a wide temperature range which required relatively high temperatures and irradiation energies to provide the maximum drug release value.

6.1.3 Synthesis of PEG-MSNs

1. In chapter 5, we aimed to achieve sharper gel-liquid phase transitions by replacing the PAA layer with a PEG nanoshell. The phase transition temperature of PEG polymers could be adjusted within the hyperthermia range by controlling their molecular weight. It was assumed that sharp gel-liquid phase transition of PEG shell under hyperthermia condition could result in a faster diffusion of chemotherapeutics into the target medium.
2. Different PEG molecular weights including 1000 Da, 1500 Da, and 2000 Da were examined to determine the optimal formulation which offers a phase transition within the hyperthermia temperature range. The selected PEG was then employed to encapsulate doxorubicin within a mesoporous silica core.
3. By increase of the molecular weight from 1000 Da to 2000 Da, the onset and peak phase transitions temperatures were respectively increased from 25.3±2.5°C and 37.1±2.3°C to 45.4±1.5°C and 50.0±1.3°C, whereas the phase transition ranges

decreased from 11.8°C to 4.6°C. Therefore, heavier PEGs exhibited sharper phase transition behaviours compared to those with lower molecular weights.

4. The optimal range of phase transition temperature for hyperthermia application was observed in PEG1500 which provided the onset and peak phase transition temperatures of 40.4±1.8°C and 48.3±1.7°C, respectively. Therefore, this molecular weight was selected in order to synthesize the PEG-MSNs for thermal-triggered drug release at hyperthermia range.

5. The MSNs were uniformly covered with a thin PEG layer using the graft-to method which not only acted as an encapsulating shell, could also minimize the particle agglomeration in aqueous solutions. However, a relatively low nanoshell thickness was obtained, probably due to the short length of the PEG1500 chains.

6. The onset temperature of phase transition in the PEG1500 nanoshell (43.5±2.5°C) was comparable to that of PAA layer (45.1±3.4°C). However, the PEG1500 nanoshell showed a significantly sharper transition temperature range as well as a lower peak phase transition temperature (49.3±2.7°C) in contrast to the PAA shell (68.3±4.2°C).

7. The optimal incubation time for loading of doxorubicin into the PEG-MSNs was identical to that observed in the PAA-MSNs. However, the quantity of loaded drug in PEG-MSNs (183±14 mg in 1 g of PEG-MSNs) was significantly lower than that obtained in PAA-MSNs. This might be due to the lower thickness of the PEG shell compared to the PAA layer which resulted in less amounts of drug entrapped within the polymer shell.

8. Incubation of PEG-MSNs at 37°C for 30 minutes resulted in a 20.2±4.3% drug leakage which was statistically higher than the values obtained at 30°C. Therefore, it may be concluded that the PEG shell could partially melt at these temperature, leading to some amounts of immature drug release.
9. The maximum ratio of drug release (68.2±3.7%) was obtained at 50°C and then no significant increase in this value was observed. Although this ratio was not statistically different from that obtained using PAA-MSNs (67.6±2.5%), it was achieved at approximately 10°C lower than PAA-MSNs.
10. The rapid release of 45.5±3.1% doxorubicin after MRgFUS sonication for 5×20 seconds also showed the potential of PEG-MSNs for rapid release of encapsulated therapeutic drugs when employed in the clinical practice.

6.2 Recommendation for Further Research

Based on the results obtained in the current project, experimental and time limitations, as well as the shortcomings of the developed thermosensitive nanocarriers, the following areas are recommended for further studies:

1. The phantom fabricated in the current project was blue-coloured at room temperature and colourless at temperatures above a specific level. Although this discolouration could be easily visualized in small phantoms, recognition of the thermal lesion was challenging when the phantom diameter was above 10 cm. Therefore, these phantoms could be more applicable when thermosensitive dyes

with opposite phase transition behaviour (i.e. transparent at room temperature and coloured at hyperthermia temperature range) are employed.

2. Although the ratios of immature drug release from the PAA-MSNs and PEG-MSNs were significantly less than most similar thermosensitive nanocarriers, these values could be minimized using nanoshells with sharper melting profiles in contrast to PAA and PEG polymers.

3. The gel-liquid phase transition of the PEG shell was significantly influenced by alteration of its molecular weight. However, the molecular weight which provided an appropriate phase transition behaviour, generated an excessively thin protective shell and thereby higher immature drug leakage ratios. Therefore, utilizing the protective layers with higher thicknesses may result in reduced immature leakage at physiological temperatures.

4. In this study, drug loading was carried out after formation of the polymer shells in order to minimize the negative effects of polymer coating procedure on the drug stability. However, this approach could significantly reduce the loading quantity, increase the optimal loading interval, and cause drug entrapment inside the polymer shell. Therefore, the experimental procedure need be enhanced to allow drug encapsulation prior fabrication of the core-shell structure.

5. The polymer shells used in this research were hydrophilic compounds which could absorb significant amounts of water in their structure and thus facilitate undesired drug leakage of the encapsulated hydrophilic drugs. The immature leakage ratios could be decreased when the hydrophobic polymers are used to

encapsulate hydrophilic agents and conversely, the hydrophilic shells are employed for delivery of hydrophobic drugs.

6. In order to perform the MRgFUS experiments, the doxorubicin-loaded nanocarriers were decanted inside a plastic tube which was previously placed in the tissue-mimicking phantom. This method allowed collecting the sonicated mixture and accurately quantifying the drug release ratios. However, this plastic tube could result in significant attenuation of the ultrasound beams and negatively affect the experiment outcomes. Therefore, a sophisticated phantom design that could simulate the capillary system will be fabricated in future studies.

7. The stability tests in complete serum as well as in vivo comparative studies at both hyperthermia and thermal ablation ranges must also be conducted to determine the in vivo efficacy of the newly synthesized product.

8. Replacement of the MSN core with superparamagnetic compounds could enhance the MR contrast properties and allow their navigation using external magnetic fields. Moreover, high thermal conductivity of metallic compartment could accelerate polymer melting under hyperthermia condition. However, limited loading capacities is the critical shortcoming of these metallic compounds which may result in low drug dosages available in target tissue. Synthesis of porous superparamagnetic nanoparticles could be an effective approach to obtain increased drug loadings combined with intrinsic benefits of these superparamagnetic materials.

REFERENCES

Al-Ahmady, Z. S., Al-Jamal, W. T., Bossche, J. V., Bui, T. T., Drake, A. F., Mason, A. J., and Kostarelos, K. (2012). Lipid–peptide vesicle nanoscale hybrids for triggered drug release by mild hyperthermia in vitro and in vivo. *ACS Nano, 6*(10): 9335-9346.

Alexander, A., Khan, J., Saraf, S., and Saraf, S. (2013). Poly (ethylene glycol)–poly (lactic-co-glycolic acid) based thermosensitive injectable hydrogels for biomedical applications. *Journal of Controlled Release, 172*(3): 715-729.

Amato, E., Italiano, A., Leotta, S., Pergolizzi, S., and Torrisi, L. (2013). Monte Carlo study of the dose enhancement effect of gold nanoparticles during X-ray therapies and evaluation of the anti-angiogenic effect on tumour capillary vessels. *Journal of X-ray Science and Technology, 21*(2): 237-247.

Amstad, E., Kohlbrecher, J., Müller, E., Schweizer, T., Textor, M., and Reimhult, E. (2011). Triggered release from liposomes through magnetic actuation of iron oxide nanoparticle containing membranes. *Nano Letters, 11*(4): 1664-1670.

Anderson, B. C., Pandit, N. K., and Mallapragada, S. K. (2001). Understanding drug release from poly (ethylene oxide)-b-poly (propylene oxide)-b-poly (ethylene oxide) gels. *Journal of Controlled Release, 70*(1): 157-167.

Anderson, J. J., Herd, M. T., King, M. R., Haak, A., Hafez, Z. T., Jun, S., Oelze, M. L., Madsen, E. L., Zagzebski, J. A., O'Brien, W. D., and Hall, T. J. (2010a). Interlaboratory comparison of backscatter coefficient estimates for tissue-mimicking phantoms. *Ultrasonic Imaging, 32*(1): 48-64.

Anderson, L. J. E., Hansen, E., Lukianova-Hleb, E. Y., Hafner, J. H., and Lapotko, D. O. (2010b). Optically guided controlled release from liposomes with tunable plasmonic nanobubbles. *Journal of Controlled Release, 144*(2): 151-158.

Anderson, P. G., Rouze, N. C., and Palmeri, M. L. (2011). Effect of graphite concentration on shear-wave speed in gelatin-based tissue-mimicking phantoms. *Ultrasonic Imaging, 33*(2): 134-142.

Andhariya, N., Chudasama, B., Mehta, R. V., and Upadhyay, R. V. (2011). Biodegradable thermoresponsive polymeric magnetic nanoparticles: A new drug delivery platform for doxorubicin. *Journal of Nanoparticle Research, 13*(4): 1677-1688.

Andreani, T., de Souza, A. L., Kiill, C. P., Lorenzon, E. N., Fangueiro, J. F., Calpena, A. C., Chaud, M. V., Garcia, M. L., Gremiao, M. P., Silva, A. M., and Souto, E. B. (2014). Preparation and characterization of PEG-coated silica nanoparticles for oral insulin delivery. *International Journal of Pharmaceutics, 473*(1-2): 627-635.

Andreuccetti, D., Bini, M., Ignesti, A., Olmi, R., Rubino, N., and Vanni, R. (1988). Use of polyacrylamide as a tissue-equivalent material in the microwave range. *IEEE Transactions on Biomedical Engineering, 35*(4): 275-277.

Annaka, M., Tanaka, T., and Osada, Y. (1992). Volume phase transitions of gels in hydrocarbons. *Macromolecules, 25*(18): 4826-4827.

Anyarambhatla, G. R., and Needham, D. (1999). Enhancement of the phase transition permeability of DPPC liposomes by incorporation of MPPC: A new temperature-sensitive liposome for use with mild hyperthermia. *Journal of Liposome Research, 9*(4): 491-506.

Arora, D., Skliar, M., Cooley, D., Blankespoor, A., Moellmer, J., and Roemer, R. (2004, June 30-July 2). *Nonlinear model predictive thermal dose control of thermal therapies: experimental validation with phantoms.* Paper presented at the IEEE Proceedings of the American Control Conference, Boston, MA.

Arora, M., Arvanitis, C., Cox, E., and Coussios, C. C. (2008). Localization and enhancement of cavitation and heating during HIFU exposure using microparticles of high surface roughness. *Journal of the Acoustical Society of America, 123*(5): 2997.

Arruebo, M., Fernández Pacheco, R., Ibarra, M. R., and Santamaría, J. (2007). Magnetic nanoparticles for drug delivery. *Nano Today, 2*(3): 22-32.

Babincova, M., Sourivong, P., Leszczynska, D., and Babinec, P. (2003). Fullerenosomes: Design of a novel nanomaterial for laser controlled topical drug release. *Physica Medica, 19*(3): 213-216.

Bae, K. H., Choi, S. H., Park, S. Y., Lee, Y., and Park, T. G. (2006). Thermosensitive pluronic micelles stabilized by shell cross-linking with gold nanoparticles. *Langmuir, 22*(14): 6380-6384.

Baldock, C., Burford, R. P., Billingham, N., Wagner, G. S., Patval, S., Badawi, R. D., and Keevil, S. F. (1998). Experimental procedure for the manufacture and calibration

of polyacrylamide gel (PAG) for magnetic resonance imaging (MRI) radiation dosimetry. *Physics in Medicine and Biology, 43*(3): 695-702.

Balivada, S., Rachakatla, R. S., Wang, H., Samarakoon, T. N., Dani, R. K., Pyle, M., Kroh, F. O., Walker, B., Leaym, X., and Koper, O. B. (2010). A/C magnetic hyperthermia of melanoma mediated by iron (0)/iron oxide core/shell magnetic nanoparticles: A mouse study. *BMC Cancer, 10*(1): 119.

Banno, B., Ickenstein, L. M., Chiu, G. N., Bally, M. B., Thewalt, J., Brief, E., and Wasan, E. K. (2010). The functional roles of poly (ethylene glycol)-lipid and lysolipid in the drug retention and release from lysolipid-containing thermosensitive liposomes in vitro and in vivo. *Journal of Pharmaceutical Sciences, 99*(5): 2295-2308.

Bartczak, D., Muskens, O. L., Sanchez Elsner, T., Kanaras, A. G., and Millar, T. M. (2013). Manipulation of in vitro angiogenesis using peptide-coated gold nanoparticles. *ACS Nano, 7*(6): 5628-5636.

Bazrafshan, B., Hubner, F., Farshid, P., Larson, M. C., Vogel, V., Mantele, W., and Vogl, T. J. (2011). A liver-mimicking MRI phantom for thermal ablation experiments. *Medical Physics, 38*(5): 2674-2684.

Bekhradnia, S., Zhu, K., Knudsen, K. D., Sande, S. A., and Nyström, B. (2014). Structure, swelling, and drug release of thermoresponsive poly(amidoamine) dendrimer–poly(N-isopropylacrylamide) hydrogels. *Journal of Materials Science, 49*(17): 6102-6110.

Bhardwaj, R., and Blanchard, J. (1996). Controlled-release delivery system for the α-MSH analog Melanotan-I using poloxamer 407. *Journal of Pharmaceutical Sciences, 85*(9): 915-919.

Bigi, A., Cojazzi, G., Panzavolta, S., Roveri, N., and Rubini, K. (2002). Stabilization of gelatin films by crosslinking with genipin. *Biomaterials, 23*(24): 4827-4832.

Bini, M. G., Ignesti, A., Millanta, L., Olmi, R., Rubino, N., and Vanni, R. (1984). The polyacrylamide as a phantom material for electromagnetic hyperthermia studies. *IEEE Transactions on Biomedical Engineering, 31*(3): 317-322.

Bouchard, L. S., and Bronskill, M. J. (2000). Magnetic resonance imaging of thermal coagulation effects in a phantom for calibrating thermal therapy devices. *Medical Physics, 27*(5): 1141-1145.

Bu Lin, Z., Bing, H., Sheng-Li, K., Huang, Y., Rong, W., and Jia, L. (2008). A polyacrylamide gel phantom for radiofrequency ablation. *International Journal of Hyperthermia, 24*(7): 568-576.

Bu, X., Zhou, D., Li, J., Zhang, X., Zhang, K., Zhang, H., and Yang, B. (2014). Copper sulfide self-assembly architectures with improved photothermal performance. *Langmuir, 30*(5): 1416-1423.

Burlew, M. M., Madsen, E. L., Zagzebski, J. A., Banjavic, R. A., and Sum, S. W. (1980). A new ultrasound tissue-equivalent material. *Radiology, 134*(2): 517-520.

Busetti, A., Soncin, M., Reddi, E., Rodgers, M. A. J., Kenney, M. E., and Jori, G. (1999). Photothermal sensitization of amelanotic melanoma cells by Ni(II)-octabutoxy-naphthalocyanine. *Journal of Photochemistry and Photobiology B: Biology, 53*(1–3): 103-109.

Canney, M. S., Khokhlova, V. A., Bessonova, O. V., Bailey, M. R., and Crum, L. A. (2010). Shock-induced heating and millisecond boiling in gels and tissue due to high intensity focused ultrasound. *Ultrasound in Medicine & Biology, 36*(2): 250-267.

Cauda, V., Argyo, C., and Bein, T. (2010). Impact of different PEGylation patterns on the long-term bio-stability of colloidal mesoporous silica nanoparticles. *Journal of Materials Chemistry, 20*(39): 8693-8699.

Caulfield, M. J., Qiao, G. G., and Solomon, D. H. (2002). Some aspects of the properties and degradation of polyacrylamides. *Chemical Reviews, 102*(9): 3067-3084.

Chen, C. L., Kuo, L. R., Lee, S. Y., Hwu, Y. K., Chou, S. W., Chen, C. C., Chang, F. H., Lin, K. H., Tsai, D. H., and Chen, Y. Y. (2013a). Photothermal cancer therapy via femtosecond-laser-excited FePt nanoparticles. *Biomaterials, 34*(4): 1128-1134.

Chen, K. J., Liang, H. F., Chen, H. L., Wang, Y., Cheng, P. Y., Liu, H. L., Xia, Y., and Sung, H. W. (2013b). A thermoresponsive bubble-generating liposomal system for triggering localized extracellular drug delivery. *ACS Nano, 7*(1): 438-446.

Chen, S., Li, Y., Guo, C., Wang, J., Ma, J., Liang, X., Yang, L. R., and Liu, H.-Z. (2007). Temperature-responsive magnetite/PEO-PPO-PEO block copolymer nanoparticles for controlled drug targeting delivery. *Langmuir, 23*(25): 12669-12676.

Chen, W. R., Adams, R. L., Higgins, A. K., Bartels, K. E., and Nordquist, R. E. (1996). Photothermal effects on murine mammary tumors using indocyanine green and an 808-nm diode laser: An in vivo efficacy study. *Cancer Letters, 98*(2): 169-173.

Chen, Y. C., Lo, C. L., and Hsiue, G. H. (2014). Multifunctional nanomicellar systems for delivering anticancer drugs. *Journal of Biomedical Materials Research Part A, 102*(6): 2024-2038.

Cherukuri, P., Glazer, E. S., and Curley, S. A. (2010). Targeted hyperthermia using metal nanoparticles. *Advanced Drug Delivery Reviews, 62*(3): 339-345.

Chiappetta, D. A., and Sosnik, A. (2007). Poly (ethylene oxide)–poly (propylene oxide) block copolymer micelles as drug delivery agents: Improved hydrosolubility, stability and bioavailability of drugs. *European Journal of Pharmaceutics and Biopharmaceutics, 66*(3): 303-317.

Chiu, G. N. C., Abraham, S. A., Ickenstein, L. M., Ng, R., Karlsson, G., Edwards, K., Wasan, E. K., and Bally, M. B. (2005). Encapsulation of doxorubicin into thermosensitive liposomes via complexation with the transition metal manganese. *Journal of Controlled Release, 104*(2): 271-288.

Choi, M. J., Guntur, S. R., Lee, K. I. L., Paeng, D. G., and Coleman, A. (2013). A Tissue mimicking polyacrylamide hydrogel phantom for visualizing thermal lesions generated by high intensity focused ultrasound. *Ultrasound in Medicine & Biology, 39*(3): 439-448.

Choi, Y., Kang, T., and Lee, L. P. (2009). Plasmon resonance energy transfer (PRET)-based molecular imaging of cytochrome c in living cells. *Nano Letters, 9*(1): 85-90.

Chou, C. K., Chen, G. W., Guy, A. W., and Luk, K. H. (1984). Formulas for preparing phantom muscle tissue at various radiofrequencies. *Bioelectromagnetics, 5*(4): 435-441.

Chrastina, A., Massey, K. A., and Schnitzer, J. E. (2011). Overcoming in vivo barriers to targeted nanodelivery. *Wiley Interdisciplinary Reviews: Nanomedicine and Nanobiotechnology, 3*(4): 421-437.

Chung, M. F., Chen, K. J., Liang, H. F., Liao, Z. X., Chia, W. T., Xia, Y., and Sung, H. W. (2012). A liposomal system capable of generating CO_2 bubbles to induce

transient cavitation, lysosomal rupturing, and cell necrosis. *Angewandte Chemie, 124*(40): 10236-10240.

Croy, S. R., and Kwon, G. S. (2006). Polymeric micelles for drug delivery. *Current Pharmaceutical Design, 12*(36): 4669-4684.

Cubeddu, R., Pifferi, A., Taroni, P., Torricelli, A., and Valentini, G. (1997). A solid tissue phantom for photon migration studies. *Physics in Medicine and Biology, 42*(10): 1971-1979.

Dabbagh, A., Abdullah, B. J., Ramasindarum, C., and Abu Kasim, N. H. (2014). Tissue-mimicking gel phantoms for thermal therapy studies. *Ultrasonic Imaging, 36*(4): 291-316.

Davidson, S. R., and Sherar, M. D. (2003). Measurement of the thermal conductivity of polyacrylamide tissue-equivalent material. *International Journal of Hyperthermia, 19*(5): 551-562.

De Smet, M., Heijman, E., Langereis, S., Hijnen, N. M., and Grüll, H. (2011). Magnetic resonance imaging of high intensity focused ultrasound mediated drug delivery from temperature-sensitive liposomes: An in vivo proof-of-concept study. *Journal of Controlled Release, 150*(1): 102-110.

De Smet, M., Langereis, S., den Bosch, S. v., and Grüll, H. (2010). Temperature-sensitive liposomes for doxorubicin delivery under MRI guidance. *Journal of Controlled Release, 143*(1): 120-127.

Derfus, A. M., von Maltzahn, G., Harris, T. J., Duza, T., Vecchio, K. S., Ruoslahti, E., and Bhatia, S. N. (2007). Remotely triggered release from magnetic nanoparticles. *Advanced Materials, 19*(22): 3932-3936.

Deshmukh, S. A., Kamath, G., Suthar, K. J., Mancini, D. C., and Sankaranarayanan, S. K. R. S. (2014). Non-equilibrium effects evidenced by vibrational spectra during the coil-to-globule transition in poly (N-isopropylacrylamide) subjected to an ultrafast heating–cooling cycle. *Soft Matter, 10*(10): 1462-1480.

DeWitt, M. R., Pekkanen, A. M., Robertson, J., Rylander, C. G., and Rylander, M. N. (2014). Influence of hyperthermia on efficacy and uptake of carbon nanohorn-cisplatin conjugates. *Journal of Biomechanical Engineering, 136*(2): 021003.

Dicheva, B. M., and Koning, G. A. (2014). Targeted thermosensitive liposomes: An attractive novel approach for increased drug delivery to solid tumors. *Expert Opinion on Drug Delivery, 11*(1): 83-100.

Divkovic, G. W., Liebler, M., Braun, K., Dreyer, T., Huber, P. E., and Jenne, J. W. (2007). Thermal properties and changes of acoustic parameters in an egg white phantom during heating and coagulation by high intensity focused ultrasound. *Ultrasound in Medicine & Biology, 33*(6): 981-986.

Dobson, J. (2006). Magnetic nanoparticles for drug delivery. *Drug Development Research, 67*(1): 55-60.

El-Sayed, I. H., Huang, X., and El-Sayed, M. A. (2005). Surface plasmon resonance scattering and absorption of anti-EGFR antibody conjugated gold nanoparticles in cancer diagnostics: Applications in oral cancer. *Nano Letters, 5*(5): 829-834.

El-Sayed, I. H., Huang, X., and El-Sayed, M. A. (2006). Selective laser photo-thermal therapy of epithelial carcinoma using anti-EGFR antibody conjugated gold nanoparticles. *Cancer Letters, 239*(1): 129-135.

El-Sayed, M. A., Shabaka, A. A., El-Shabrawy, O. A., Yassin, N. A., Mahmoud, S. S., El-Shenawy, S. M., Al-Ashqar, E., Eisa, W. H., Farag, N. M., and El-Shaer, M. A. (2013). Tissue distribution and efficacy of gold nanorods coupled with laser induced photoplasmonic therapy in ehrlich carcinoma solid tumor model. *PloS One, 8*(10): e76207.

Elliott, A. M., Shetty, A. M., Wang, J., Hazle, J. D., and Jason Stafford, R. (2010). Use of gold nanoshells to constrain and enhance laser thermal therapy of metastatic liver tumours. *International Journal of Hyperthermia, 26*(5): 434-440.

Faria, M. R., Cruz, M. M., Gonçalves, M. C., Carvalho, A., Feio, G., and Martins, M. B. F. (2013). Synthesis and characterization of magnetoliposomes for MRI contrast enhancement. *International Journal of Pharmaceutics, 446*(1–2): 183-190.

Farny, C. H., Holt, R. G., and Roy, R. A. (2010). The correlation between bubble-enhanced HIFU heating and cavitation power. *IEEE Transactions on Biomedical Engineering, 57*(1): 175-184.

Gaber, M. H., Hong, K., Huang, S. K., and Papahadjopoulos, D. (1995). Thermosensitive sterically stabilized liposomes: Formulation and in vitro studies on mechanism of

doxorubicin release by bovine serum and human plasma. *Pharmaceutical Research, 12*(10): 1407-1416.

Gan, D., and Lyon, L. A. (2002). Synthesis and protein adsorption resistance of PEG-modified poly (N-isopropylacrylamide) core/shell microgels. *Macromolecules, 35*(26): 9634-9639.

Gandhi, S., Venkatesh, S., Sharma, U., Jagannathan, N. R., Sethuraman, S., and Krishnan, U. M. (2011). Superparamagnetic nanosystems based on iron oxide nanoparticles & mesoporous silica: Synthesis & evaluation of their magnetic, relaxometric and biocompatability properties. *Journal of Materials Chemistry, 21*(39): 15698-15707.

Ganta, S., Devalapally, H., Shahiwala, A., and Amiji, M. (2008). A review of stimuli-responsive nanocarriers for drug and gene delivery. *Journal of Controlled Release, 126*(3): 187-204.

Gasselhuber, A., Dreher, M. R., Partanen, A., Yarmolenko, P. S., Woods, D., Wood, B. J., and Haemmerich, D. (2012a). Targeted drug delivery by high intensity focused ultrasound mediated hyperthermia combined with temperature-sensitive liposomes: Computational modelling and preliminary in vivo validation. *International Journal of Hyperthermia, 28*(4): 337-348.

Gasselhuber, A., Dreher, M. R., Rattay, F., Wood, B. J., and Haemmerich, D. (2012b). Comparison of conventional chemotherapy, stealth liposomes and temperature-sensitive liposomes in a mathematical model. *PloS One, 7*(10): e47453.

Gil, E. S., and Hudson, S. M. (2004). Stimuli-reponsive polymers and their bioconjugates. *Progress in Polymer Science, 29*(12): 1173-1222.

Gilstrap, K., Hu, X., Lu, X., and He, X. (2011). Nanotechnology for energy-based cancer therapies. *American Journal of Cancer Research, 1*(4): 508-520.

Giustetto, P., Castelli, D. D., Boffa, C., Rizzitelli, S., Durando, D., Cutrin, J. C., Aime, S., and Terreno, E. (2013). Release of a paramagnetic magnetic resonance imaging agent from liposomes triggered by low intensity non-focused ultrasound. *Journal of Medical Imaging and Health Informatics, 3*(3): 356-366.

Glatter, O., Scherf, G., Schillen, K., and Brown, W. (1994). Characterization of a poly (ethylene oxide)-poly (propylene oxide) triblock copolymer (EO_{27}-PO_{39}-EO_{27}) in aqueous solution. *Macromolecules, 27*(21): 6046-6054.

Gollavelli, G., and Ling, Y. C. (2014). Magnetic and fluorescent graphene for dual modal imaging and single light induced photothermal and photodynamic therapy of cancer cells. *Biomaterials, 35*(15): 4499-4507.

Gong, C., Qi, T., Wei, X., Qu, Y., Wu, Q., Luo, F., and Qian, Z. (2013). Thermosensitive polymeric hydrogels as drug delivery systems. *Current Medicinal Chemistry, 20*(1): 79-94.

Govorov, A. O., and Richardson, H. H. (2007). Generating heat with metal nanoparticles. *Nano Today, 2*(1): 30-38.

Hainfeld, J. F., O'Connor, M. J., Lin, P., Qian, L., Slatkin, D. N., and Smilowitz, H. M. (2014). Infrared-transparent gold nanoparticles converted by tumors to infrared absorbers cure tumors in mice by photothermal therapy. *PloS One, 9*(2): e88414.

Han, H. D., Choi, M. S., Hwang, T., Song, C. K., Seong, H., Kim, T. W., Choi, H. S., and Shin, B. C. (2006). Hyperthermia-induced antitumor activity of thermosensitive polymer modified temperature-sensitive liposomes. *Journal of Pharmaceutical Sciences, 95*(9): 1909-1917.

Hayashi, H., Kono, K., and Takagishi, T. (1999). Temperature sensitization of liposomes using copolymers of N-isopropylacrylamide. *Bioconjugate Chemistry, 10*(3): 412-418.

Hays, L. M., Crowe, J. H., Wolkers, W., and Rudenko, S. (2001). Factors affecting leakage of trapped solutes from phospholipid vesicles during thermotropic phase transitions. *Cryobiology, 42*(2): 88-102.

Hervault, A., and Thanh, N. T. K. (2014). Magnetic nanoparticle-based therapeutic agents for thermo-chemotherapy treatment of cancer. *Nanoscale, 6*(20): 11553-11573.

Holt, R. G., and Roy, R. A. (2001). Measurements of bubble-enhanced heating from focused, MHz-frequency ultrasound in a tissue-mimicking material. *Ultrasound in Medicine & Biology, 27*(10): 1399-1412.

Hon, N. K., Shaposhnik, Z., Diebold, E. D., Tamanoi, F., and Jalali, B. (2012). Tailoring the biodegradability of porous silicon nanoparticles. *Journal of Biomedical Materials Research Part A, 100*(12): 3416-3421.

Huang, J., Holt, R. G., Cleveland, R. O., and Roy, R. A. (2004). Experimental validation of a tractable numerical model for focused ultrasound heating in flow-through tissue phantoms. *Journal of the Acoustical Society of America, 116*: 2451-2458.

Huang, N., Wang, H., Zhao, J., Lui, H., Korbelik, M., and Zeng, H. (2010). Single-wall carbon nanotubes assisted photothermal cancer therapy: Animal study with a murine model of squamous cell carcinoma. *Lasers in Surgery and Medicine, 42*: 638-648.

Huang, X., El-Sayed, I. H., Qian, W., and El-Sayed, M. A. (2006). Cancer cell imaging and photothermal therapy in the near-infrared region by using gold nanorods. *Journal of the American Chemical Society, 128*(6): 2115-2120.

Huang, X., and El-Sayed, M. A. (2011). Plasmonic photo-thermal therapy (PPTT). *Alexandria Journal of Medicine, 47*(1): 1-9.

Huff, T. B., Tong, L., Zhao, Y., Hansen, M. N., Cheng, J. X., and Wei, A. (2007). Hyperthermic effects of gold nanorods on tumor cells. *Nanomedicine: Nanotechnology, Biology, and Medicine, 2*(1): 125-132.

Iancu, C., and Mocan, L. (2011). Advances in cancer therapy through the use of carbon nanotube-mediated targeted hyperthermia. *International Journal of Nanomedicine, 6*: 1675-1684.

Iizuka, M. N., Sherar, M. D., and Vitkin, I. A. (1999). Optical phantom materials for near infrared laser photocoagulation studies. *Lasers in Surgery and Medicine, 25*(2): 159-169.

Ilmain, F., Tanaka, T., and Kokufuta, E. (1991). Volume transition in a gel driven by hydrogen bonding. *Nature, 349*(6308): 400-401.

Ishida, T., and Kato, H. (1980). Muscle equivalent agar phantom for 13.56mhz RF-induced hyperthermia. *Shimane Journal of Medical Science, 4*(2): 134-140.

Issels, R. D. (2008). Hyperthermia adds to chemotherapy. *European Journal of Cancer, 44*(17): 2546-2554.

Ito, K., Furuya, K., Okano, Y., and Hamada, L. (2001). Development and characteristics of a biological tissue-equivalent phantom for microwaves. *Electronics and Communications in Japan (Part I: Communications), 84*(4): 67-77.

Jabeen, F., Najam-ul-Haq, M., Javeed, R., Huck, C. W., and Bonn, G. K. (2014). Au-Nanomaterials as a Superior Choice for Near-Infrared Photothermal Therapy. *Molecules, 19*(12): 20580-20593.

Jain, R. K., and Stylianopoulos, T. (2010). Delivering nanomedicine to solid tumors. *Nature Reviews Clinical Oncology, 7*(11): 653-664.

Jain, S., Hirst, D. G., and O'sullivan, J. M. (2012). Gold nanoparticles as novel agents for cancer therapy. *The British Journal of Radiology, 85*(1010): 101-113.

Jang, J. T., Nah, H., Lee, J. H., Moon, S. H., Kim, M. G., and Cheon, J. (2009). Critical enhancements of MRI contrast and hyperthermic effects by dopant-controlled magnetic nanoparticles. *Angewandte Chemie, 121*(7): 1260-1264.

Jeong, B., Bae, Y. H., and Kim, S. W. (1999). Thermoreversible gelation of PEG-PLGA-PEG triblock copolymer aqueous solutions. *Macromolecules, 32*(21): 7064-7069.

Jeong, B., Bae, Y. H., and Kim, S. W. (2000). Drug release from biodegradable injectable thermosensitive hydrogel of PEG–PLGA–PEG triblock copolymers. *Journal of Controlled Release, 63*(1): 155-163.

Jeong, B., and Gutowska, A. (2002). Lessons from nature: Stimuli-responsive polymers and their biomedical applications. *Trends in Biotechnology, 20*(7): 305-311.

Jeun, M., Kim, Y. J., Park, K. H., Paek, S. H., and Bae, S. (2013). Physical contribution of Néel and Brown relaxation to interpreting intracellular hyperthermia characteristics using superparamagnetic nanofluids. *Journal of Nanoscience and Nanotechnology, 13*(8): 5719-5725.

Jiang, C. P., Wu, M. C., and Wu, Y. S. (2012). Inducing occlusion effect in Y-shaped vessels using high-intensity focused ultrasound: finite element analysis and phantom validation. *Computer Methods in Biomechanics and Biomedical Engineering, 15*(4): 323-332.

Jokerst, J. V., Lobovkina, T., Zare, R. N., and Gambhir, S. S. (2011). Nanoparticle PEGylation for imaging and therapy. *Nanomedicine: Nanotechnology, Biology, and Medicine, 6*(4): 715-728.

Kanda, M. Y., Ballen, M., Salins, S., Chung-Kwang, C., and Balzano, Q. (2004). Formulation and characterization of tissue equivalent liquids used for RF

densitometry and dosimetry measurements. *IEEE Transactions on Microwave Theory and Techniques, 52*(8): 2046-2056.

Kaneko, Y., Nakamura, S., Sakai, K., Aoyagi, T., Kikuchi, A., Sakurai, Y., and Okano, T. (1998). Rapid deswelling response of poly (N-isopropylacrylamide) hydrogels by the formation of water release channels using poly (ethylene oxide) graft chains. *Macromolecules, 31*(18): 6099-6105.

Kang, S. M., Lee, K. B., Kim, D. J., and Choi, I. S. (2006). Biomimetic approach to the formation of gold nanoparticle/silica core/shell structures and subsequent bioconjugation. *Nanotechnology, 17*(18): 4719-4725.

Kao, T. J., Saulnier, G. J., Isaacson, D., Szabo, T. L., and Newell, J. C. (2008). A versatile high-permittivity phantom for EIT. *IEEE Transactions on Biomedical Engineering, 55*(11): 2601-2607.

Kato, H., Hiraoka, M., and Ishida, T. (1986). An agar phantom for hyperthermia. *Medical Physics, 13*(3): 396-398.

Kato, H., and Ishida, T. (1987). Development of an agar phantom adaptable for simulation of various tissues in the range 5-40 MHz. *Physics in Medicine and Biology, 32*(2): 221-226.

Kato, H., Yoshimura, K., Kuroda, M., Yoshida, A., Hanamoto, K., Kawasaki, S., Shibuya, K., Yamamoto, Y., Tsunoda, M., Takemoto, M., and Hiraki, Y. (2004). Development of a phantom compatible for MRI and hyperthermia using carrageenan gel--relationship between dielectric properties and NaCl concentration. *International Journal of Hyperthermia, 20*(5): 529-538.

Katono, H., Maruyama, A., Sanui, K., Ogata, N., Okano, T., and Sakurai, Y. (1991). Thermo-responsive swelling and drug release switching of interpenetrating polymer networks composed of poly (acrylamide-co-butyl methacrylate) and poly (acrylic acid). *Journal of Controlled Release, 16*(1): 215-227.

Kedar, U., Phutane, P., Shidhaye, S., and Kadam, V. (2010). Advances in polymeric micelles for drug delivery and tumor targeting. *Nanomedicine: Nanotechnology, Biology and Medicine, 6*(6): 714-729.

Khokhlova, V. A., Bailey, M. R., Reed, J. A., Cunitz, B. W., Kaczkowski, P. J., and Crum, L. A. (2006). Effects of nonlinear propagation, cavitation, and boiling in lesion

formation by high intensity focused ultrasound in a gel phantom. *Journal of the Acoustical Society of America, 119*(3): 1834-1848.

Kim, D. H., Nikles, D. E., Johnson, D. T., and Brazel, C. S. (2008). Heat generation of aqueously dispersed $CoFe_2O_4$ nanoparticles as heating agents for magnetically activated drug delivery and hyperthermia. *Journal of Magnetism and Magnetic Materials, 320*(19): 2390-2396.

Klingeler, R., Hampel, S., and Büchner, B. (2008). Carbon nanotube based biomedical agents for heating, temperature sensoring and drug delivery. *International Journal of Hyperthermia, 24*(6): 496-505.

Kneidl, B., Peller, M., Winter, G., Lindner, L. H., and Hossann, M. (2014). Thermosensitive liposomal drug delivery systems: State of the art review. *International Journal of Nanomedicine, 9*: 4387-4398.

Koning, G. A., Eggermont, A. M. M., Lindner, L. H., and ten Hagen, T. L. M. (2010). Hyperthermia and thermosensitive liposomes for improved delivery of chemotherapeutic drugs to solid tumors. *Pharmaceutical Research, 27*(8): 1750-1754.

Kono, K. (2001). Thermosensitive polymer-modified liposomes. *Advanced Drug Delivery Reviews, 53*(3): 307-319.

Kono, K., Hayashi, H., and Takagishi, T. (1994). Temperature-sensitive liposomes: Liposomes bearing poly (N-isopropylacrylamide). *Journal of Controlled Release, 30*(1): 69-75.

Kono, K., Yoshino, K., and Takagishi, T. (2002). Effect of poly (ethylene glycol) grafts on temperature-sensitivity of thermosensitive polymer-modified liposomes. *Journal of Controlled Release, 80*(1): 321-332.

Kujawa, P., Tanaka, F., and Winnik, F. M. (2006). Temperature-dependent properties of telechelic hydrophobically modified poly(N-isopropylacrylamides) in water: Evidence from light scattering and fluorescence spectroscopy for the formation of stable mesoglobules at elevated temperatures. *Macromolecules, 39*(8): 3048-3055.

Kulčar, R., Friškovec, M., Hauptman, N., Vesel, A., and Gunde, M. K. (2010). Colorimetric properties of reversible thermochromic printing inks. *Dyes and Pigments, 86*(3): 271-277.

Kumar, C. S. S. R., and Mohammad, F. (2011). Magnetic nanomaterials for hyperthermia-based therapy and controlled drug delivery. *Advanced Drug Delivery Reviews, 63*(9): 789-808.

Kuruppuarachchi, M., Savoie, H., Lowry, A., Alonso, C., and Boyle, R. W. (2011). Polyacrylamide nanoparticles as a delivery system in photodynamic therapy. *Molecular Pharmaceutics, 8*(3): 920-931.

Labuda, C. P., and Church, C. C. (2011). Augmentation of HIFU-induced heating with fibers embedded in a phantom. *Ultrasound in Medicine & Biology, 37*(3): 442-449.

Lafon, C., Zderic, V., Noble, M. L., Yuen, J. C., Kaczkowski, P. J., Sapozhnikov, O. A., Chavrier, F., Crum, L. A., and Vaezy, S. (2005). Gel phantom for use in high-intensity focused ultrasound dosimetry. *Ultrasound in Medicine & Biology, 31*(10): 1383-1389.

Lai, C. Y., Kruse, D. E., Caskey, C. F., Stephens, D. N., Sutcliffe, P. L., and Ferrara, K. W. (2010). Noninvasive thermometry assisted by a dual-function ultrasound transducer for mild hyperthermia. *IEEE Transactions on Ultrasonics, Ferroelectrics, and Frequency Control, 57*(12): 2671-2684.

Landon, C. D., Park, J. Y., Needham, D., and Dewhirst, M. W. (2011). Nanoscale drug delivery and hyperthermia: The materials design and preclinical and clinical testing of low temperature-sensitive liposomes used in combination with mild hyperthermia in the treatment of local cancer. *The Open Nanomedicine Journal, 3*: 38-64.

Lasic, D. D., and Needham, D. (1995). The" stealth" liposome: A prototypical biomaterial. *Chemical Reviews, 95*(8): 2601-2628.

Lazebnik, M., Madsen, E. L., Frank, G. R., and Hagness, S. C. (2005). Tissue-mimicking phantom materials for narrowband and ultrawideband microwave applications. *Physics in Medicine and Biology, 50*(18): 4245-4258.

Lee, J. H., Jang, J. T., Choi, J. S., Moon, S. H., Noh, S. H., Kim, J. W., Kim, J. G., Kim, I. S., Park, K. I., and Cheon, J. (2011). Exchange-coupled magnetic nanoparticles for efficient heat induction. *Nature Nanotechnology, 6*(7): 418-422.

Li, H., Yu, G. E., Price, C., Booth, C., Hecht, E., and Hoffmann, H. (1997). Concentrated aqueous micellar solutions of diblock copoly (oxyethylene/oxybutylene) E41B8: A study of phase behavior. *Macromolecules, 30*(5): 1347-1354.

Li, J., Wang, B., and Liu, P. (2008). Possibility of active targeting to tumor by local hyperthermia with temperature-sensitive nanoparticles. *Medical Hypotheses, 71*(2): 249-251.

Li, L., Ten Hagen, T. L. M., Bolkestein, M., Gasselhuber, A., Yatvin, J., Van Rhoon, G. C., Eggermont, A. M. M., Haemmerich, D., and Koning, G. A. (2013a). Improved intratumoral nanoparticle extravasation and penetration by mild hyperthermia. *Journal of Controlled Release, 167*(2): 130-137.

Li, L., Ten Hagen, T. L. M., Hossann, M., Süss, R., Van Rhoon, G. C., Eggermont, A. M. M., Haemmerich, D., and Koning, G. A. (2013b). Mild hyperthermia triggered doxorubicin release from optimized stealth thermosensitive liposomes improves intratumoral drug delivery and efficacy. *Journal of Controlled Release, 168*(2): 142-150.

Li, L., Ten Hagen, T. L. M., Schipper, D., Wijnberg, T. M., Van Rhoon, G. C., Eggermont, A. M. M., Lindner, L. H., and Koning, G. A. (2010). Triggered content release from optimized stealth thermosensitive liposomes using mild hyperthermia. *Journal of Controlled Release, 143*(2): 274-279.

Li, P., Xu, R., Wang, W., Li, X., Xu, Z., Yeung, K. W., and Chu, P. K. (2013c). Thermosensitive poly (N-isopropylacrylamide-co-glycidyl methacrylate) microgels for controlled drug release. *Colloids and Surfaces B: Biointerfaces, 101*: 251-255.

Li, Y., Kröger, M., and Liu, W. K. (2014). Endocytosis of PEGylated nanoparticles accompanied by structural and free energy changes of the grafted polyethylene glycol. *Biomaterials, 35*(30): 8467-8478.

Lien, Y. H., and Wu, T. M. (2008). The application of thermosensitive magnetic nanoparticles in drug delivery. *Advanced Materials Research, 47*: 528-531.

Lin, Y. S., Abadeer, N., and Haynes, C. L. (2011). Stability of small mesoporous silica nanoparticles in biological media. *Chemical Communications, 47*(1): 532-534.

Lindner, L. H., Eichhorn, M. E., Eibl, H., Teichert, N., Schmitt Sody, M., Issels, R. D., and Dellian, M. (2004). Novel temperature-sensitive liposomes with prolonged circulation time. *Clinical Cancer Research, 10*(6): 2168-2178.

Lindner, U., Lawrentschuk, N., Weersink, R. A., Raz, O., Hlasny, E., Sussman, M. S., Davidson, S. R., Gertner, M. R., and Trachtenberg, J. (2010). Construction and evaluation of an anatomically correct multi-image modality compatible phantom for prostate cancer focal ablation. *Journal of Urology, 184*(1): 352-357.

Link, S., and El-Sayed, M. A. (2003). Optical properties and ultrafast dynamics of metallic nanocrystals. *Annual Review of Physical Chemistry, 54*(1): 331-366.

Liu, Z., Ahmed, M., Weinstein, Y., Yi, M., Mahajan, R. L., and Goldberg, S. N. (2006). Characterization of the RF ablation-induced 'oven effect': The importance of background tissue thermal conductivity on tissue heating. *International Journal of Hyperthermia, 22*(4): 327-342.

Loo, C., Lin, A., Hirsch, L., Lee, M. H., Barton, J., Halas, N., West, J., and Drezek, R. (2004). Nanoshell-enabled photonics-based imaging and therapy of cancer. *Technology in Cancer Research & Treatment, 3*(1): 33-40.

Lorenzato, C., Cernicanu, A., Meyre, M. E., Germain, M., Pottier, A., Levy, L., Senneville, B. D., Bos, C., Moonen, C., and Smirnov, P. (2013). MRI contrast variation of thermosensitive magnetoliposomes triggered by focused ultrasound: A tool for image-guided local drug delivery. *Contrast Media & Molecular Imaging, 8*(2): 185-192.

Lutz, J. F., Akdemir, Ö., and Hoth, A. (2006). Point by point comparison of two thermosensitive polymers exhibiting a similar LCST: Is the age of poly (NIPAM) over? *Journal of the American Chemical Society, 128*(40): 13046-13047.

Ma, Y., Liang, X., Tong, S., Bao, G., Ren, Q., and Dai, Z. (2013). Gold nanoshell nanomicelles for potential magnetic resonance imaging, light-triggered drug release, and photothermal therapy. *Advanced Functional Materials, 23*(7): 815-822.

MacKinnon, N., Guérin, G., Liu, B., Gradinaru, C. C., Rubinstein, J. L., and Macdonald, P. M. (2009). Triggered instability of liposomes bound to hydrophobically modified core−shell PNIPAM hydrogel beads. *Langmuir, 26*(2): 1081-1089.

Madsen, E. L., Dong, F., Frank, G. R., Garra, B. S., Wear, K. A., Wilson, T., Zagzebski, J. A., Miller, H. L., Shung, K. K., Wang, S. H., Feleppa, E. J., Liu, T., O'Brien, W. D., Jr., Topp, K. A., Sanghvi, N. T., Zaitsev, A. V., Hall, T. J., Fowlkes, J. B., Kripfgans, O. D., and Miller, J. G. (1999). Interlaboratory comparison of ultrasonic backscatter, attenuation, and speed measurements. *Journal of Ultrasound in Medicine, 18*(9): 615-631.

Madsen, E. L., Frank, G. R., and Dong, F. (1998). Liquid or solid ultrasonically tissue-mimicking materials with very low scatter. *Ultrasound in Medicine & Biology, 24*(4): 535-542.

Madsen, E. L., Frank, G. R., Krouskop, T. A., Varghese, T., Kallel, F., and Ophir, J. (2003). Tissue-mimicking oil-in-gelatin dispersions for use in heterogeneous elastography phantoms. *Ultrasonic Imaging, 25*(1): 17-38.

Maestro, L. M., Haro Gonzalez, P., Del Rosal, B., Ramiro, J., Caamano, A. J., Carrasco, E., Juarranz, A., Sanz Rodriguez, F., Sole, J. G., and Jaque, D. (2013). Heating efficiency of multi-walled carbon nanotubes in the first and second biological windows. *Nanoscale, 5*(17): 7882-7889.

Mahoney, M. J., and Anseth, K. S. (2006). Three-dimensional growth and function of neural tissue in degradable polyethylene glycol hydrogels. *Biomaterials, 27*(10): 2265-2274.

Marchal, C., Nadi, M., Tosser, A. J., Roussey, C., and Gaulard, M. L. (1989). Dielectric properties of gelatine phantoms used for simulations of biological tissues between 10 and 50 MHz. *International Journal of Hyperthermia, 5*(6): 725-732.

Martina, M. S., Fortin, J. P., Ménager, C., Clément, O., Barratt, G., Grabielle Madelmont, C., Gazeau, F., Cabuil, V., and Lesieur, S. (2005). Generation of superparamagnetic liposomes revealed as highly efficient MRI contrast agents for in vivo imaging. *Journal of the American Chemical Society, 127*(30): 10676-10685.

Mathew, S., Murakami, T., Nakatsuji, H., Okamoto, H., Morone, N., Heuser, J. E., Hashida, M., and Imahori, H. (2013). Exclusive photothermal heat generation by a gadolinium bis(naphthalocyanine) complex and inclusion into modified high-density lipoprotein nanocarriers for therapeutic applications. *ACS Nano, 7*(10): 8908-8916.

May, J. P., and Li, S. D. (2013). Hyperthermia-induced drug targeting. *Expert Opinion on Drug Delivery, 10*(4): 511-527.

Maya, S., Sarmento, B., Nair, A., Rejinold, N. S., Nair, S. V., and Jayakumar, R. (2013). Smart stimuli sensitive nanogels in cancer drug delivery and imaging: A review. *Current Pharmaceutical Design, 19*(41): 7203-7218.

McDaniel, J. R., Dewhirst, M. W., and Chilkoti, A. (2013). Actively targeting solid tumours with thermoresponsive drug delivery systems that respond to mild hyperthermia. *International Journal of Hyperthermia, 29*(6): 501-510.

McDonald, M., Lochhead, S., Chopra, R., and Bronskill, M. J. (2004). Multi-modality tissue-mimicking phantom for thermal therapy. *Physics in Medicine and Biology, 49*(13): 2767-2778.

Mendoza Nava, H., Ferro Flores, G., Ocampo García, B., Serment Guerrero, J., Santos Cuevas, C., Jiménez Mancilla, N., Luna Gutiérrez, M., and Camacho López, M. A. (2013). Laser heating of gold nanospheres functionalized with octreotide: In vitro effect on HeLa cell viability. *Photomedicine and Laser Surgery, 31*(1): 17-22.

Mills, J. K., and Needham, D. (2005). Lysolipid incorporation in dipalmitoylphosphatidylcholine bilayer membranes enhances the ion permeability and drug release rates at the membrane phase transition. *Biochimica et Biophysica Acta (BBA)-Biomembranes, 1716*(2): 77-96.

Miyakawa, M., Takahashi, N., and Hoshina, S. (1995). A method for observing the three-dimensional patterns of electromagnetic power absorbed by the human body-the gel phantom of the human body used to study the electromagnetic environmental problem. *Electronics and Communications in Japan (Part I: Communications), 78*(8): 99-112.

Miyako, E., Nagata, H., Hirano, K., Makita, Y., Nakayama, K. I., and Hirotsu, T. (2007). Near-infrared laser-triggered carbon nanohorns for selective elimination of microbes. *Nanotechnology, 18*(47): 475103.

Mocan, L., Ilie, I., Tabaran, F. A., Dana, B., Zaharie, F., Zdrehus, C., Puia, C., Mocan, T., Muntean, V., and Teodora, P. (2013). Surface plasmon resonance-induced photoactivation of gold nanoparticles as mitochondria-targeted therapeutic agents for pancreatic cancer. *Expert Opinion on Therapeutic Targets, 17*(12): 1383-1393.

Mortensen, K., Brown, W., and Joergensen, E. (1994). Phase behavior of poly(propylene oxide)-poly(ethylene oxide)-poly(propylene oxide) triblock copolymer melt and aqueous solutions. *Macromolecules, 27*(20): 5654-5666.

Mura, S., Nicolas, J., and Couvreur, P. (2013). Stimuli-responsive nanocarriers for drug delivery. *Nature Materials, 12*(11): 991-1003.

Mylonopoulou, E., Bazán Peregrino, M., Arvanitis, C. D., and Coussios, C. C. (2013). A non-exothermic cell-embedding tissue-mimicking material for studies of ultrasound-induced hyperthermia and drug release. *International Journal of Hyperthermia, 29*(2): 133-144.

Nadi, M., Marchal, C., Rouane, A., Hedjiedj, A., Kourtiche, D., and Prieur, G. (1992, Oct. 29). *Effect of temperature variations on the dielectric properties of a radiofrequency, gelatin water phantom.* Paper presented at the IEEE Engineering in Medicine & Biology Society Conference, Paris, France.

Needham, D., Anyarambhatla, G., Kong, G., and Dewhirst, M. W. (2000). A new temperature-sensitive liposome for use with mild hyperthermia: Characterization and testing in a human tumor xenograft model. *Cancer Research, 60*(5): 1197-1201.

Needham, D., and Dewhirst, M. W. (2001). The development and testing of a new temperature-sensitive drug delivery system for the treatment of solid tumors. *Advanced Drug Delivery Reviews, 53*(3): 285-305.

Needham, D., Park, J. Y., Wright, A. M., and Tong, J. (2013). Materials characterization of the low temperature sensitive liposome (LTSL): Effects of the lipid composition (lysolipid and DSPE–PEG2000) on the thermal transition and release of doxorubicin. *Faraday Discussions, 161*: 515-534.

Nibu, Y., Inoue, T., and Motoda, I. (1995). Effect of headgroup type on the miscibility of homologous phospholipids with different acyl chain lengths in hydrated bilayer. *Biophysical Chemistry, 56*(3): 273-280.

O'Neal, D. P., Hirsch, L. R., Halas, N. J., Payne, J. D., and West, J. L. (2004). Photo-thermal tumor ablation in mice using near infrared-absorbing nanoparticles. *Cancer Letters, 209*(2): 171-176.

Okada, Y., and Tanaka, F. (2005). Cooperative hydration, chain collapse, and flat LCST behavior in aqueous poly(N-isopropylacrylamide) solutions. *Macromolecules, 38*(10): 4465-4471.

Ortega, R., Téllez, A., Leija, L., and Vera, A. (2010). Measurement of ultrasonic properties of muscle and blood biological phantoms. *Physics Procedia, 3*(1): 627-634.

Otsuka, H., Nagasaki, Y., and Kataoka, K. (2012). PEGylated nanoparticles for biological and pharmaceutical applications. *Advanced Drug Delivery Reviews, 64*: 246-255.

Ozen, S., and Koylu, H. (2005). Phantom model of human brain tissue for cellular phone frequencies in electromagnetic field radiation absorption studies. *Gazi University Journal of Science, 18*(2): 193-200.

Pankhurst, Q. A., Connolly, J., Jones, S., and Dobson, J. (2003). Applications of magnetic nanoparticles in biomedicine. *Journal of Physics D: Applied Physics, 36*(13): R167–R181.

Park, S. K., Anjaneya Reddy Guntur, S. R., Lee, K. I., Paeng, D. G., and Choi, M. J. (2010). Reusable ultrasonic tissue mimicking hydrogels containing nonionic surface-active agents for visualizing thermal lesions. *IEEE Transactions on Biomedical Engineering, 57*(1): 194-202.

Parodi, A., Quattrocchi, N., Van de Ven, A. L., Chiappini, C., Evangelopoulos, M., Martinez, J. O., Brown, B. S., Khaled, S. Z., Yazdi, I. K., Enzo, M. V., Isenhart, L., Ferrari, M., and Tasciotti, E. (2013). Synthetic nanoparticles functionalized with biomimetic leukocyte membranes possess cell-like functions. *Nature Nanotechnology, 8*(1): 61-68.

Partanen, A., Yarmolenko, P. S., Viitala, A., Appanaboyina, S., Haemmerich, D., Ranjan, A., Jacobs, G., Woods, D., Enholm, J., and Wood, B. J. (2012). Mild hyperthermia with magnetic resonance-guided high-intensity focused ultrasound for applications in drug delivery. *International Journal of Hyperthermia, 28*(4): 320-336.

Patel, J. M., Evrensel, C. A., Fuchs, A., and Sutrisno, J. (2015). Laser irradiation of ferrous particles for hyperthermia as cancer therapy, a theoretical study. *Lasers in Medical Science, 30*(1): 165-172.

Patenaude, M., and Hoare, T. (2012). Injectable, degradable thermoresponsive poly (N-isopropylacrylamide) hydrogels. *ACS Macro Letters, 1*(3): 409-413.

Pattani, V. P., and Tunnell, J. W. (2012). Nanoparticle-mediated photothermal therapy: A comparative study of heating for different particle types. *Lasers in Surgery and Medicine, 44*(8): 675-684.

Paulides, M. M., Stauffer, P. R., Neufeld, E., Maccarini, P. F., Kyriakou, A., Canters, R. A. M., Diederich, C. J., Bakker, J. F., and Van Rhoon, G. C. (2013). Simulation techniques in hyperthermia treatment planning. *International Journal of Hyperthermia, 29*(4): 346-357.

Peidaee, P., Almansour, N., Shukla, R., and Pirogova, E. (2013). The cytotoxic effects of low intensity visible and infrared light on human breast cancer (MCF7) cells. *Computational and Structural Biotechnology Journal, 6*(7): e201303015.

Pennadam, S. S., Firman, K., Alexander, C., and Górecki, D. C. (2004). Protein-polymer nano-machines. Towards synthetic control of biological processes. *Journal of Nanobiotechnology, 2*(1): 8.

Piazza, J., Hoare, T., Molinaro, L., Terpstra, K., Bhandari, J., Selvaganapathy, P. R., Gupta, B., and Mishra, R. K. (2014). Haloperidol-loaded intranasally administered lectin functionalized poly (ethylene glycol)–block-poly (d, l)-lactic-co-glycolic acid (PEG–PLGA) nanoparticles for the treatment of schizophrenia. *European Journal of Pharmaceutics and Biopharmaceutics, 87*(1): 30-39.

Pitto Barry, A., and Barry, N. P. E. (2014). Pluronic® block-copolymers in medicine: From chemical and biological versatility to rationalisation and clinical advances. *Polymer Chemistry, 5*(10): 3291-3297.

Podaru, G., Dani, R., Wang, H., Basel, M. T., Prakash, P., Bossmann, S. H., and Chikan, V. (2014). Pulsed magnetic field induced fast drug release from magneto liposomes via ultrasound generation. *Journal of Physical Chemistry B, 118*(40): 11715–11722.

Poepping, T. L., Nikolov, H. N., Rankin, R. N., Lee, M., and Holdsworth, D. W. (2002). An in vitro system for Doppler ultrasound flow studies in the stenosed carotid artery bifurcation. *Ultrasound in Medicine & Biology, 28*(4): 495-506.

Polotsky, A. A., Plamper, F. A., and Borisov, O. V. (2013). Collapse-to-swelling transitions in pH- and thermoresponsive microgels in aqueous dispersions: The thermodynamic theory. *Macromolecules, 46*(21): 8702-8709.

Pradhan, L., Srivastava, R., and Bahadur, D. (2014). pH- and thermosensitive thin lipid layer coated mesoporous magnetic nanoassemblies as a dual drug delivery system towards thermochemotherapy of cancer. *Acta Biomaterialia, 10*(7): 2976-2987.

Prakash, P., Converse, M. C., Mahvi, D. M., and Webster, J. G. (2006). Measurement of the specific heat capacity of liver phantom. *Physiological Measurement, 27*(10): N41-N46.

Qiu, D., and An, X. (2013). Controllable release from magnetoliposomes by magnetic stimulation and thermal stimulation. *Colloids and Surfaces B: Biointerfaces, 104*: 326-329.

Qiu, Y., and Park, K. (2001). Environment-sensitive hydrogels for drug delivery. *Advanced Drug Delivery Reviews, 53*(3): 321-339.

Rezaei, S. J. T., Nabid, M. R., Niknejad, H., and Entezami, A. A. (2012). Folate-decorated thermoresponsive micelles based on star-shaped amphiphilic block copolymers for efficient intracellular release of anticancer drugs. *International Journal of Pharmaceutics, 437*(1): 70-79.

Rickey, D. W., Picot, P. A., Christopher, D. A., and Fenster, A. (1995). A wall-less vessel phantom for Doppler ultrasound studies. *Ultrasound in Medicine & Biology, 21*(9): 1163-1176.

Robinson, M. P., Richardson, M. J., Green, J. L., and Preece, A. W. (1991). New materials for dielectric simulation of tissues. *Physics in Medicine and Biology, 36*(12): 1565-1571.

Romberg, B., Flesch, F. M., Hennink, W. E., and Storm, G. (2008). Enzyme-induced shedding of a poly (amino acid)-coating triggers contents release from dioleoyl phosphatidylethanolamine liposomes. *International Journal of Pharmaceutics, 355*(1): 108-113.

Romberg, B., Metselaar, J. M., De Vringer, T., Motonaga, K., Kettenes van den Bosch, J. J., Oussoren, C., Storm, G., and Hennink, W. E. (2005). Enzymatic degradation of liposome-grafted poly (hydroxyethyl l-glutamine). *Bioconjugate Chemistry, 16*(4): 767-774.

Romberg, B., Oussoren, C., Snel, C. J., Carstens, M. G., Hennink, W. E., and Storm, G. (2007a). Pharmacokinetics of poly (hydroxyethyl-l-asparagine)-coated liposomes is superior over that of PEG-coated liposomes at low lipid dose and upon repeated

administration. *Biochimica et Biophysica Acta (BBA)-Biomembranes, 1768*(3): 737-743.

Romberg, B., Oussoren, C., Snel, C. J., Hennink, W. E., and Storm, G. (2007b). Effect of liposome characteristics and dose on the pharmacokinetics of liposomes coated with poly (amino acid)s. *Pharmaceutical Research, 24*(12): 2394-2401.

Rosenholm, J. M., Mamaeva, V., Sahlgren, C., and Lindén, M. (2012). Nanoparticles in targeted cancer therapy: Mesoporous silica nanoparticles entering preclinical development stage. *Nanomedicine: Nanotechnology, Biology, and Medicine, 7*(1): 111-120.

Rösler, A., Vandermeulen, G. W., and Klok, H. A. (2012). Advanced drug delivery devices via self-assembly of amphiphilic block copolymers. *Advanced Drug Delivery Reviews, 64*: 270-279.

Rossi, L. M., Shi, L., Quina, F. H., and Rosenzweig, Z. (2005). Stöber synthesis of monodispersed luminescent silica nanoparticles for bioanalytical assays. *Langmuir, 21*(10): 4277-4280.

Roy, D., Brooks, W. L. A., and Sumerlin, B. S. (2013). New directions in thermoresponsive polymers. *Chemical Society Reviews, 42*(17): 7214-7243.

Ruiz Hernandez, E., Baeza, A., and Vallet Regí, M. (2011). Smart drug delivery through DNA/magnetic nanoparticle gates. *ACS Nano, 5*(2): 1259-1266.

Ruiz, J. C., Burillo, G., and Bucio, E. (2007). Interpenetrating thermo and pH stimuli-responsive polymer networks of PAAc/PNIPAAm grafted onto PP. *Macromolecular Materials and Engineering, 292*(10-11): 1176-1188.

Rytkönen, J., Miettinen, R., Kaasalainen, M., Lehto, V. P., Salonen, J., and Närvänen, A. (2012). Functionalization of Mesoporous Silicon Nanoparticles for Targeting and Bioimaging Purposes. *Journal of Nanomaterials, 2012*: 896562.

Sadhukha, T., Wiedmann, T. S., and Panyam, J. (2013). Inhalable magnetic nanoparticles for targeted hyperthermia in lung cancer therapy. *Biomaterials, 34*(21): 5163-5171.

Saffer, E. M., Tew, G. N., and Bhatia, S. R. (2011). Poly (lactic acid)-poly (ethylene oxide) block copolymers: New directions in self-assembly and biomedical applications. *Current Medicinal Chemistry, 18*(36): 5676-5686.

Salmaso, S., and Caliceti, P. (2013). Stealth properties to improve therapeutic efficacy of drug nanocarriers. *Journal of Drug Delivery, 2013*: 374252.

Sandström, M. C., Ickenstein, L. M., Mayer, L. D., and Edwards, K. (2005). Effects of lipid segregation and lysolipid dissociation on drug release from thermosensitive liposomes. *Journal of Controlled Release, 107*(1): 131-142.

Sarkar, S., Gurjarpadhye, A. A., Rylander, C. G., and Nichole Rylander, M. (2011a). Optical properties of breast tumor phantoms containing carbon nanotubes and nanohorns. *Journal of Biomedical Optics, 16*(5): 051304.

Sarkar, S., Zimmermann, K., Leng, W., Vikesland, P., Zhang, J., Dorn, H., Diller, T., Rylander, C., and Rylander, M. N. (2011b). Measurement of the thermal conductivity of carbon nanotube--tissue phantom composites with the hot wire probe method. *Annals of Biomedical Engineering, 39*(6): 1745-1758.

Scherzinger, C., Schwarz, A., Bardow, A., Leonhard, K., and Richtering, W. (2014). Cononsolvency of poly-N-isopropyl acryl amide (PNIPAM): Microgels versus linear chains and macrogels. *Current Opinion in Colloid & Interface Science, 19*(2): 84-94.

Schmaljohann, D. (2006). Thermo-and pH-responsive polymers in drug delivery. *Advanced Drug Delivery Reviews, 58*(15): 1655-1670.

Seuring, J., and Agarwal, S. (2012). Polymers with upper critical solution temperature in aqueous solution. *Macromolecular Rapid Communications, 33*(22): 1898-1920.

Shao, P., Wang, B., Wang, Y., Li, J., and Zhang, Y. (2011). The application of thermosensitive nanocarriers in controlled drug delivery. *Journal of Nanomaterials, 2011*: 389640.

Sharifi, I., Shokrollahi, H., and Amiri, S. (2012). Ferrite-based magnetic nanofluids used in hyperthermia applications. *Journal of Magnetism and Magnetic Materials, 324*(6): 903-915.

Shen, Z., Terao, K., Maki, Y., Dobashi, T., Ma, G., and Yamamoto, T. (2006). Synthesis and phase behavior of aqueous poly (N-isopropylacrylamide-co-acrylamide), poly (N-isopropylacrylamide-co-N, N-dimethylacrylamide) and poly (N-isopropylacrylamide-co-2-hydroxyethyl methacrylate). *Colloid and Polymer Science, 284*(9): 1001-1007.

Shibayama, M., and Tanaka, T. (1993). Volume phase transition and related phenomena of polymer gels. In K. Dušek (Ed.), *Responsive Gels: Volume Transitions I* (Vol. 109, pp. 1-62). Berlin, Germany: Springer Berlin Heidelberg.

Shin, Y., Lee, D., Lee, K., Ahn, K. H., and Kim, B. (2008). Surface properties of silica nanoparticles modified with polymers for polymer nanocomposite applications. *Journal of Industrial and Engineering Chemistry, 14*(4): 515-519.

Siddiqi, A. K., and Cho, S. H. (2013). Agar-based heat-sensitive gel with linear thermal response over 65–80° C. *Journal of Thermal Analysis and Calorimetry, 111*: 1805-1809.

Singh, R., and Torti, S. V. (2013). Carbon nanotubes in hyperthermia therapy. *Advanced Drug Delivery Reviews, 65*(15): 2045-2060.

Smith, A. M., Mancini, M. C., and Nie, S. (2009). Bioimaging: Second window for in vivo imaging. *Nature Nanotechnology, 4*(11): 710-711.

Soenen, S. J. H., Baert, J., and De Cuyper, M. (2007). Optimal conditions for labelling of 3T3 fibroblasts with magnetoliposomes without affecting cellular viability. *ChemBioChem, 8*(17): 2067-2077.

Soenen, S. J. H., Hodenius, M., and De Cuyper, M. (2009). Magnetoliposomes: Versatile innovative nanocolloids for use in biotechnology and biomedicine. *Nanomedicine: Nanotechnology, Biology, and Medicine, 4*(2): 177-191.

Solazzo, S. A., Liu, Z., Lobo, S. M., Ahmed, M., Hines Peralta, A. U., Lenkinski, R. E., and Goldberg, S. N. (2005). Radiofrequency ablation: Importance of background tissue electrical conductivity--an agar phantom and computer modeling study. *Radiology, 236*(2): 495-502.

Soncin, M., Busetti, A., Fusi, F., Jori, G., and Rodgers, M. A. J. (1999). Irradiation of amelanotic melanoma cells with 532 nm high peak power pulsed laser radiation in the presence of the photothermal sensitizer Cu(II)-hematoporphyrin: A new approach to cell photoinactivation. *Photochemistry and Photobiology, 69*(6): 708-712.

Song, Z., Feng, R., Sun, M., Guo, C., Gao, Y., Li, L., and Zhai, G. (2011). Curcumin-loaded PLGA-PEG-PLGA triblock copolymeric micelles: Preparation, pharmacokinetics and distribution in vivo. *Journal of Colloid and Interface Science, 354*(1): 116-123.

Spera, R., Petralito, S., Liberti, M., Merla, C., D'Inzeo, G., Pinto, R., and Apollonio, F. (2014). Controlled release from magnetoliposomes aqueous suspensions exposed to a low intensity magnetic field. *Bioelectromagnetics, 35*(4): 309-312.

Stauffer, P. R., Rossetto, F., Prakash, M., Neuman, D. G., and Lee, T. (2003). Phantom and animal tissues for modelling the electrical properties of human liver. *International Journal of Hyperthermia, 19*(1): 89-101.

Sun, X., Zhang, G., Keynton, R. S., O'Toole, M. G., Patel, D., and Gobin, A. M. (2013). Enhanced drug delivery via hyperthermal membrane disruption using targeted gold nanoparticles with PEGylated Protein-G as a cofactor. *Nanomedicine: Nanotechnology, Biology and Medicine, 9*(8): 1214-1222.

Sunaga, T., Ikehira, H., Furukawa, S., Tamura, M., Yoshitome, E., Obata, T., Shinkai, H., Tanada, S., Murata, H., and Sasaki, Y. (2003). Development of a dielectric equivalent gel for better impedance matching for human skin. *Bioelectromagnetics, 24*(3): 214-217.

Surowiec, A., Shrivastava, P. N., Astrahan, M., and Petrovich, Z. (1992). Utilization of a multilayer polyacrylamide phantom for evaluation of hyperthermia applicators. *International Journal of Hyperthermia, 8*(6): 795-807.

Ta, T., Bartolak Suki, E., Park, E. J., Karrobi, K., McDannold, N. J., and Porter, T. M. (2014). Localized delivery of doxorubicin in vivo from polymer-modified thermosensitive liposomes with MR-guided focused ultrasound-mediated heating. *Journal of Controlled Release, 194*: 71-81.

Ta, T., Convertine, A. J., Reyes, C. R., Stayton, P. S., and Porter, T. M. (2010). Thermosensitive liposomes modified with poly (N-isopropylacrylamide-co-propylacrylic acid) copolymers for triggered release of doxorubicin. *Biomacromolecules, 11*(8): 1915-1920.

Ta, T., and Porter, T. M. (2013). Thermosensitive liposomes for localized delivery and triggered release of chemotherapy. *Journal of Controlled Release, 169*(1): 112-125.

Takegami, K., Kaneko, Y., Watanabe, T., Maruyama, T., Matsumoto, Y., and Nagawa, H. (2004). Polyacrylamide gel containing egg white as new model for irradiation experiments using focused ultrasound. *Ultrasound in Medicine & Biology, 30*(10): 1419-1422.

Talelli, M., and Hennink, W. E. (2011). Thermosensitive polymeric micelles for targeted drug delivery. *Nanomedicine: Nanotechnology, Biology, and Medicine, 6*(7): 1245-1255.

Tang, H., Guo, J., Sun, Y., Chang, B., Ren, Q., and Yang, W. (2011). Facile synthesis of pH sensitive polymer-coated mesoporous silica nanoparticles and their application in drug delivery. *International Journal of Pharmaceutics, 421*(2): 388-396.

Thomas, C. R., Ferris, D. P., Lee, J. H., Choi, E., Cho, M. H., Kim, E. S., Stoddart, J. F., Shin, J. S., Cheon, J., and Zink, J. I. (2010). Noninvasive remote-controlled release of drug molecules in vitro using magnetic actuation of mechanized nanoparticles. *Journal of the American Chemical Society, 132*(31): 10623-10625.

Torchilin, V. P. (2005). Recent advances with liposomes as pharmaceutical carriers. *Nature Reviews Drug Discovery, 4*(2): 145-160.

Turner, D., Moshkelani, D., Shemesh, C., Luc, D., and Zhang, H. (2012). Near-infrared image-guided delivery and controlled release using optimized thermosensitive liposomes. *Pharmaceutical Research, 29*(8): 2092-2103.

Vaupel, P. W., and Kelleher, D. K. (2010). Pathophysiological and vascular characteristics of tumours and their importance for hyperthermia: Heterogeneity is the key issue. *International Journal of Hyperthermia, 26*(3): 211-223.

Vigderman, L., and Zubarev, E. R. (2013). Therapeutic platforms based on gold nanoparticles and their covalent conjugates with drug molecules. *Advanced Drug Delivery Reviews, 65*(5): 663-676.

Viglianti, B. L., Dewhirst, M. W., Boruta, R. J., Park, J. Y., Landon, C., Fontanella, A. N., Guo, J., Manzoor, A., Hofmann, C. L., and Palmer, G. M. (2014). Systemic anti-tumour effects of local thermally sensitive liposome therapy. *International Journal of Hyperthermia, 30*(6): 385-392.

Vihola, H., Laukkanen, A., Tenhu, H., and Hirvonen, J. (2008). Drug release characteristics of physically cross-linked thermosensitive poly(N-vinylcaprolactam) hydrogel particles. *Journal of Pharmaceutical Sciences, 97*(11): 4783-4793.

Wang, H., Zhao, P., Liang, X., Gong, X., Song, T., Niu, R., and Chang, J. (2010). Folate-PEG coated cationic modified chitosan–cholesterol liposomes for tumor-targeted drug delivery. *Biomaterials, 31*(14): 4129-4138.

Wang, L., Shi, J., Jia, X., Liu, R., Wang, H., Wang, Z., Li, L., Zhang, J., Zhang, C., and Zhang, Z. (2013). NIR-/pH-responsive drug delivery of functionalized single-walled carbon nanotubes for potential application in cancer chemo-photothermal therapy. *Pharmaceutical Research, 30*(11): 2757-2771.

Wang, X., and Wu, C. (1999). Light-scattering study of coil-to-globule transition of a poly (N-isopropylacrylamide) chain in deuterated water. *Macromolecules, 32*(13): 4299-4301.

Ward, M. A., and Georgiou, T. K. (2011). Thermoresponsive polymers for biomedical applications. *Polymers, 3*(3): 1215-1242.

Wear, K. A., Stiles, T. A., Frank, G. R., Madsen, E. L., Cheng, F., Feleppa, E. J., Hall, C. S., Kim, B. S., Lee, P., and O'Brien, W. D. (2005). Interlaboratory comparison of ultrasonic backscatter coefficient measurements from 2 to 9 MHz. *Journal of Ultrasound in Medicine, 24*(9): 1235-1250.

Wei, H., Zhang, X. Z., Chen, W. Q., Cheng, S. X., and Zhuo, R. X. (2007). Self-assembled thermosensitive micelles based on poly (L-lactide-star block-N-isopropylacrylamide) for drug delivery. *Journal of Biomedical Materials Research Part A, 83*(4): 980-989.

Weissleder, R. (2001). A clearer vision for in vivo imaging. *Nature Biotechnology, 19*(4): 316-317.

Wilhelm, C., Fortin, J. P., and Gazeau, F. (2007). Tumour cell toxicity of intracellular hyperthermia mediated by magnetic nanoparticles. *Journal of Nanoscience and Nanotechnology, 7*(8): 2933-2937.

Woodle, M. C., Engbers, C. M., and Zalipsky, S. (1994). New amphipatic polymer-lipid conjugates forming long-circulating reticuloendothelial system-evading liposomes. *Bioconjugate Chemistry, 5*(6): 493-496.

Wu, G., Chen, S. C., Zhan, Q., and Wang, Y. Z. (2011). Well-defined amphiphilic biodegradable comb-like graft copolymers: Their unique architecture-determined LCST and UCST thermoresponsivity. *Macromolecules, 44*(4): 999-1008.

Xie, R., Li, Y., and Chu, L. Y. (2007). Preparation of thermo-responsive gating membranes with controllable response temperature. *Journal of Membrane Science, 289*(1): 76-85.

Xing, Z., Wang, C., Yan, J., Zhang, L., Li, L., and Zha, L. (2011). Dual stimuli responsive hollow nanogels with IPN structure for temperature controlling drug loading and pH triggering drug release. *Soft Matter, 7*(18): 7992-7997.

Yamamoto, M., Ikada, Y., and Tabata, Y. (2001). Controlled release of growth factors based on biodegradation of gelatin hydrogel. *Journal of Biomaterials Science, Polymer Edition, 12*(1): 77-88.

Yamauchi, H., and Maeda, Y. (2007). LCST and UCST behavior of poly(N-isopropylacrylamide) in DMSO/water mixed solvents studied by IR and micro-raman spectroscopy. *Journal of Physical Chemistry B, 111*(45): 12964-12968.

Yamazaki, A., Winnik, F. M., Cornelius, R. M., and Brash, J. L. (1999). Modification of liposomes with N-substituted polyacrylamides: Identification of proteins adsorbed from plasma. *Biochimica et Biophysica Acta (BBA)-Biomembranes, 1421*(1): 103-115.

Yan, R., Zhang, M., Zhang, W., and Liu, S. (2011). Temperature dependent synthesis of micro-and meso-porous silica employing the thermo-responsive polymer of poly (N-isopropylacrylamide) as structure-directing agent. *Journal of Sol-Gel Science and Technology, 59*(2): 315-326.

Yang, L., Liu, T., Song, K., Wu, S., and Fan, X. (2013). Effect of intermolecular and intramolecular forces on hydrodynamic diameters of poly (N-isopropylacrylamide) copolymers in aqueous solutions. *Journal of Applied Polymer Science, 127*(6): 4280-4287.

Yang, X., Lee, H. Y., and Kim, J. C. (2011). Effect of hydrophobic comonomer content on assembling of poly (N-isopropylacrylamide) and thermal properties. *Journal of Applied Polymer Science, 120*(4): 2346-2353.

Yang, Y., Yan, X., Cui, Y., He, Q., Li, D., Wang, A., Fei, J., and Li, J. (2008). Preparation of polymer-coated mesoporous silica nanoparticles used for cellular imaging by a "graft-from" method. *Journal of Materials Chemistry, 18*(47): 5731-5737.

Yang, Y. W., Yang, Z., Zhou, Z. K., Attwood, D., and Booth, C. (1996). Association of triblock copolymers of ethylene oxide and butylene oxide in aqueous solution. A study of $B_nE_mB_n$ copolymers. *Macromolecules, 29*(2): 670-680.

Yapar, E. A., and Ýnal, Ö. (2013). Poly (ethylene oxide)–poly (propylene oxide)-based copolymers for transdermal drug delivery: An overview. *Tropical Journal of Pharmaceutical Research, 11*(5): 855-866.

Yatvin, M. B., Weinstein, J. N., Dennis, W. H., and Blumenthal, R. (1978). Design of liposomes for enhanced local release of drugs by hyperthermia. *Science, 202*(4374): 1290-1293.

Yin, J., Hu, J., Zhang, G., and Liu, S. (2014). Schizophrenic core–shell microgels: Thermoregulated core and shell swelling/collapse by combining UCST and LCST phase transitions. *Langmuir, 30*(9): 2551-2558.

Yoshida, A., Kato, H., Kuroda, M., Hanamoto, K., Yoshimura, K., Shibuya, K., Kawasaki, S., Tsunoda, M., Kanazawa, S., and Hiraki, Y. (2004). Development of a phantom compatible for MRI and hyperthermia using carrageenan gel-relationship between T1 and T2 values and NaCl concentration. *International Journal of Hyperthermia, 20*(8): 803-814.

Yoshino, K., Kadowaki, A., Takagishi, T., and Kono, K. (2004). Temperature sensitization of liposomes by use of N-isopropylacrylamide copolymers with varying transition endotherms. *Bioconjugate Chemistry, 15*(5): 1102-1109.

You, Y. Z., and Oupický, D. (2007). Synthesis of temperature-responsive heterobifunctional block copolymers of poly (ethylene glycol) and poly (N-isopropylacrylamide). *Biomacromolecules, 8*(1): 98-105.

Yu, L., and Ding, J. (2008). Injectable hydrogels as unique biomedical materials. *Chemical Society Reviews, 37*(8): 1473-1481.

Yu, L., Xu, W., Shen, W., Cao, L., Liu, Y., Li, Z., and Ding, J. (2014). Poly (lactic acid-co-glycolic acid)–poly (ethylene glycol)–poly (lactic acid-co-glycolic acid) thermogel as a novel submucosal cushion for endoscopic submucosal dissection. *Acta Biomaterialia, 10*(3): 1251-1258.

Yuan, Y., Wyatt, C., Maccarini, P., Stauffer, P., Craciunescu, O., Macfall, J., Dewhirst, M. W., and Das, S. K. (2012). A heterogeneous human tissue mimicking phantom

for RF heating and MRI thermal monitoring verification. *Physics in Medicine and Biology, 57*(7): 2021-2037.

Zalipsky, S., Hansen, C. B., Oaks, J. M., and Allen, T. M. (1996). Evaluation of blood clearance rates and biodistribution of poly(2-oxazoline)-grafted liposomes. *Journal of Pharmaceutical Sciences, 85*(2): 133-137.

Zarzyka, I., Pyda, M., and Di Lorenzo, M. L. (2014). Influence of crosslinker and ionic comonomer concentration on glass transition and demixing/mixing transition of copolymers poly(N-isopropylacrylamide) and poly(sodium acrylate) hydrogels. *Colloid and Polymer Science, 292*(2): 485-492.

Zhang, J., Chu, L. Y., Li, Y. K., and Lee, Y. M. (2007). Dual thermo-and pH-sensitive poly (N-isopropylacrylamide-co-acrylic acid) hydrogels with rapid response behaviors. *Polymer, 48*(6): 1718-1728.

Zhang, P., and Porter, T. (2010). An in vitro study of a phase-shift nanoemulsion: A potential nucleation agent for bubble-enhanced HIFU tumor ablation. *Ultrasound in Medicine & Biology, 36*(11): 1856-1866.

Zhang, W., Guo, Z., Huang, D., Liu, Z., Guo, X., and Zhong, H. (2011). Synergistic effect of chemo-photothermal therapy using PEGylated graphene oxide. *Biomaterials, 32*(33): 8555-8561.

Zhang, W., Shi, L., Wu, K., and An, Y. (2005). Thermoresponsive micellization of poly (ethylene glycol)-b-poly (N-isopropylacrylamide) in water. *Macromolecules, 38*(13): 5743-5747.

Zhang, Y. Z., Venugopal, J., Huang, Z. M., Lim, C. T., and Ramakrishna, S. (2006). Crosslinking of the electrospun gelatin nanofibers. *Polymer, 47*(8): 2911-2917.

Zhao, Z., Shi, S., Huang, Y., Tang, S., and Chen, X. (2014). Simultaneous photodynamic and photothermal therapy using photosensitizer-functionalized Pd nanosheets by single continuous wave laser. *ACS Applied Materials & Interfaces, 6*(11): 8878-8885.

Zhou, F., Xing, D., Ou, Z., Wu, B., Resasco, D. E., and Chen, W. R. (2009a). Cancer photothermal therapy in the near-infrared region by using single-walled carbon nanotubes. *Journal of Biomedical Optics, 14*(2): 021009.

Zhou, T., Meaney, P. M., Fanning, M. W., Geimer, S. D., and Paulsen, K. D. (2009b, Jan. 25-26). *Integrated microwave thermal imaging system with mechanically steerable HIFU therapy device.* Paper presented at the Energy-based Treatment of Tissue and Assessment V ({roceedings of SPIE), San Jose, CA.

Zhou, W., An, X., Wang, J., Shen, W., Chen, Z., and Wang, X. (2012). Characteristics, phase behavior and control release for copolymer–liposome with both pH and temperature sensitivities. *Colloids and Surfaces A: Physicochemical and Engineering Aspects, 395*: 225-232.

LIST OF PUBLICATIONS

Dabbagh, A., Abdullah, B. J., Ramasindarum, C., and Abu Kasim, N. H. (2014). Tissue-mimicking gel phantoms for thermal therapy studies. *Ultrasonic Imaging, 36*(4): 291-316.

Dabbagh, A., Abdullah, B. J., Abu Kasim, N. H, and Ramasindarum, C. (2014). Reusable heat-sensitive phantom for precise estimation of thermal profile in hyperthermia application. *International Journal of Hyperthermia, 30*(1): 66-74.

Dabbagh, A., Abu Kasim, N. H., Bakri, M. M., Wakily, H., Ramasindarum, C., and Abdullah, B. J. (2014). Polyethylene-glycol coated maghemite nanoparticles for treatment of dental hypersensitivity. *Materials Letters, 121*: 89-92.

Dabbagh, A., Abdullah, B. J., Abdullah, H., Hamdi, M., and Abu Kasim, N. H. (2015). Triggering mechanisms of thermosensitive nanoparticles under hyperthermia condition. *Journal of Pharmaceutical Sciences, 104*(8): 2414-2428.

Dabbagh, A., Abdullah, B. J., Abu Kasim, N. H., Abdullah, H., and Hamdi, M. (2015). A new mechanism of thermal sensitivity for rapid drug release and low systemic toxicity in hyperthermia and thermal ablation temperature ranges. *International Journal of Hyperthermia, 31*(4): 375-385.

Dabbagh, A., Abdullah, B. J., Abu Kasim, N. H., Abdullah, H., and Hamdi, M. (2015). Low-melting-point Polymeric Nanoshells for Thermal-triggered Drug release under Hyperthermia Condition, *International Journal of Hyperthermia, 31*(8): 920-929.

APPENDICES

REPRINT PERMISSIONS

(FIGURE 2.7)

(FIGURE 2.9)

ELSEVIER LICENSE
TERMS AND CONDITIONS

Aug 05, 2015

This is a License Agreement between Ali Dabbagh ("You") and Elsevier ("Elsevier") provided by Copyright Clearance Center ("CCC"). The license consists of your order details, the terms and conditions provided by Elsevier, and the payment terms and conditions.

All payments must be made in full to CCC. For payment instructions, please see information listed at the bottom of this form.

Supplier	Elsevier Limited The Boulevard,Langford Lane Kidlington,Oxford,OX5 1GB,UK
Registered Company Number	1982084
Customer name	Ali Dabbagh
Customer address	Faculty of Engineering Kuala Lumpur, Kuala Lumpur 50603
License number	3682400681144
License date	Aug 05, 2015
Licensed content publisher	Elsevier
Licensed content publication	Ultrasound in Medicine & Biology
Licensed content title	Gel phantom for use in high-intensity focused ultrasound dosimetry
Licensed content author	Cyril Lafon,Vesna Zderic,Misty L. Noble,Jonathan C. Yuen,Peter J. Kaczkowski,Oleg A. Sapozhnikov,Francoise Chavrier,Lawrence A. Crum,Shahram Vaezy
Licensed content date	October 2005
Licensed content volume number	31
Licensed content issue number	10
Number of pages	7
Start Page	1383
End Page	1389
Type of Use	reuse in a thesis/dissertation
Intended publisher of new work	other
Portion	figures/tables/illustrations
Number of figures/tables/illustrations	1
Format	both print and electronic
Are you the author of this	No

Elsevier article?	
Will you be translating?	No
Title of your thesis/dissertation	A NEW DRUG TRIGGERING MECHANISM IN THERMOSENSITIVE NANOROBOTS USING LOW-MELTING-POINT POLYMER NANOSHELLS
Expected completion date	Sep 2015
Estimated size (number of pages)	220
Elsevier VAT number	GB 494 6272 12
Permissions price	0.00 USD
VAT/Local Sales Tax	0.00 USD / 0.00 GBP
Total	0.00 USD
Terms and Conditions	

(FIGURE 2.10)

ELSEVIER LICENSE
TERMS AND CONDITIONS

Aug 05, 2015

This is a License Agreement between Ali Dabbagh ("You") and Elsevier ("Elsevier") provided by Copyright Clearance Center ("CCC"). The license consists of your order details, the terms and conditions provided by Elsevier, and the payment terms and conditions.

All payments must be made in full to CCC. For payment instructions, please see information listed at the bottom of this form.

Supplier	Elsevier Limited The Boulevard,Langford Lane Kidlington,Oxford,OX5 1GB,UK
Registered Company Number	1982084
Customer name	Ali Dabbagh
Customer address	Faculty of Engineering Kuala Lumpur, Kuala Lumpur 50603
License number	3682400441539
License date	Aug 05, 2015
Licensed content publisher	Elsevier
Licensed content publication	Ultrasound in Medicine & Biology
Licensed content title	Polyacrylamide gel containing egg white as new model for irradiation experiments using focused ultrasound
Licensed content author	Kenji Takegami,Yukio Kaneko,Toshiaki Watanabe,Toshiyuki Maruyama,Yoichiro Matsumoto,Hirokazu Nagawa
Licensed content date	October 2004
Licensed content volume number	30
Licensed content issue number	10
Number of pages	4
Start Page	1419
End Page	1422
Type of Use	reuse in a thesis/dissertation
Portion	figures/tables/illustrations
Number of figures/tables/illustrations	1
Format	both print and electronic
Are you the author of this Elsevier article?	No
Will you be translating?	No

Original figure numbers	Figure 3
Title of your thesis/dissertation	A NEW DRUG TRIGGERING MECHANISM IN THERMOSENSITIVE NANOROBOTS USING LOW-MELTING-POINT POLYMER NANOSHELLS
Expected completion date	Sep 2015
Estimated size (number of pages)	220
Elsevier VAT number	GB 494 6272 12
Permissions price	0.00 USD
VAT/Local Sales Tax	0.00 USD / 0.00 GBP
Total	0.00 USD
Terms and Conditions	
Will you be translating?	No

(TABLE 2.4)

JOHN WILEY AND SONS LICENSE TERMS AND CONDITIONS

Aug 05, 2015

This Agreement between Ali Dabbagh ("You") and John Wiley and Sons ("John Wiley and Sons") consists of your license details and the terms and conditions provided by John Wiley and Sons and Copyright Clearance Center.

License Number	3682401325506
License date	Aug 05, 2015
Licensed Content Publisher	John Wiley and Sons
Licensed Content Publication	Bioelectromagnetics
Licensed Content Title	Formulas for preparing phantom muscle tissue at various radiofrequencies
Licensed Content Author	Chung-Kwang Chou,Gang-Wu Chen,Arthur W. Guy,Kenneth H. Luk
Licensed Content Date	Oct 19, 2005
Pages	7
Type of use	Dissertation/Thesis
Requestor type	University/Academic
Format	Print and electronic
Portion	Figure/table
Number of figures/tables	1
Original Wiley figure/table number(s)	Table 1
Will you be translating?	No
Title of your thesis / dissertation	A NEW DRUG TRIGGERING MECHANISM IN THERMOSENSITIVE NANOROBOTS USING LOW-MELTING-POINT POLYMER NANOSHELLS
Expected completion date	Sep 2015
Expected size (number of pages)	220
Requestor Location	Ali Dabbagh Faculty of Engineering University of Malaya Kuala Lumpur, Malaysia 50603 Attn: Ali Dabbagh
Billing Type	Invoice
Billing Address	Ali Dabbagh Faculty of Engineering University of Malaya Kuala Lumpur, Malaysia 50603 Attn: Ali Dabbagh
Total	0.00 USD